MODE I FRACTURE TOUGHNESS AND TENSILE STRENGTH INVESTIGATION ON MOLDED SHOTCRETE BRAZILIAN SPECIMEN

A THESIS SUBMITTED TO
THE GRADUATE SCHOOL OF NATURAL AND APPLIED SCIENCES
OF
MIDDLE EAST TECHNICAL UNIVERSITY

BY

TUĞÇE TAYFUNER

IN PARTIAL FULFILLMENT OF THE REQUIREMENTS
FOR
THE DEGREE OF MASTER OF SCIENCE
IN
MINING ENGINEERING

SEPTEMBER 2019

Approval of the thesis:

MODE I FRACTURE TOUGHNESS AND TENSILE STRENGTH INVESTIGATION ON MOLDED SHOTCRETE BRAZILIAN SPECIMEN

submitted by **TUĞÇE TAYFUNER** in partial fulfillment of the requirements for the degree of **Master of Science in Mining Engineering Department, Middle East Technical University** by,

Prof. Dr. Halil Kalıpçılar
Dean, Graduate School of **Natural and Applied Sciences** _____

Prof. Dr. Celal Karpuz
Head of Department, **Mining Engineering** _____

Prof. Dr. Levend Tutluoğlu
Supervisor, **Mining Engineering, METU** _____

Examining Committee Members:

Prof. Dr. Celal Karpuz
Mining Engineering, METU _____

Prof. Dr. Levend Tutluoğlu
Mining Engineering, METU _____

Assoc. Prof. Dr. Mehmet Ali Hindistan
Mining Engineering, Hacettepe Uni. _____

Date: 13.09.2019

I hereby declare that all information in this document has been obtained and presented in accordance with academic rules and ethical conduct. I also declare that, as required by these rules and conduct, I have fully cited and referenced all material and results that are not original to this work.

Name, Surname: Tuğçe Tayfuner

Signature:

ABSTRACT

MODE I FRACTURE TOUGHNESS AND TENSILE STRENGTH INVESTIGATION ON MOLDED SHOTCRETE BRAZILIAN SPECIMEN

Tayfuner, Tuğçe
Master of Science, Mining Engineering
Supervisor: Prof. Dr. Levend Tutluoğlu

September 2019, 141 pages

Tensile opening mode I loading state is important for shotcrete-concrete type materials, since these are weak under tension. Brazilian type splitting tests are commonly used for checking the structural effectiveness of concrete in opening mode. Tensile strength is measured indirectly by these tests.

In concrete industry, beam tests under three- and four-point bending loads are used to measure tensile strength and mode I fracture toughness of beams and columns under almost pure tensile loading state. However, some structural parts are under compression and indirect tensile loading may result in these. Flattened Brazilian Disc (FBD) is a modified splitting type geometry. It is preferred due to its simplicity of specimen preparation and the compressive load application. Testing this geometry under compression provides means to measure both tensile strength and mode I fracture toughness with a single specimen and test.

This work is original in the sense that FBD geometry and the testing method are successfully applied to measure the tensile strength and fracture toughness of molded shotcrete with a water/cement ratio of 0.5. Molds are designed in different sizes and 3D printing technology are used to produce these accurately in desired geometries.

The aim of this study is to investigate the relations between fracture toughness, specimen size, curing time and the tensile strength of shotcrete for a particular mixture design. Loading angle that is defined as the angle between the paths drawn from the specimen center to the edges of flattened loading ends, are kept constant at *22*° in all testing work. This corresponds to a half of the flattened end/radius ratio of *L/R*=0.19.

For investigating the effect of specimen size on the fracture toughness, specimen diameters were varied between 100 mm and 200 mm. Curing time was constant as 7-day for this group of tests. Fracture toughness of shotcrete was found to increase from 0.93 to 1.46 MPa√m while specimen diameters were changing between 100 mm to 200 mm.

The effect of curing time on fracture toughness was investigated with constant 160 mm diameter disc specimen geometry. One to seven-day air cured FBD specimens were tested. It was found that mode I fracture toughness of shotcrete increased from 0.66 to 1.18 MPa√m with increasing curing time.

The tensile strength calculated from Flattened Brazilian Disc tests were compared to the results of the conventional Brazilian Disc tests. Processing the experimental results, a size independent fracture toughness/tensile strength ratio was proposed for concrete type of materials.

Keywords: Shotcrete, mode I fracture toughness, Flattened Brazilian disc method, size effect, curing time

ÖZ

BRAZİLYAN DÖKÜLMÜŞ PÜSKÜRTME BETON NUMUNELERİNDE MOD I KIRILMA TOKLUĞUNUN VE ÇEKME DAYANIMININ İNCELENMESİ

Tayfuner, Tuğçe
Yüksek Lisans, Maden Mühendisliği
Tez Danışmanı: Prof. Dr. Levend Tutluoğlu

Eylül 2019, 141 sayfa

Beton-püskürtme beton tipi malzemelerin gerilme yüklenmesi karşısında zayıf olduklarından mod I diye isimlendirilen açılma modu, bu tarzda numunelerin kırılma tokluklarının incelenmesi için en kritik yükleme modudur. Düzleştirilmiş Brazilyan disk yöntemi bu yükleme modunda kırılma tokluğu araştırılması yapılması için şekil yapısından ötürü önerilen bir yöntemdir.Bu test yöntemi kullanılarak çekme dayanımının dolaylı yolla elde edilmiştir.

Beton endüstrisinde, üç ve dört noktalı eğilme yükleri altındaki kiriş testleri, mod I, neredeyse saf çekme yükü durumunda kirişlerin ve kolonların çekme dayanımını ve kırılma tokluğunu ölçmek için kullanılır. Bununla birlikte, yapısal olarak bazı bölgeler sıkıştırma etkisi altında kalabilir ve bu bölgeler dolaylı çekme yükü ile sonuçlanabilir. Düzleştirilmiş Brezilyan Disk (FBD), değiştirilmiş bir ayrılma tipi geometridir. Bu geometri hem sıkıştırma altında test edildiği hem de numune hazırlamasında sağladığı kolaylıktan dolayı tercih edilmektedir. Sıkıştırma yükü altında test edilen bu numuneden hem Mod I kırılma tokluğunu hem de çekme mukavemeti ölçülebilir.

Bu çalışma, FBD geometrisi ve test yönteminin, 0.5 su çimento oranına sahip kalıplanmış püskürtme betonun çekme dayanımını ve kırılma tokluğunu ölçmek için başarılı bir şekilde uygulanması anlamında orijinaldir. Kalıplar farklı boyutlarda

tasarlanır ve bunları istenen geometrilerde doğru şekilde üretmek için 3D baskı teknolojisi kullanılır.

Bu çalışmanın amacı, seçilen beton karışım tasarımı için, püskürtme betonun kırılma tokluğunun numune büyüklüğü, kür süresi ve çekme dayanımı ile ilişkisini incelemektir.

Numunenin merkezinden düzleştirilmiş yükleme uçlarının kenarlarına doğru çizgiler olduğu farzedilirse bu çizgiler arasındaki açı olarak tanımlanan yükleme açısı, tüm test çalışmalarında 22 ° olacak şekilde sabit tutulur. Bu açı düzleştirilmiş yükleme yüzeyinin uzunluğunun yarısının yarıçapa oranı olan, *L/R* = 0.19 'a karşılık gelmektedir.

Numune büyüklüğünün mod I kırılma tokluğuna etkisi araştırılırken, sabit karışım oranı, sabit yükleme açısı ve 7 gün olarak belirlenen sabit kür süresinde çaplar 100 mm ile 200 mm arasında değiştirilmiştir. Sonuçlar mod I kırılma tokluğunun, numune çapları 100 mm ile 200 mm arasında değişirken, 0.93-1.46 MPa$\sqrt{m}$ aralığında değiştiğini göstermektedir.

Devamında yapılan kür süresinin kırılma tokluğu üzerindeki etkisinin araştırıldığı çalışmada çapı 160 mm olan numuneler ile çalışılmış, kür süresi 1 gün ile 7 gün arası değişirken karışım oranı, yükleme açısı ve numune çapı sabit tutulmuştur. Bu çalışma sonucunda ise 1 gün ile 7 gün arasında değişen kür alma sürelerinde püskürtme betonun mod I kırılma tokluğu 0.66-1.18 MPa$\sqrt{m}$ arasında değişmiştir.

Tüm bunlara ek olarak, çalışmanın son bölümünde Düzleştirilmiş Brazilyan disk testlerinen çekme dayanımı hesaplanması ve bunların geleneksel Brazilyan disk test sonuçları ile karşılaştırılması çalışılmışır. Elde edilen deney sonuçlarından ve bu sonuçların excel grafiklerinden, beton tipi Düzleştirilmiş Brazilyan Disk numunelerinde,160 mm çapa sahip olanlar için, numune çapından bağımsız kırılma tokluğu/ çekme dayanımı oranı (katsayısı) geliştirilmiştir.

Anahtar Kelimeler: Püskürtme beton, mod I kırılma tokluğu, düzleştirilmiş Brazilyan disk yöntemi, boyut etkisi, kür süresi

To My Family

ACKNOWLEDGEMENTS

I would like to express my deepest gratitude to my supervisor Prof. Dr. Levend Tutluoğlu for his patient guidance, scientific insight, precious comments and trust in me. I want to thank to the examining committee the members, Prof. Dr. Celal Karpuz and Assoc. Prof. Dr. Mehmet Ali Hindistan for their valuable contributions.

I am deeply grateful to Selin Yoncacı, who will soon get her PhD degree, for not leaving me alone during the whole process and for answering all my questions all that time. Moreover, I want to thank my chief engineer Koray Önal and my manager Ömer Şansal Gülcüoğlu for their support during my thesis period.

I would like to thank my friends, research assistants Enver Yılmaz and Ceren Karataş Batan for staying with me in the laboratory when it necessary and no matter how long it took.

I would like to show my gratitude to my dearest friends Gizem Özcan, Müge Öztürk, Onur Can Kaplan. They are always with me, in my best and worst times. I also want to thank Hazal Varol, Buse Ceren Otaç, Merve Özköse and Elif Naz Şar for their support and motivation.

I would also like to extend my thanks to Hakan Uysal for his support during my laboratory works.

I would like to offer all my loving thanks to my family Senar Tayfuner, Serdal Tayfuner and Berk Tayfuner for their limitless support and encouragement.

Finally, I want to express my deepest gratitude and appreciation to Onur Can Yağmur being with me whenever I need. I will never forget your support and help during this process.

TABLE OF CONTENTS

LIST OF TABLES

TABLES

LIST OF FIGURES

FIGURES

LIST OF ABBREVIATIONS

ABBREVIATIONS

2D: two-dimensional

3D: three-dimensional

BDT : Brazilian disc test

CB : Chevron bend

CCNBD : Cracked chevron notched Brazilian disc

CPD: Crack propagation direction

CPE8: Continuum plane strain eight noded element

CSTBD : Cracked straight through Brazilian disc

FBD : Flattened Brazilian disc

ISRM : International Society for Rock Mechanics

LEFM: Linear elastic fracture mechanics

LVDT: Linear variable differential transformer

MTS: Maximum tangential stress

SCB : Semi-circular bending

SIF: Stress intensity factor

SNDB : Straight-notched disc bending

SR: Short-rod

UCS : Uniaxial Compressive Strength

LIST OF SYMBOLS

SYMBOLS

a: half of crack length

A: mesh size

A: andesite

D: specimen diameter

d_e: distance of crack tip to central load application point

E: Elastic Modulus

G : energy release rate

G_c : critical energy release rate

J: J integral

K: stress intensity factor

K_C*:* critical stress intensity factor

K_I *:* mode I stress intensity factor (opening mode)

K_{II} : mode II stress intensity factor (shearing mode)

K_{III} : mode III stress intensity factor (tearing mode)

K_{Ic} : mode I fracture toughness

K_{IIc} : mode II fracture toughness

L: half of flattened length

P: applied concentrated load

P_{max}: failure load

P_{min}: local minimum load

R: disc radius

r_c: radius of contour integral region

S_{11} : normal stress in x-direction

S_{22} : normal stress in y-direction

S_{33} : normal stress in z-direction

S_{12} : shear stress in xy-direction

S: span length

t: specimen thickness

Y : dimensionless stress intensity factor

Y_I : mode I dimensionless stress intensity factor

Y_{II} : mode II dimensionless stress intensity factor

$Y_{\imath max}$: maximum dimensionless stress intensity factor

w : projected width over loaded section

α: half of loading angle

ε : Strain

σ : stress

σ_1 : maximum principal stress

σ_3 : minimum principal stress

σ_t : tensile strength

α : a/R

τ : shear stress

μ: shear modulus

ϑ : Poisson's Ratio

θ : crack propagation angle

t_c: curing time in days

σ_t: tensile strength

CHAPTER 1

INTRODUCTION

1.1. General

According to the data from the National Institute for Science and Technology and the Bettelle Memorial Institute, in one year 119 billion dollars were spent because of fracture related failures in 1983. The money has an incontrovertible significance; however, the price of many failures in human life and also physical injuries are more important than the dollars, (Anderson, 2005).

Defects in the materials, lack of information about the loading or environment, improper design and defects in structures can cause catastrophic failures.

In the respect of both structural and mining engineering, Rossmanith said that the main questions are respectively: “how the failure load of these flawed structures can be estimated? Which kind of combinations of load and parameters of flaw geometry causes the failure? Moreover, which material variables are the fracture process conducted by?” (Rossmanith, 1983).

In 1950’s and 1960’s, Fracture Engineering eventually arise to find out the causes of cracks in various engineering materials. There are several engineering materials such as metal, rock, concrete and ceramics. Rock fracture mechanics is the science that identifies how the crack starts and disseminates under the applied loads in rock engineering. The crack resistance at the beginning of the crack growth is specified by fracture toughness parameter and this is a very active area of the current research.

The stability of underground engineering structures may be possible by supporting the cavities opened in the structures rapidly with lower cost. Shotcrete technology has improved recently with the findings and innovations in installation equipment and

material technology. Although, shotcrete applications go back a long way around the beginning of 20th century, structural integrity of shotcrete is a relatively a new field of research area which needs to be investigated in detail. Nowadays, underground mine openings, tunnels, and the galleries of many purposes are being stabilized by shotcrete support systems. As most of the time shotcrete is applied just after its preparation on site, it is difficult to conduct a detailed laboratory analysis. Detailed laboratory testing can be done if a proper mixture of shotcrete can be prepared; so that shotcrete in the field practice is simulated closely.

1.2. Statement of the Problem

Although, shotcrete is a widely used heterogeneous material that particularly used as a support system, the crack behavior of it has not been focused enough even though one of the most important weakness of it is cracks. Most of the studies on shotcrete is based on laboratory tests to determine its mechanical properties, strength, setting time or rebound rate. So far, not enough attention is paid to the fracture mechanics and crack propagation characteristics of shotcrete, which is one of the most important consideration for the field of engineering.

Mode I fracture toughness is a measure of the fracture energy to propagate a crack under tension in materials. This parameter is important also in the preventing efforts of propagation of a pre-existing defect. Fracture toughness tests are commonly carried out with beam and disc or cylinder-type specimen geometries. One current trend in fracture toughness testing is to minimize the specimen geometry effect on pure tensile mode crack opening. Specimen geometry is associated with a size effect issue.

Size effect on facture toughness of rocks has been frequently investigated. However, rock fracture toughness testing is usually restricted to the core sample diameters which may go up to around 100 mm in practice. It has not been possible to work with large range of diameters. Sizes of specimens were limited, in particular in circular geometries such as FBD geometry, depending on the diameter of the core drilling

machine. Research on internal characteristics and mechanical properties of shotcrete is still in progress in literature. It is worth to carry out an investigation about the size effect on fracture toughness of cementitious material.

A few studies investigate the shotcrete behavior at early ages of curing. There is a need for information on crack formation or crack mechanisms, since shotcrete is used to provide temporary surface control for local stability before the primary support is installed. Because the shotcrete must become self-supporting before miners and equipment can work safely underneath, the curing characteristics of the shotcrete are critical to the speed of the mining cycle. Thus, in order to understand the time-dependent response of fracture behavior in shotcrete, more research is to be done on the basis of laboratory tests.

Under mode I fracture loading, the opening mode, brittle or quasi-brittle materials commonly yield in tension. Thus, one might expect that there is a relationship between the fracture toughness and the tensile strength of shotcrete.

Therefore, studying the initiation of cracks or fracture toughness of the shotcrete specimens depending on the geometry and the curing time is a challenging topic. The relation of the fracture toughness to the tensile strength of the shotcrete is an innovative area that needs to be investigated.

1.3. Objectives of the Study

The main objectives of performing this thesis are to understand the relation between fracture toughness of shotcrete with the specimen size, curing time and the tensile strength for a particular mix design.

1.4. Methodology of the Study

Cementitious materials like shotcrete-concrete generally exhibit high compressive strength, low tensile strength. So the mode I, in other words tensile opening mode is a crucial loading mode for not only shotcrete but also for brittle materials such as rocks. ISRM and ASTM suggested many methods to measure the rock fracture toughness. The main proposed methods by International Society for Rock Mechanics (ISRM), are:

- Short rod (SR) (Ouchterlony, 1988),
- Chevron bend (CB) (Ouchterlony, 1988),
- Cracked chevron notched Brazilian disc (CCNBD) (Fowell, 1995)
- Semi-circular bending (Kuruppu et al., 2015)

Brazilian type methods which were preferable since relatively simple both in specimen preparation and also compressive loading on disc specimens while testing include;

- Cracked chevron notched Brazilian disc (CCNBD), (Sheity, D. K., Rosenfield, A. R., & Duckworth, W. H. (1985)
- Cracked straight through Brazilian disc (CSTBD)
- Semi-circular bending test (SCB) (Chong and Kuruppu, 1984)
- Brazilian disc (BD) (Guo et al., 1993)
- Flattened Brazilian disc (FBD) (Wang and Xing, 1999)

The reason for selection of the Flattened Brazilian Disc method is the easiness of sample preparation and testing procedure. Compressive loading in fracture testing and indirectly generating tensile splitting are attractive for brittle materials. Although, it is necessary to prepare a very precise samples for FBD testing, the usage of 3D printing technology for shotcrete casting process provided the desired geometric accuracy. Moreover, 3D printing technology made preparation of specimens in different sizes

possible. A wide range of specimen with varying diameters were tested to measure tensile strength and mode I fracture toughness of shotcrete.

The experimental work started with the preparation of the shotcrete specimens. In the preparation of shotcrete samples, attention was paid to use the same ingredients for each sample and to prepare with the same equipment under the same laboratory conditions in order to interpret the test results correctly. Five samples were molded and tested for each group of varying specimen sizes in order to increase statistical quality of the test results.

For all tests, MTS 815 Rock Testing Machine in laboratory was used. Five specimens were prepared for each diameter and curing time group.

First, conventional mechanical property testing work was conducted. Static deformability test and uniaxial compressive strength tests were conducted in order both to check the mechanical properties of the shotcrete and to validate the mixture according to its mechanical properties in the literature. The conventional Brazilian disc test was conducted next to measure the tensile strength with regular testing method.

Finally, as the main part, mode I fracture toughness tests with Flattened Brazilian Disc geometry were carried out to split the samples into two. One investigation was the size effect on fracture toughness with constant curing time and changing diameters and the second one was performed to analyse the effect of curing time on fracture toughness with constant diameter and various curing time. Moreover, in order to determine the relation between fracture toughness and the tensile strength, conventional Brazilian test results were compared to the results of Flattened Brazilian Disk tests. For the evaluation of experimental results, equations from a similar work were adopted.

1.5. Organization of Thesis

This thesis is divided into six chapter. Following this introduction. Chapter 2 presents a general review of the literature about the basics of fracture mechanic and its significance for the main research problem. In Chapter 2, description of the different fracture toughness testing methods is provided. Experimental method used to determine mode I fracture toughness and its background are explained as well as fracture mechanics of shotcrete. Chapter 3 presents a description of the properties of shotcrete mixture and its ingredients. It continues with the shotcrete mix design and laboratory work related to the casting process. Chapter 4 presents a detailed description of the laboratory work and the results of all conventional experimental study, including static deformability tests, Brazilian disc test, and the most importantly Flattened Brazilian Disc tests to investigate fracture toughness and to the factors affecting its value. Chapter 5 presents evaluation of the results, discussion of the all experiments carried out, and the interpretation of these results with the help of previous studies in literature. Finally, Chapter 6 presents conclusion and the findings of this study as well as recommendations for further research in this field.

CHAPTER 2

THEORETICAL BACKGROUND OF FRACTURE MECHANICS

2.1. History of Fracture Mechanics

In the early Renaissance, the concept of fracture had been scientifically evaluated as scaling of fracture and experiments were conducted on iron wires by Leonardo da Vinci for the first time (1452-1519), (Figure 2.1), (Gross,2014).

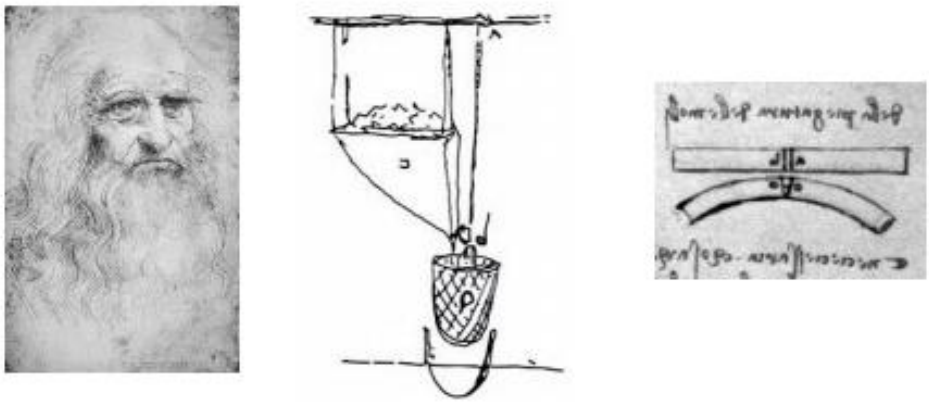

Figure 2.1. Leonardo da Vinci fracture test setup (Gross, 2014)

Afterwards, Galileo Galilei (1564–1642) who was known as the founder of modern mechanics by his contributions from his well-known “Dialog”, made correct inferences that the fracture forces of column under tension were related to the cross sectional area, and also he stated that the bending moment was the crucial loading type for the fracture of beams, (Figure 2.2), (Cotterel, 2002).

Figure 2.2. Galileo Galilei tensile test setup (Gross, 2014)

The most punctual work was done by Griffith (1921). He carried out an analysis for actual cracks. Even though, Griffith's theory was so important, it was limited for some highly brittle materials such as glass. In the early 1960s, with the development of the discipline that we called "fracture mechanics", Irwin (1958) who was a professor from Lehigh University, examined plasticity in detail. He extended the Griffth's theory. Irwin proposed that the stress intensity factor concept could be used for the calculation of stress field around the crack tip.

Applications of engineering fracture mechanics to brittle materials developed with an important delay in comparison to ductile materials. Considering the underground mines, tunnels in galleries etc., rock fracture problem has a significant role in collapses. At the early sixties, Griffith's model found the roles in applications involving stone and concrete type materials. The friction between crack faces was established byMc Clintock and Walsh (1962). They modified Griffith's theory and investigated the crack closure in compression, whereas Kaplan (1961) have published the first experimental study about the possibility of applying linear elastic fracture mechanics to concrete. In 1965 Bieniawski and Hoek was performed the early research about rocks, in South Africa, where mine disappointments were earnest issues to be comprehended (Ceriolo and Tommaso, 1998).

2.2. Basics of Fracture Mechanics

2.2.1. Fracture Modes

There are three main ways named as mode I, mode II and mode III for cracks to initiate and propagate in a material, (Figure 2.3).

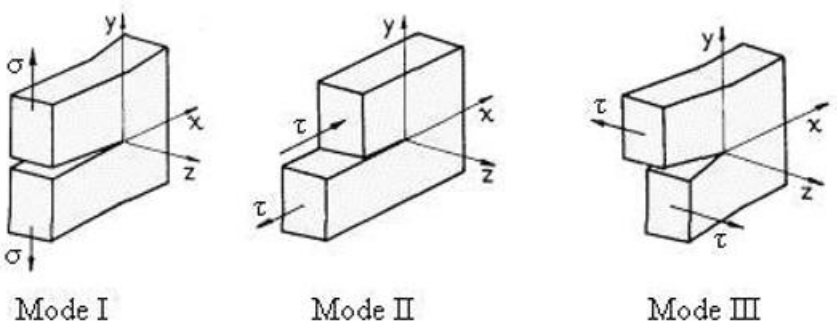

Figure 2.3. Fracture modes (Key to Metals Database, 2010)

Mode I: In mode I, also known as tensile opening mode, direction normal to the crack plane separates the faces of the cracks.

Mode II: In mode II, also named as in-plane sliding or shear mode, both crack faces are in the direction of crack front normal.

Mode III: In mode III, also named as the tearing or out of plane mode, the crack faces are sheared parallel to the crack front.

Crack formations can occur by any of these three modes. Moreover, combinations of these modes are also possible such as mode I and mode II can occur simultaneously. In such a case it is called as mixed mode. Mode I is the essential failure mode for brittle material since brittle materials are weak under tension.

2.2.2. Stress Intensity Factor

Stress intensity factor, *K* is used for predicting the stress state around the tip of the crack. *K* depends on the size and location of the crack as well as sample geometry. It is important that the maximum stress around the tip of the crack not to exceed the fracture toughness. Otherwise, if *K* exceeds the fracture toughness values, crack initiates and propagates.

Formula for calculating the stress intensity factor for beam and plate type geometries is given below:

$$K = \sigma\sqrt{a \times \pi} \times f(\frac{a}{w}) \quad (2.1)$$

where:

σ: remote stress applied to component (MPa)

a: crack length (m)

f (a/w): correction factor that depends on specimen and crack geometry

w: specimen width or beam depth (m)

2.2.3. Fracture Toughness

Fracture toughness, K_C is the critical value of stress intensity factor that represents the material's resistance to fracture. It depending on loading rate, temperature, environment, composition and microstructure with geometric effects.

The mode I, opening mode, fracture toughness of concrete can be expressed by the critical stress intensity factor, K_{IC}. Similarly, especially in concrete related studies, G_C, energy release rate usually used to express the fracture toughness. The term G_c, called

the critical strain energy release rate was generalized by the Irwin who compiled crack extension related studies and expressed the rate of change in potential energy with crack area. He indicated that in order to overcome the surface energy of the new cracks in a fracturing material, the sufficient potential energy must be required. Irwin form of energy criterion can be written as;

For plane stress;

$$\sigma = \sqrt{\frac{EG_c}{\pi a}} \tag{2.2}$$

For plane strain;

$$\sigma = \sqrt{\frac{EG_c}{(1-\nu^2)\pi a}} \tag{2.3}$$

When stress intensity factor reaches its critical value, crack propagation occurs. The relation between the critical stress intensity factor and critical energy release rate can be shown as;

For plane stress;

$$G_c = \frac{{K_C}^2}{E} \tag{2.4}$$

For plane strain;

$$G_C = {K_C}^2 \left(\frac{1-\nu^2}{E}\right) \quad (2.5)$$

G_C: Critical energy release rate (MPa.m)

E: Elastic Modulus (MPa)

υ: Poisson's ratio

K_C: Critical stress intensity factor (MPa√m)

2.2.4. Linear Elastic Fracture Mechanics

Linear Elastic Fracture Mechanics works under the assumption of the material being linear elastic and isotropic. Assuming that the material is linear elastic and isotropic indicate that the material properties are independent of direction. At the same time, elastic modulus, E and Poisson's ratio, υ are two independent elastic constant that material has. In LEFM assumption, considering the theory of elasticity, the stress field around the crack tip can be calculated. However, Linear Elastic Fracture Mechanics, LEFM, is only applicable when the inelastic deformation around the crack path is relatively smaller compare to the size of a crack.

Irwin found a method for calculating the amount of energy available for fracture.

$$\sigma_{ij} = \left(\frac{K_I}{\sqrt{2\pi r}}\right) f_{ij}(\theta) \quad (2.6)$$

σ_{ij} : Cauchy Stress

K_I : stress intensity factor

r: the distance from the crack tip

θ *:* angle with respect to the plane of the crack

f_{ij} *:* function depending on the crack geometry and loading conditions

In general, LEFM is valid when the nonlinear material deformation at the crack tip is small enough. In order to characterize nonlinear behavior like plastic deformation for many materials, there was a need for an alternative fracture mechanics model namely Elastic-Plastic Fracture Mechanics. Unlike LEFM, the material is assumed to be isotropic and elasto-plastic.

2.3. Fracture Toughness Testing with Flattened Brazilian Disc Test Method

Brazilian tensile strength testing specimen geometry was suggested by Guo et al. (1993) as a mode I fracture toughness test method so that without machining a notch or crack, mode I fracture toughness (*KIc*) may be determined.

The relation between stress intensity factors (SIF) were studied by Guo et al. (1993). A formula using dimensionless stress intensity factor, Y_I and dimensionless crack length, a*/R* was derived by numerical integration method. From the numerical solution, it was found out that dimensionless stress intensity factor could be expressed as a function of dimensionless crack length.

Changing the loading angles between 5°- 50°, Guo et al., 1993 showed the relationship between different crack lengths and the stress intensity factors for Flattened Brazilian Disk type geometry.

After numerical interpretations, formula for BDT under mode I fracture toughness was derived as follows (Guo et al., 1993):

$$K_{IC} = B \times P_{min} \times Y_I(\frac{a}{R}) \tag{2.7}$$

Where:

K_{IC}*:* mode I fracture toughness

B: the constant dependent on geometry of the specimen

$$\text{B: } \frac{2}{\sqrt{R}\times t\times a\times \pi\sqrt{\pi}} \tag{2.8}$$

P_{min}*:* local minimum load

R: disc radius

t: disc thickness

$Y_I(\frac{a}{R})$*:* dimensionless stress intensity factor

a: half of crack length

a/R: dimensionless crack length

Method suggested by Guo et. Al (1993) has some limitations and problematic cases such as: crack initiation at the center and crack propagation along vertical axis is not guaranteed, also it could not explain the relation between loading angle and where the crack initiates (Wang and Xing, 1999). In the problems that crack initiated at the center inconsistent SIF values resulted due to the assumption of uniform arc loading and wrong selection of domain, (Figure 2.4).

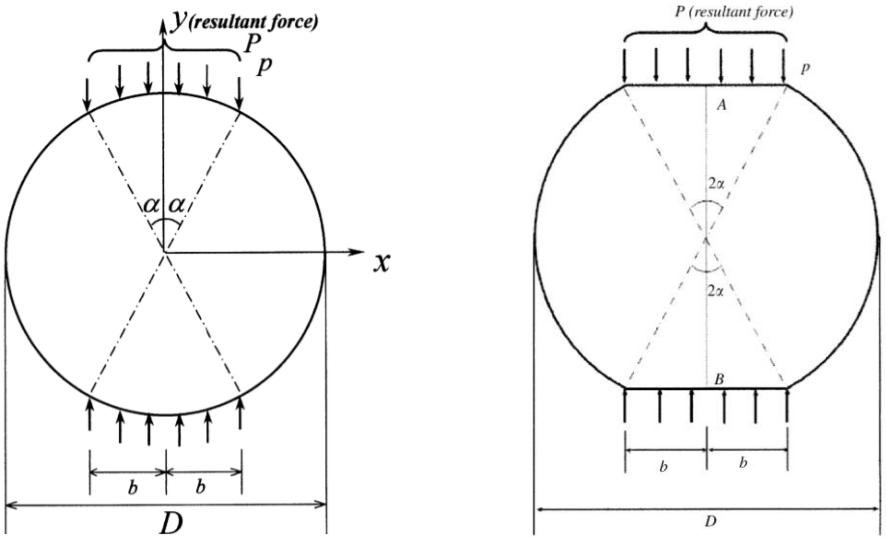

Figure 2.4. The Brazilian Disc specimen under the uniform arc loading (at left) and the Flattened Brazilian Disc specimen under the uniform diametral compression (at right) (Wang & Wu, 2004)

A better method was proposed Wang and Wu (2004) "for Flattened Brazilian Disc (FBD) in order to overcome the problems of Brazilian Disc Test (BDT) proposed by Guo et al. (1993). The geometry suggested for this method replaced opposite curved surfaces with flattened load application ends of width (*2L*). This way a simple loading configuration is provided and crack initiation at the disc center is guaranteed by discarding crushing problem at contact points. FBD geometry is illustrated in Figure 2.5 where the red solid line demonstrates the location of the crack formation during loading (*2a*), red dashed line indicates the crack path and its maximum gives the value of critical crack length ($2a_c$), orange arc shows the loading angle (2α), black *t* and *2L* indicate the thickness and flattened end width of the specimen.

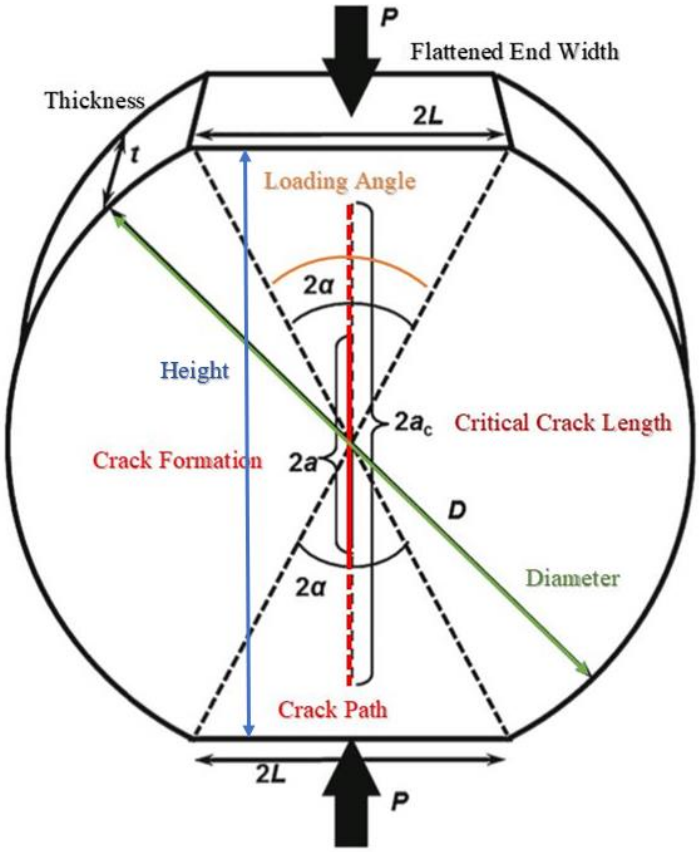

Figure 2.5. The geometric representation of Flattened Brazilian Disc (Keles and Tutluoglu, 2011)

Formula derived by Wang and Wu (2004) for mode I fracture toughness of FBD geometry is provided as:

$$K_{IC} = \frac{P_{min} \times Y_{max}}{t \times \sqrt{R}} \tag{2.9}$$

Where:

K_{IC}: mode I fracture toughness (MPa√m)

P_{min}: local minimum load (MN)

Y_{Imax}: maximum dimensionless stress intensity factor

R: disc radius (m)

t: disc thickness (m)

In Figure 2.6 a typical load displacement curve of Flattened Brazilian Disc test result is shown. In this figure, P_{max} is represented by letter a and P_{min} is represented by letter b.

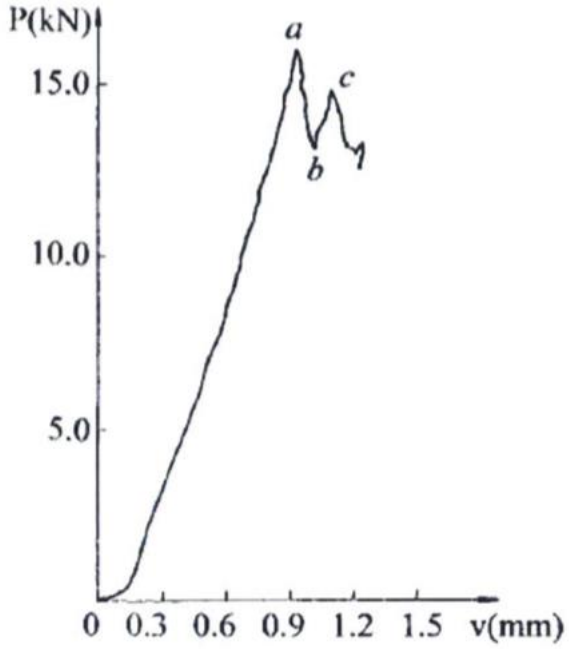

Figure 2.6. A typical load displacement curve (Wang and Xing, 1999)

In Figure 2.7 dimensionless stress intensity factor (Y_I) changing with the dimensionless crack length (*a/R*) is shown. Wang and Xing (1999) stated that, when *a/R* increasing, Y_I also increasing up to its maximum value and after that it starts to

decrease. When Y_I reaches its maximum, it is called maximum dimensionless stress intensity factor at dimensionless critical crack length. In this circumstances, dimensionless stress intensity factor only depends on the loading angle and it can be calculated numerically.

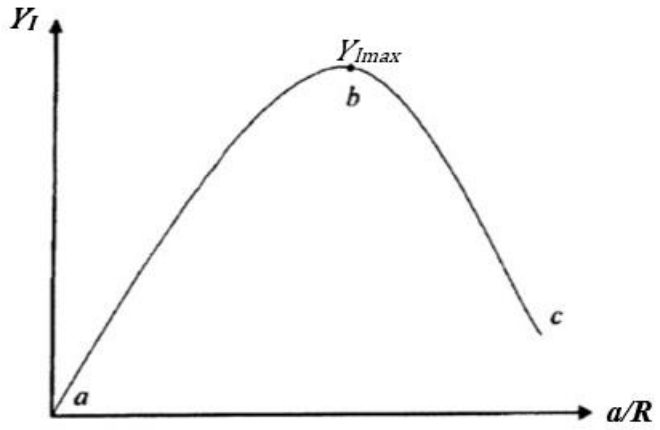

Figure 2.7. Maximum dimensionless stress intensity factor represented by Wang and Xing (Wang and Xing, 1999)

2.4. Fracture Mechanics of Concrete

Beginning of fracture mechanics of concrete was by Kaplan (Kaplan, 1961) who conducted experiments with four point bending of notched beams at various sizes. His experiments showed that fracture toughness of concrete beams were changing depending on their geometry and size. After that Kesler, Naus and Lott (1971) stated that the LEFM that Kaplan used was inapplicable on concrete structures with sharp cracks. Walsh's experimental works supported Kaplan's findings. (Walsh, 1979). In the wake of experimental results on notched concrete beams and their relation with the K_C, in order to describe the crack growth on concrete at least two fracture parameters were needed. In order to understand and model the behavior of concrete, a major improvement as made in 1976 by Hillerborg, Modeer and Petersson was

fictitious crack model. In 1976, Crack band model was proposed by Bazant in order to explain the fracture process zone on concrete with using the concept of the strain-softening, (Bazant, 1976). Jenq and Shah (1985) proposed the two-parameter model which assumed a crack tip singularity in front of the real crack. (Carpinteri, 1984) described fracture behavior of the concrete by expressing the rate of change of strain energy density with the crack growth. Two-parameter model was used by Karihaloo and Nallathambi to propose effective crack model which assumes a sharp crack in front of the real crack (Karihaloo and Nallathambi, 1989).

Almost all the work summarized is related to the size effect issues in concrete beams. Concrete and shotcrete are structurally very similar materials; the difference lies in the application. Testing work here originally involves splitting disc type specimen geometries for which tensile cracking along the central line is generated by a compressive at the ends.

CHAPTER 3

SHOTCRETE MIXTURE SETUP

In early 1900's the spraying a cement-sand mixture was developed with the trade name of Gunite and ever since it has been used in the mining industry. However, it took fifty years to use the same process with a coarse aggregate, now called shotcrete. After that, shotcrete was used for the first time on a tunnel project in Austria in mid-50's. it did not attract much attention for ten years until Burnaby-Vancouver railway tunnel on the North American continent was under construction. After it was introduced, it attracted attention in 1967 and several Canadian and American mining firms had experimented or started to use shotcrete. (Miner, 1973)

The reason why shotcrete is widely used especially in underground works and tunnel construction as a rock support is due to the continuously developed mining industry and their constant search for ways and methods to reduce costs at the same time. Thus, investigation of the fracture properties of all composites (concrete, shotcrete, etc.) that are used in the underground openings is crucial in order to reach safe working environment and conduct safe operations in mining and civil engineering industry.

3.1. Shotcrete Mixture Ingredients

The ingredients of shotcrete mixture are Portland cement, aggregate, water and additives when necessary. In order to get the optimum strength and proper spraying ability of shotcrete mixture, correct proportions of ingredients and correct water/cement ratio are essential.

It is known that the water/cement ratio of the shotcrete should be between 0.35-0.50 (M.G. Alexander and R. Heiyantuduwa, 2009). The required 7 days strength of

shotcrete is between 25-30 MPa and 28 days strength is 35-40 MPa. In this study water/cement ratio selected as 0.5. According to the suggested concrete mixture properties standard TS EN 2016-1, concrete with 0.5 water cement ratio refer to C30 which is the minimum concrete grade for durable and long-lasting structures.

3.1.1. Portland Cement

Portland cement is a binding material produced by pulverizing a small amount of gypsum along with the Portland cement clinker which is obtained by burning an appropriate combination of calcareous and clayey materials, (Figure 3.1).

Figure 3.1. Cement

According to the Turkish Standard namely TS EN 197-1, in Turkey, produced cement are divided into five groups, which are;

CEM I; Portland Cement

CEM II; Portland-Composed Cement

CEM III; Blast Furnace Slag Cement

CEM IV; Pozzolanic Cement

CEM V; Composed Cement (Erdoğan, 2013)

The amount of cement usage is directly effective in determining the mechanical properties, especially strength, of the shotcrete. According to the application area the amount of cement should be selected. In experimental studies, CEM I 42.5 R was used in the shotcrete mixture. 42.5 means the 28-day strength of shotcrete should be 42.5 MPa and the R represents high early strength. The cement content of the mixture is in generally should be between 300-450 kg/m^3.

3.1.2. Aggregate

Aggregates are granular materials such as sand, gravel, crushed stone used with cement and water in concrete construction. Approximately 75% of the concrete/shotcrete volume is formed by aggregate. In this study, only fine aggregates from the ready-mixed concrete plant was used for all laboratory experiments because of the mold dimensions. d_{max}, the maximum grain size used for the experimental works was 0.4 mm which is referred to as fine aggregate in the literature, (Figure 3.2).

Figure 3.2. Aggregate

According to the TS EN 1097-6 standard the density of aggregate for shotcrete-concrete type of specimen should be between 2.5-3 g/cm^3. Therefore, the pycnometer test (Figure 3.3) was the precursor test that should be done in order to get specific gravity of aggregates.

Pycnometer Test method and Calculation;

M1: mass of clean and dry empty pycnometer container

M2: mass of dry soil and pycnometer container together

M3: mass of dry soil and water mix with pycnometer container

M4: mass of pure water and pycnometer container

Figure 3.3. Pycnometer tests

The specific gravity of soil is determined using the relation below:

$$\frac{M_2 - M_1}{(M_2 - M_1) - (M_3 - M_4)} \tag{3.1}$$

Table 3.1. *Pycnometer test parameters*

M_1 (g)	M_2 (g)	M_3 (g)	M_4 (g)	G (Specific gravity of aggregate)
28.55	34.75	82.49	78.61	2.67
28.55	37.09	83.94	78.61	2.66
28.55	43.59	88.07	78.61	2.69
			Average	2.68

3.1.3. Water

Water is used for two purposes. One of them is for washing aggregates to be used in shotcrete, since aggregates may include clay, silt or organic materials that may decrease surface adherence character of the pieces. The other one is for the preparation of shotcrete mixture. Water and cement are combined in specified proportions to start chemical reaction, namely hydration. Water and cement provide the desired workability as fresh shotcrete mixture, following the washing of aggregate surfaces and cement grains in the mixing process of shotcrete.

3.1.4. Admixtures/Additives

There are three purpose for using plasticizer, as an additive. The first one is by reducing the water/cement ratio in the shotcrete mixture, it provides higher strength. The second one is increasing the workability of fresh concrete without changing the material quantities or proportion in the mixture. The third one is it provides technical and economic benefits by keeping the water/cement ratio to be used in the mixture constant, while reducing the water and cement quantities. The used admixture as plasticizer is SIKA ViscoCrete Hi-Tech 2001, (Figure 3.4). The amount of plasticizer should be 1% by weight of the cement amount.

Figure 3.4. Additives

3.2. 3D Molds and Recipe for Shotcrete

For fracture toughness testing work special molds of varying diameters were prepared. SolidWorks software was used for the technical drawings of 3D-molds, (Figure 3.5). The thickness/radius (t/R ratio) of the specimens was kept constant as 1.3 for all sizes. Wall thickness and the solidity percentage of the molds were adjusted according to the changing diameters in order to get high performance like resistance to the repeated usage, and to prevent any damage to the sample during extraction out of the mold.

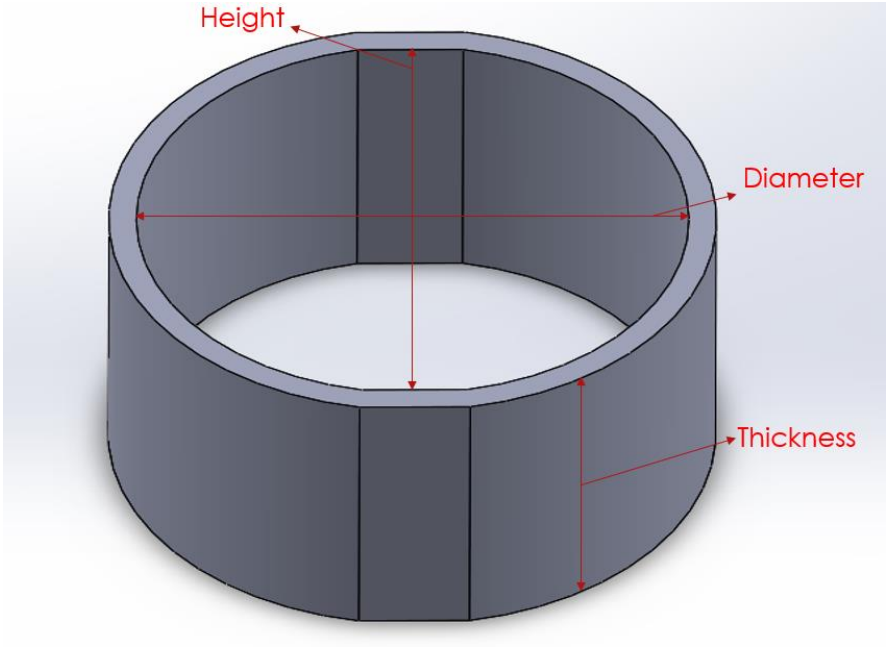

Figure 3.5. Drawing of FBD mold in SolidWorks

In Table 3.2, dimensions of the FBD specimens extracted from the 3D molds are tabulated.

Table 3.2. *Dimensions of the specimens extracted from the molds*

Mold Name	*Diameter (mm)*	*Thickness (mm)*	*Height (mm)*
M-1	100	67	98
M-2	120	80	118
M-3	140	94	137
M-4	160	107	157
M-5	180	120	177
M-6	200	133	196

The picture of molds used for the investigation of size effect on fracture toughness test is shown in Figure 3.6.

Figure 3.6. Used molds with varying diameters 100 mm to 200 mm

The 3D mold of each diameter group has its own mixture recipe which was adjusted accordingly the volume of each mold and keeping recipe proportions the same. In general, the recipe for shotcrete is expressed as for volume of $1dm^3$.

Recipe for 0.5 water/cement ratio shotcrete-concrete type of specimens for 1dm^3 mixture;

- Cement: 300 g
- Water: 150 g
- Aggregate: 2015 g
- Admixture: 3 g

Recipe for all mold diameters were tabulated in Table 3.3 including the recipe for the mold prepared specially for static deformability and Brazilian disc tests.

Table 3.3. *Recipe for all diameters*

Ingredient (g)	*Specimen Diameter (mm)*					
	100	120	140	160	180	200
Cement	180	300	450	600	930	1260
Water	90	150	225	300	465	630
Admixture (plasticizer)	1.8	3	4.5	6	9.3	12.6
Aggregates	1209	2015	3023	4030	6247	8463
Total Weight (g)	1480.8	2468	3702.5	4936	7651.3	10365.6

3.3. Preparation of Shotcrete Samples

For the preparation of the shotcrete samples, UTEST mixer with almost 10 dm^3 capacity with adjustable speed was used, (Figure 3.7).

Figure 3.7. UTEST mixer

For the casting procedure, first, aggregate and then cement was put in the mixer and materials were mixed for 40 seconds at slow speed in dry condition. After that the liquid mixture was prepared including water and additive in it and poured into the dry mixture. All materials were mixed at slow speed in first 40 seconds and then mixed for 40 seconds in fast speed to achieve the homogeneity in the mixture. For each sample, attention was given for the consistency and the homogeneity of the mixture. As the shotcrete mixture design was set to the desired composition to get an early strength, it was poured into molds without wasting any time. Before starting the casting process, the molds were lubricated with motor oil in order to avoid difficulty in demolding process, (Figure 3.8).

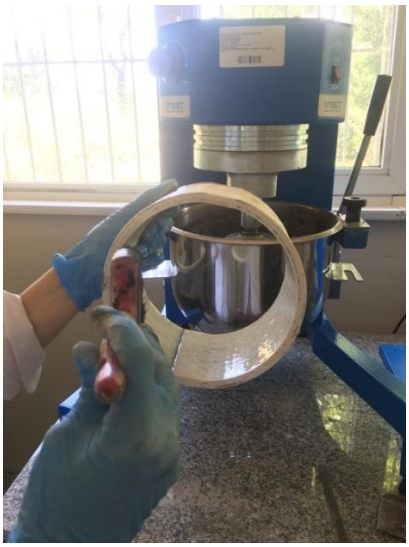

Figure 3.8. Lubrication process

During the casting procedure in order to avoid the air voids, vibration action was needed and this was performed manually by hand shaking of the mixture in the mold, (Figure 3.9).

Figure 3.9. Casted Shotcrete

Casting process is very important to obtain homogeneity. If the vibration process is not performed well or nor done at all, layering occurs according to the casting order. Homogeneity is disrupted by the formation of air voids in the upper side while the remaining parts are well-settled on the bottom side, (Figure 3.10).

Figure 3.10. Successful and unsuccessful casting products

CHAPTER 4

TESTING FOR MECHANICAL PROPERTIES OF SHOTCRETE

Preparation of the shotcrete specimens were the first step for the conventional testing work. Mix design were made according to the concrete-specification, performance, production and conformity standard namely EN 206. Casting process was carried out according to the specific geometry requirements of the particular tests. Cylindrical core samples which had length/diameter of L/D=2.5 and D=70 mm were prepared for static deformability tests. Cylindrical disc samples with thickness/diameter ratio of t/D=0.5 were prepared for Brazilian Disc tests from the molds illustrated in Figure 4.1.

Figure 4.1. Prepared molds for conventional testing

In Figure 4.2, shotcrete cores taken out of molds are shown. These are seven day-cured samples.

Figure 4.2. Cylindrical samples taken out of molds for static deformability test

For Static deformability tests and Brazilian Disc tests to obtain tensile strength, MTS 815 testing system was used in loading the specimens. Tests were conducted according to ISRM suggested procedures summarized given in Ulusay, 2007.

4.1. Static Deformability Test

Young's Modulus and Poisson's Ratio of shotcrete specimens were measured by the static deformability test that ISRM (1979) suggested. Tests were performed on five seven day-cured shotcrete specimens by using MTS 815 servo-controlled loading machine. Two MTS external displacement transducers (having 10 mm capacity with $\pm$0.005 mm accuracy) were mounted on the specimens to measure longitudinal strain.

An Epsilon circumferential extensometer was attached to measure lateral strain and to determine Poisson's Ratio, (Figure 4.3). To measure UCS results also, samples were kept under continuing compressive loading until failure.

Figure 4.3. Static Deformability Test Setup

During displacement-controlled testing, rate was kept constant at 0.005mm/s. Data acquisition frequency was kept as 8Hz. A typical test took about 15 minutes to be completed.

Results of static deformability tests are tabulated in Table 4.1.

Table 4.1. *Static deformability test results*

Specimen	*Length (mm)*	*Diameter (mm)*	*UCS (MPa)*	*Elastic Modulus (GPa)*	*Poisson's Ratio*
S_SD_1	177.5	71.4	25.9	20.03	0.18
S_SD_2	176.0	70.4	22.9	20.64	0.17
S_SD_3	173.5	71.0	29.7	20.96	0.18
S_SD_4	175.0	71.1	29.5	21.59	0.20
S_SD_5	175.0	70.4	24.8	23.81	0.18
Average	175.40	70.9	26.6±3.0	21.41±1.46	0.18±0.01

Average Uniaxial Compressive Strength (UCS) was calculated as 27 MPa. Elastic Modulus (E) and Poisson's Ratio (υ) were calculated as 21 GPa and 0.18, respectively.

A typical lateral strain- axial strain curve and stress-strain curve for shotcrete core specimen are shown in Table 4.4 and Table 4.5, respectively.

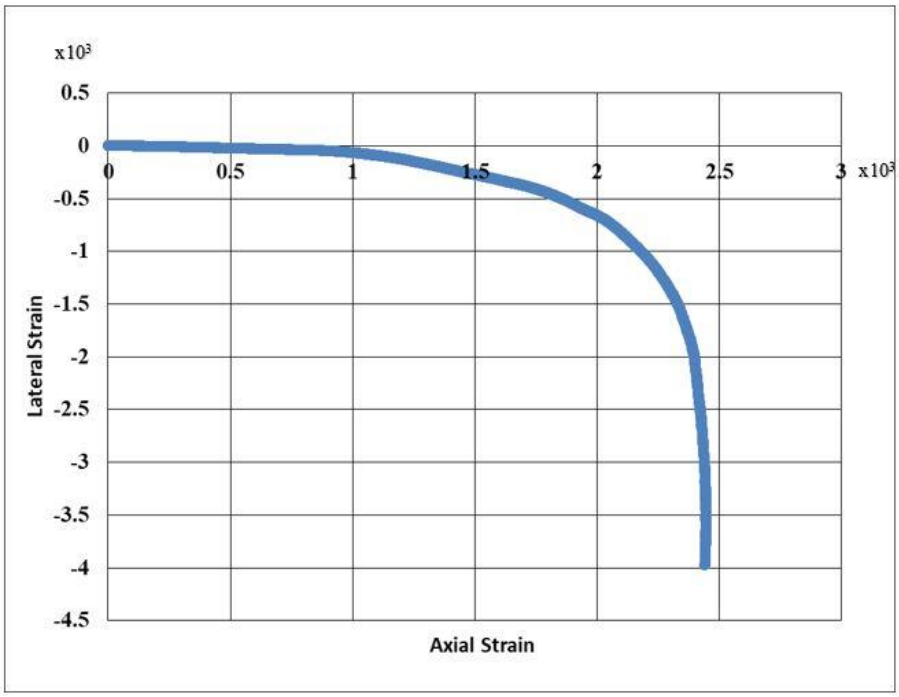

Figure 4.4. Lateral strain vs axial strain graph

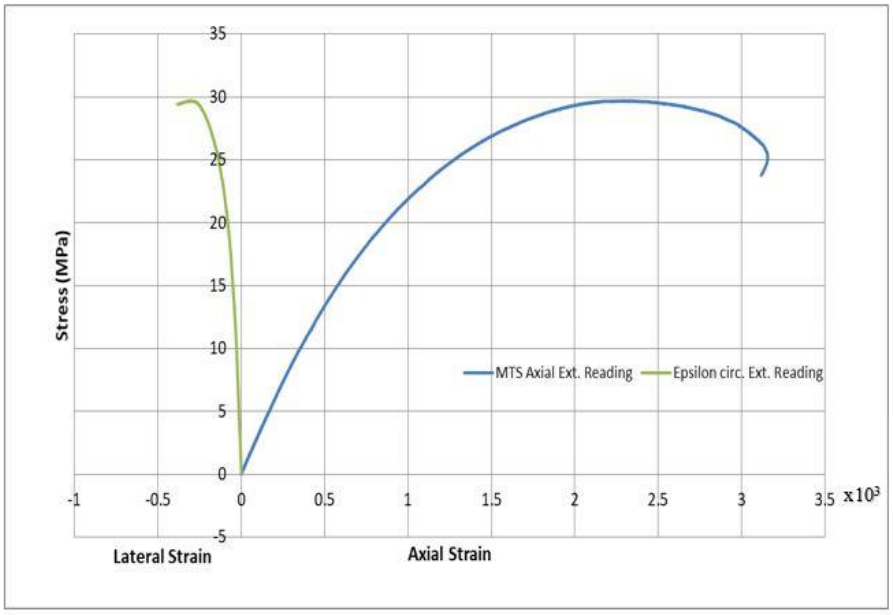

Figure 4.5. Stress vs lateral strain and axial strain graph

Test results presented in Table 4.1 are compared to some results reported in literature to assess the representative shotcrete quality of the mixture used here.

The pioneers of studying mechanical properties of early age shotcrete was Huber (Schutz, 2010). Including their experimental work and other researchers, changing the Young's modulus with time was compiled by Chang, 1994 in Figure 4.6. Elastic Modulus of seven day-cured shotcrete samples with the mixture in this work, *E*=21GPa, is compatible with the results in literature, (Figure 4.6).

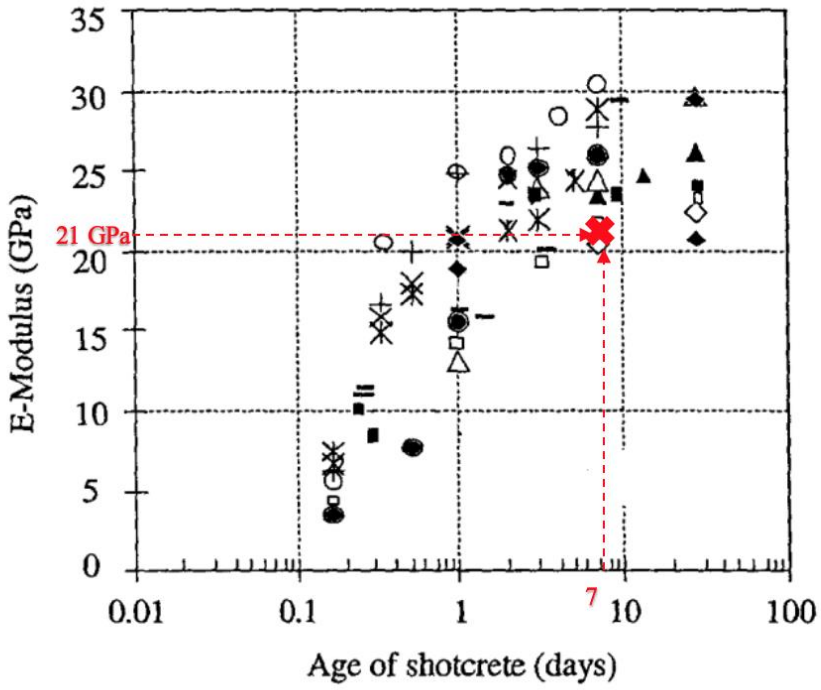

Figure 4.6. Development of Young's modulus with early age of shotcrete compiled from various research by (Chang, 1994)

In literature, the development of the UCS of early age concrete is available for both dry and wet mix shotcrete. In Figure 4.7, UCS results of various researchers are compiled by Chang, 1994. It is known that the mix design and the application

technique of the mixture have a great influence on the strength results. So, it is difficult to know the exact strength at a certain shotcrete age. It is necessary to validate the results with some preliminary experiments first. Uniaxial compressive strength of seven day-cured shotcrete samples with mixture recipe of this work yielded UCS=26.6 MPa. This is compatible with the results in literature, (Figure 4.7).

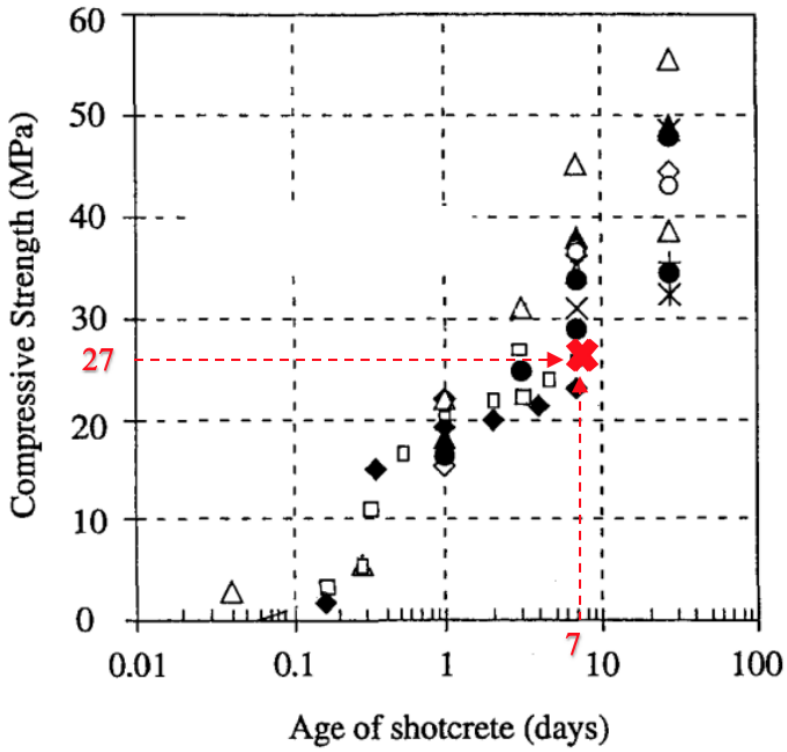

Figure 4.7. UCS results of various researchers compiled by Chang (1994)

In literature, the required 7 days strength of the shotcrete is approximately 25-30 MPa. According to the suggested concrete mixture properties of standard TS EN 206-1, concrete with a water/cement ratio of 0.5 is classified as C30 and its 28-day strength is around 30 MPa for a characteristic cylinder sample. The static deformability tests showed that the 28-day strength was gained in 7 days to a great extent, this supports

the compatibility of the mixture prepared here to represent the shotcrete which is aimed to provide high-early strength.

Experimental work related to the Poisson's ratio of early age shotcrete is limited. Neville (1981) stated that Poisson's ratio of concrete should be 0.11 to 0.21. According to Byfors (1980), development of the Poisson's ratio with time depended on the quantity and type of aggregates used for the mixture of shotcrete. Aydan, Sezaki and Kawamoto (1992) conducted experiments to identify the behavior of Poisson's ratio with time. Results of their experiments showed that after three days the Poisson's ratio of shotcrete was almost fixed at the value of 0.18. In Figure 4.8, corresponding test results are shown.

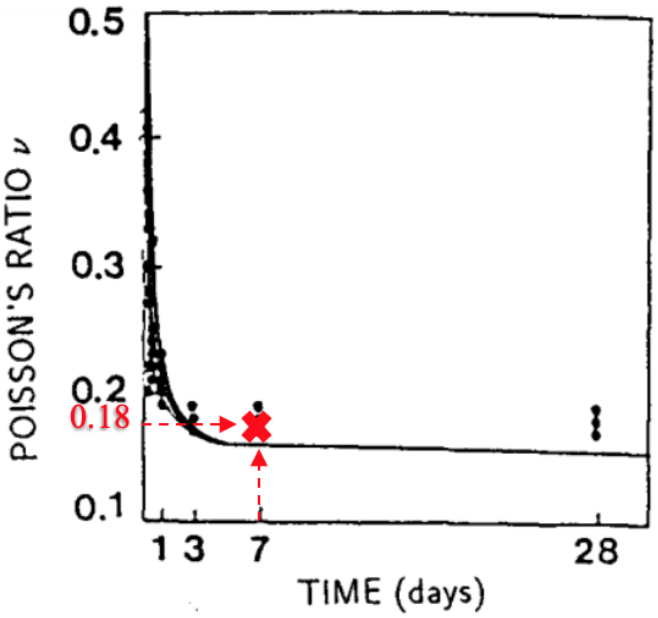

Figure 4.8. Variation of Poisson's ratio with time (Aydan et al., 1992)

Equation derive from this work is given as:

$$\upsilon = 0.18 + 0.32\, e^{-5.6t_c} \tag{4.1}$$

Where t_c is the curing time in days.

According to the static deformability test results, Poisson's ratio (υ=0.18) of seven day-cured samples here is compatible with the results of Aydan et al. (1992) as illustrated in Figure 4.8.

4.2. Indirect Tensile Strength Test (Brazilian Disc Test)

In order to calculate the tensile strength of rocks and concrete materials, The Brazilian Disc Test is preferred since it is a convenient and easy method. In 1978, it was officially proposed by the International Society for Rock Mechanics (ISRM) for the rock materials. Since concrete and rock have the same mechanics properties, their mechanical properties test method can be reference each other. Standardization of this test method for obtaining the tensile strength of concrete specimens by both the American Society for Testing and Materials (ASTM) and European Committee for Standardization.

Indirect Tensile Strength tests were conducted according to the ISRM (1979) suggested method. These tests were performed on five shotcrete specimens. MTS 815 servo-controlled loading machine was used with constant displacement rate of 0.005mm/s and 8Hz data acquisition frequency. In order to eliminate infinite compressive stress concentration at loading ends, jaws were used during the tests, (Figure 4.9).

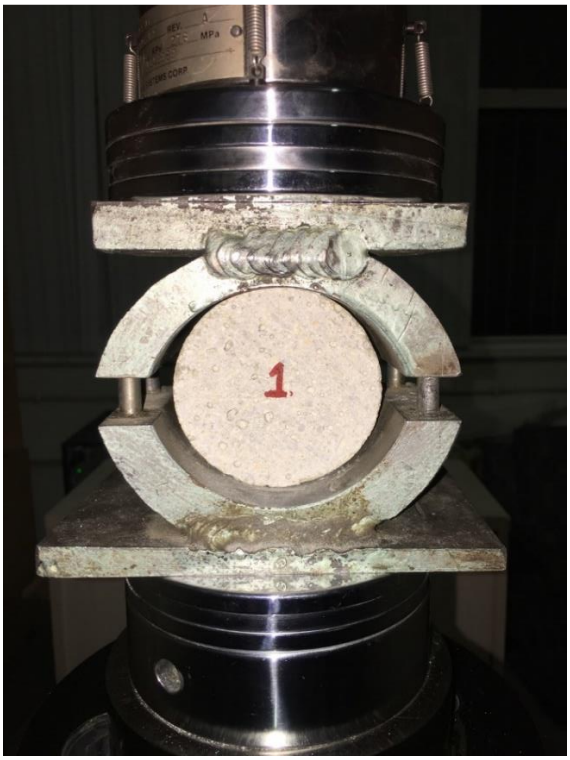

Figure 4.9. Brazilian Disc Test set up

In Table 4.2, Brazilian disc test results including peak loads and calculated tensile strengths were tabulated, (Table 4.2). Diameter and thickness of all Brazilian Disc specimens were around 71mm and 33 mm, respectively,

Table 4.2. *Brazilian disc test results*

Specimen Name	*Peak Load (kN)*	σ_t *(MPa)*
S_BD_1	16.60	4.30
S_BD_2	17.89	4.60
S_BD_3	15.59	4.03
S_BD_4	14.45	3.66
S_BD_5	10.50	3.53
Average	15.01±2.82	4.02±0.44

According to the test results, the average peak load was 15 kN, and the average tensile strength was calculated as $\sigma_t = 4$ MPa.

A typical Brazilian Disc Test sample namely S_BD_2 with central crack clearly visible is shown in Figure 4.10.

Figure 4.10. A typical Brazilian Disc sample with central crack clearly visible

A typical force-displacement curve of the same specimen namely S_BD_2 during the Indirect Tensile Strength Test with Brazilian Disc geometry is shown Figure 4.11.

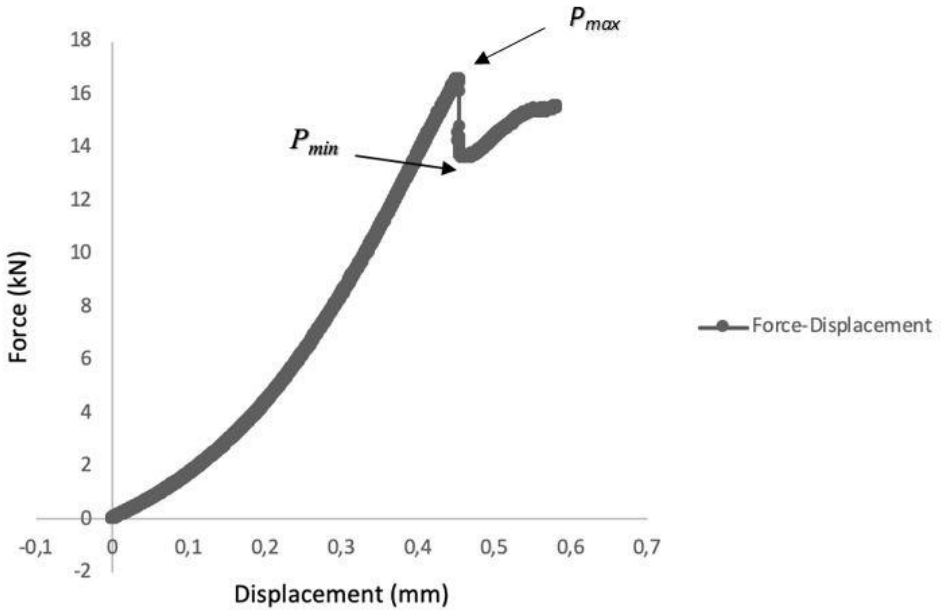

Figure 4.11. Force-Displacement curve of a Brazilian Disc test specimen

It should be noted that load-displacement curve has a local minimum load (P_{min}) point similar to those observed in FBD fracture toughness tests. This is believed to be caused by the use of jaws on the upper and lower loading boundaries of the discs. The use of jaws is distributing the line load and artificially imposing a loading angle which is estimated to be around 20°.

4.3. Tensile Strength Estimation from Brazilian Disc Tests

Cementitious materials like concrete generally exhibit high compressive strength, low tensile strength, and brittle failure under tensile loading. So, in order to avoid local collapse or failure on the structure because of this weakness and the consequences of the stress distributions related to it, determination of the tensile strength of concrete is as an important parameter related the structure design of concrete work. (Liang & Tao, 2014)

It is possible to estimate tensile strength from FBD tests. P_{max} values before the load drop can be used in some recently developed expressions to compute tensile strength. There are two well-known formulations for this purpose one is by Wang and the other one is Keles and Tutluoglu. These are explained below.

4.3.1. Wang's Approach

By assuming that the specimen is under uniformly distributed tensile stress, in 1953 Carneiro and Barcellos stated that the tensile strength can be expressed as:

$$\sigma_t = \frac{2P_{max}}{\pi Dt} \tag{4.2}$$

Where σ_T is tensile strength, P_{max} is the failure load of the specimen, D is the diameter of the specimen, t is the thickness of the specimen, (Japaridze, 2015).

However, the Brazilian test has the disadvantage that high shear stresses are induced close to the loading platens apart from the tensile stresses, which are developed in the disc. Wang and Xing (1999) introduced two mutually parallel planes to be used as surface loading application to the disc. Parallel loading ends are used to distribute the concentrated load. Griffith strength criterion (Griffith, 1924) was applied by Wang and Xing (1999); Wang and Wu (2004); Wang, Jia, Kou, Zhang and Lindqvist (2004a); Kaklis, Agioutantis, Sarris and Pateli (2005) and Keles & Tutluoglu (2011) to develop an analytical formula to calculate the tensile strength in Flattened Brazilian Disc.

According to the Griffith's theory to form cracks at the center in regular Brazilian test stress conditions required are;

$3\sigma_1 + \sigma_3 = 0$ Which yields, $\sigma_G = \frac{2P}{\pi Dt}$ (4.3)

Where σ_1 and σ_3 are maximum principle stress and minimum principle stress, respectively at the center. $\sigma_G = \sigma_\theta$ at the same time.

The failure occurs, $\sigma_t = \sigma_G$ where $\sigma_G$the equivalent stress is, and it was based on the principle stresses σ_1 maximum and σ_3 minimum and if the tensile stress is considered positive:

If $3\sigma_1 + \sigma_3 \geq 0$, then $\sigma_1 = \sigma_t$ (4.4)

If $3\sigma_1 + \sigma_3 < 0$, then $\sigma_G = \sigma_t = -\frac{(\sigma_1-\sigma_3)^2}{8(\sigma_1+\sigma_3)}$ (4.5)

In cylindrical system, the stress inside the sample can be expressed by σ_θ and σ_r .Wang et al. (2004) assumed that there is no shear stress in the direction of σ_θ and σ_r. Timoshenko and Goodier (1970) stated that when a Brazilian disc is subjected to a radial compressive force, the stress solution on the loading diameter can be expressed as:

$$\sigma_\theta = \frac{2P}{\pi Dt} \quad (4.6)$$

$$\sigma_r = \frac{2P}{\pi Dt}\left(1 - \frac{4D^2}{D^2-4r^2}\right) \quad (4.7)$$

When the Brazilian Disc is flattened loading angle comes into the problem. Wang et al. (2004) analyzed the crack initiation condition at the center and they stated that when *2α* is equal or larger than 20°, the primary tensile crack will initiate at the center and σ_G must reach a maximum value at that point.

Thus, for the Flattened Brazilian Disc at the center of disc;

$$\frac{(\sigma_r-\sigma_\theta)^2}{8(\sigma_r+\sigma_\theta)} = \sigma_G = \sigma_t \tag{4.8}$$

To determine σ_T, Wang et al. (2004) derived approximate formulae for σ_θ and σ_r and they assumed that the crack initiates at the specimen center, (Figure 4.12).

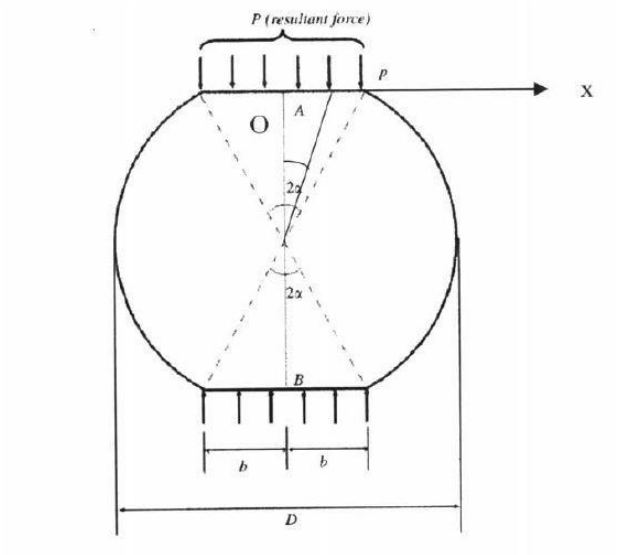

Figure 4.12. Specimen subjected to a uniform diametric loading (Wang et al.,2004)

$$\sigma_\theta = -\frac{2P}{\pi Dt}\, cos^3\alpha \frac{\alpha}{sin\alpha} \tag{4.9}$$

$$\sigma_r = \frac{2P}{\pi Dt}\left(cos^3\alpha + cos\alpha + \frac{sin\alpha}{\alpha}\right)\frac{\alpha}{sin\alpha} \tag{4.10}$$

Wang et al. (2004) expressed σ_t as:

$$\sigma_t = \frac{2P}{\pi Dt}\underbrace{\left[\frac{\left(2cos^3\alpha+cos\alpha+{sin\alpha}/{s}\right)^2}{8\left(cos\alpha+{sin\alpha}/{\alpha}\right)}\,\frac{\alpha}{sin\alpha}\right]}_{k} \tag{4.11}$$

So, In Flattened Brazilian Disc, a dimensionless correction coefficient *k* is joined to the equation to determine tensile strength formula.

$$\sigma_t = k\frac{2P_{max}}{\pi Dt} \tag{4.12}$$

In order to get tensile strength from flattened Brazilian disc geometry, correction coefficient *k* is calculated from Wang's equation for loading angle of 2α=22° (0.19 radian) and the result was equal to *k*= 0.9522.

By using k into the equation and also Flattened Brazilian disc specimens' failure loads (P_{max}), diameters (D), thickness (t), indirect tensile strength for changing diameters between 100 mm to 200mm at constant loading angle was calculated. In Table 4.3, calculated tensile strength and the geometric parameters of the specimens were tabulated. The tensile strength values computed as the average of five tests.

Table 4.3. *Average tensile strength from Wang's correction coefficient*

Group Name	D_{ave} (mm)	t_{ave} (mm)	$P_{max\ ave}$ (kN)	$\sigma_{t\,W}$ (MPa)
S100	99.0	66.62	24.98	2.30
S120	118.5	79.55	37.31	2.40
S140	138.4	83.99	45.77	2.39
S160	158.1	103.86	67.68	2.50
S180	174.4	122.38	102.92	2.87
S200	197.6	133.16	127.14	2.93

∗ $\sigma_{t\,W}$ represents calculated tensile strength by using Wang's correction coefficient.

The change in tensile strength with the specimen diameter is shown in Figure 4.13. Tensile strength increases with sample size following a fitted third degree polynomial. The lowest 2.30 for 100 mm size group and the highest is 2.87 for the 200 mm group.

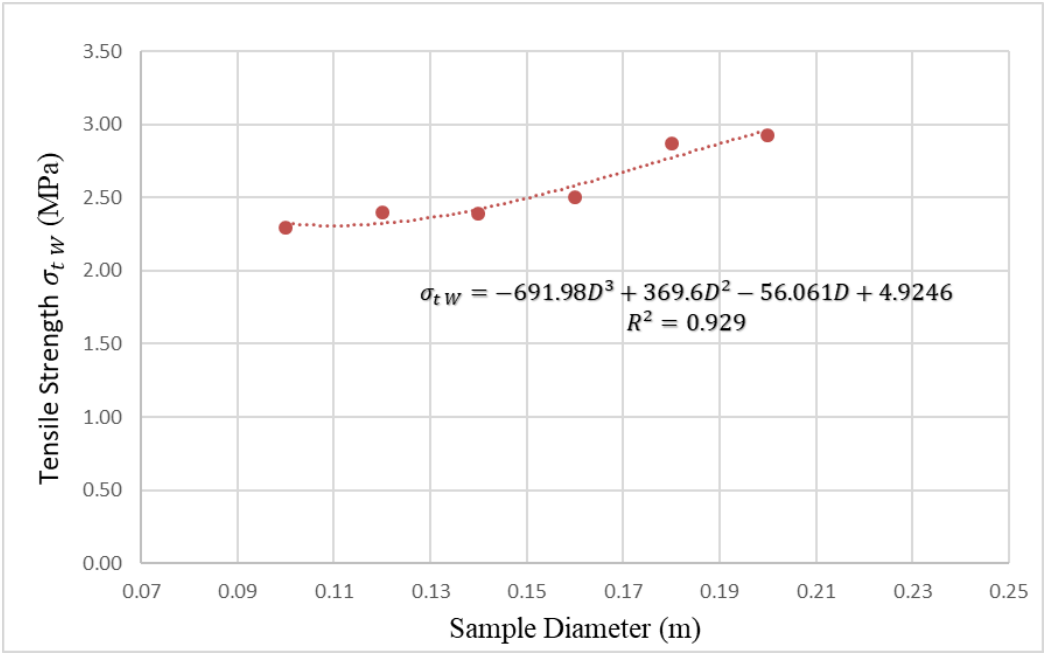

Figure 4.13. Tensile strength versus specimen diameter using Wang approach

A third-degree polynomial functional fit to the data points in Figure 4.13 is the best fit and this fitted function gives an estimated maximum at D=0.247m as the σ_t= 3.20 MPa. With conventional Brazilian disc tests using curved jaws, tensile strength of shotcrete was measured as 4.02 MPa. The ratio of the tensile strength obtained from the FBD test and the regular BD test is showed Figure 4.14.

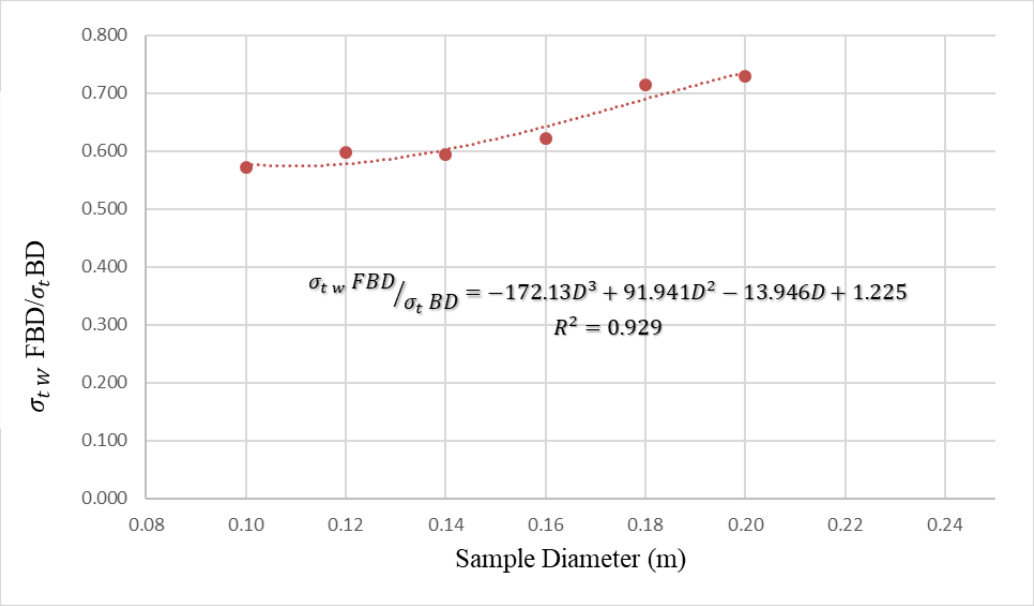

Figure 4.14. The ratio of the tensile strengths from FBD and BD with varying diameter

A third degree polynomial functional fit to the ratios in Figure 4.14 is the best fit and this fitted function gives an estimated maximum at D=0.247m as the ratio=0.796. According to the extreme points of the equation, when diameter increases, the ratio approach one but can't reach it. This can be explained as; the loading angle imposed by the curved jaws used in the regular Brazilian Disc Test is possibly lower than the loading angle of the Flattened Brazilian Disc Test (2α=22°).

4.3.2. Keles and Tutluoglu's Approach

Similar work conducted by Keles and Tutluoglu (2011). They stated that in their numerical analysis, when 2α was changed between 15° and 60° crack was initiate at the center and they determined the principle stresses to calculate tensile strength σ_t.

For each 2α dimensionless principle stresses at the center calculated and formulized as;

$$\bar{\sigma}_1 = \frac{\sigma_1}{2P/\pi Dt} = 1.08cos\alpha + 1.92 \quad (4.13)$$

$$\bar{\sigma}_3 = \frac{\sigma_3}{2P/\pi Dt} = -0.94cos\alpha - 0.04 \quad (4.14)$$

And substituting into equation:

$$\sigma_G = \sigma_t = -\frac{(\sigma_1-\sigma_3)^2}{8(\sigma_1+\sigma_3)}; \quad (4.15)$$

$$\bar{\sigma}_G = \frac{\sigma_G}{2P/\pi Dt} = 0.83cos\alpha + 0.15 \quad (4.16)$$

In fact, the coefficient defined by (Keles & Tutluoglu, 2011), $\bar{\sigma}_G$, is the same coefficient *k* as defined by Wang and Wu (2004) but different form of expression. According to the equation determined by Keles, *k* is now calculated as *k*=0.9648.

$$\sigma_T = \frac{2P}{\pi Dt}\underbrace{[0.83cos\alpha + 0.15]}_{\bar{\sigma}_G \text{ (Namely } k \text{ in Wang's approach)}} \quad (4.17)$$

This time by using Keles's correction coefficient into the equation and also Flattened Brazilian disc specimens' failure loads (P_{max}), diameters (*D*), thickness (*t*) indirect tensile strength for changing diameters between 100mm to 200mm at constant loading angle were calculated. In Table 4.4 calculated tensile strength and the parameters used were tabulated.

Table 4.4. *Tensile strength calculation from Keles and Tutluoglu's correction coefficient*

Group Name	D_{ave} (mm)	t_{ave} (mm)	P_{max} (kN)	$\sigma_{t\,K\,T}$ (MPa)
S100	99.0	66.62	24.98	2.33
S120	118.5	79.55	37.31	2.43
S140	138.4	83.99	45.77	2.42
S160	158.1	103.86	67.68	2.53
S180	174.4	122.38	102.92	2.91
S200	197.6	133.16	127.14	2.97

$*\ \sigma_{t\,K\,T}$ represents calculated tensile strength by using Keles and Tutluoglu's correction coefficient.

Calculated tensile strength according to the corresponding diameters were shown in Figure 4.15. Tensile strength increases with sample size following a fitted third degree polynomial. The lowest 2.33 MPa for 100 mm size group and the highest is 2.97 MPa for the 200 mm group.

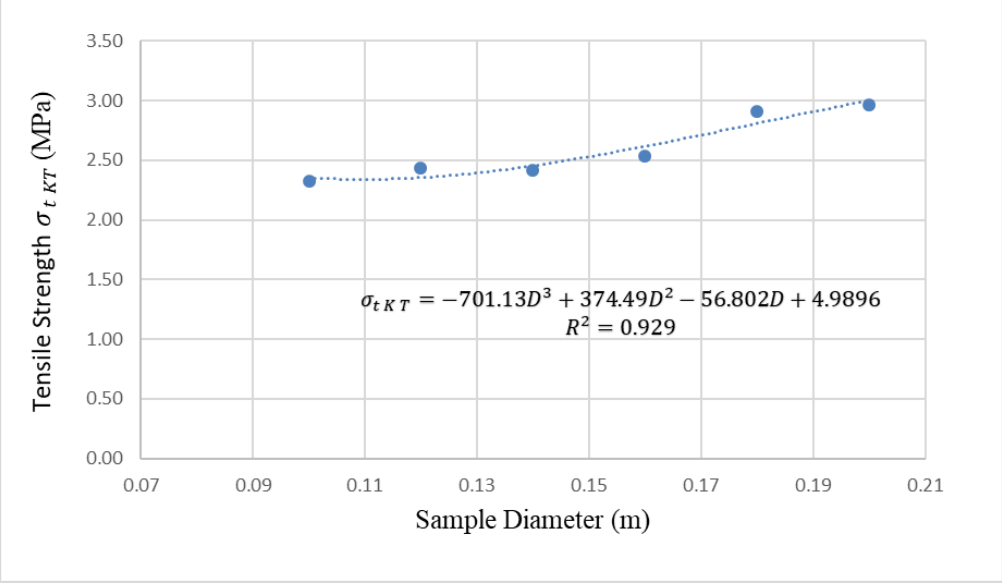

Figure 4.15. Tensile strength versus specimen diameter using Keles and Tutluoglu approach

A third-degree polynomial functional fit to the data points in Figure 4.15 is the best fit and this fitted function gives an estimated maximum at D=0.247 m as the ratio=3.24.

In Brazilian disc test experimentally calculated tensile strength of shotcrete was obtained as 4.02 MPa. Changing difference between obtained tensile strength from Brazilian Disc test and Fattened Brazilian disc test method according to the testing diameters were presented in Figure 4.16.

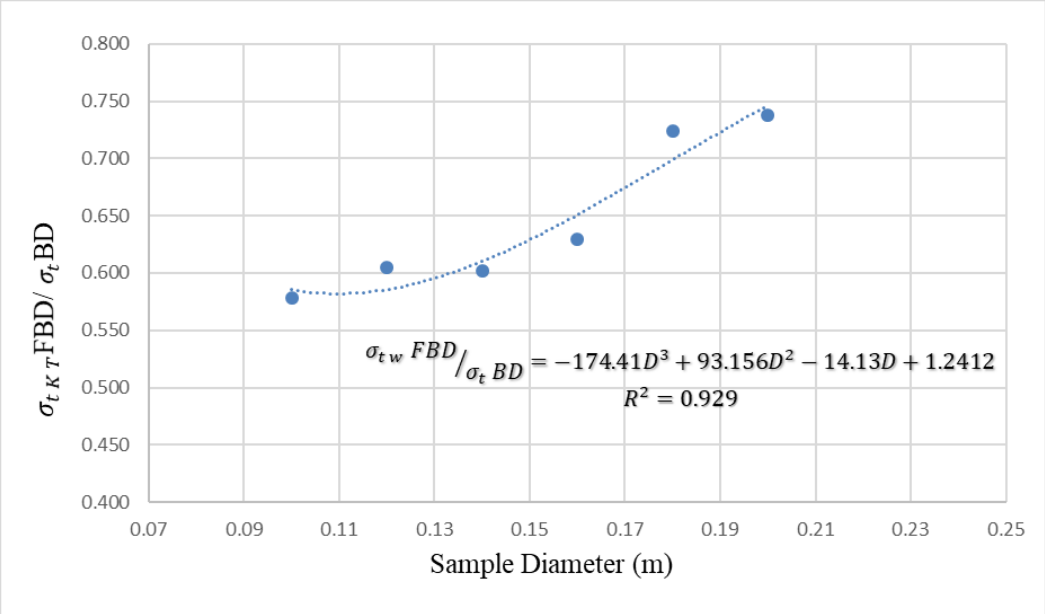

Figure 4.16. The ratio of tensile strengths from FBD and BD with related diameters

A third degree polynomial functional fit to the ratios in Figure 4.16 is the best fit and this fitted function gives an estimated maximum at *D*=0.247m as the ratio=0.806. According to the extreme points of the equation, when diameter increases, the ratio approach one but can't reach. This can be explained as; the loading angle imposed by the curved jaws used in the regular Brazilian Disc Test is possibly lower than the loading angle of the Flattened Brazilian Disc Test (*2α=22°*).

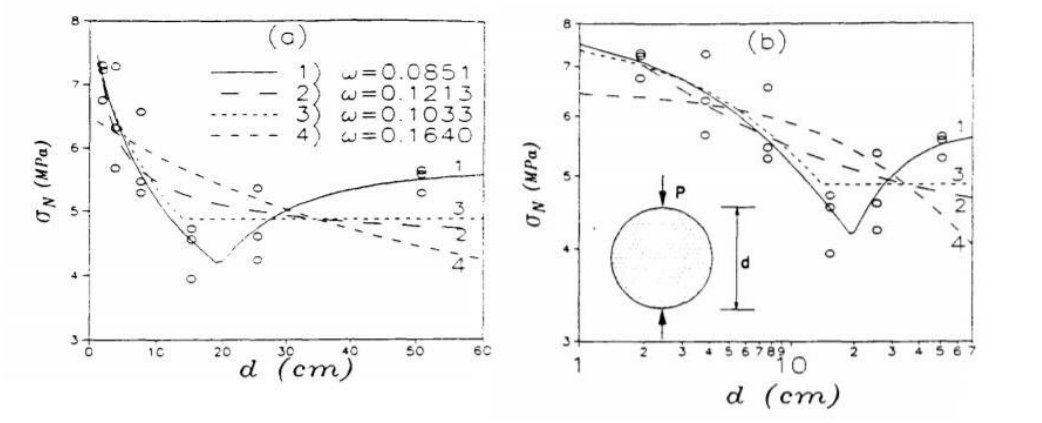

Figure 4.17. Bazant's size effect investigation (Bazant et al., 1991)

According to Bazant's study, for the small sizes, the Brazilian Disc strength decreased with increasing size until a certain diameter. As a result of experiments applied in concrete while diameter of the specimen changed from 10 to 508 mm, threshold diameter was around 200 mm. After that certain diameter, strength increased in direct proportion. In this study, for the shotcrete specimens that had 0.5 water/cement ratio, the increasing behavior of tensile with diameter was observed between 100 mm diameter and 200 mm diameter.

CHAPTER 5

MODE I FRACTURE TOUGHNESS TESTS

Understanding the fracture mechanism is crucial to solve many engineering problems. In order to be able to investigate the conditions of the fracture growth, measurement of toughness is required for fracture analysis.

When considered the other testing methods, Flattened Brazilian Disc Test method has been preferred testing method for determination of the fracture toughness due to the relatively easiness for the specimen preparation, compressive load application on the flat ends and also simple testing procedure.

For fracture toughness testing, FBD method with flat compressive load application boundaries is the simplest method among the other methods considering specimen preparation, loading type, and testing procedures.

Objective of this work is to study the variation fracture toughness of shotcrete with specimen size and curing time. 30 experiments were performed to investigate the size effect on mode I fracture toughness and 21 experiments were performed to investigate the effect of curing time on mode I fracture toughness.

5.1. Fracture Toughness Testing Work

Before conducting the experiments, dimensions of the specimens were measured since all of the specimens differed slightly due to the imperfections of casting process. Shotcrete specimens were prepared with six different diameters which are 100 mm, 120 mm, 140 mm, 160 mm, 180 mm, and 200 mm.

In the second part of the experimental program effect of curing time on K_{IC} was investigated by varying the curing time t_c as 1 day, 2 days, 3 days, 5 days and 7 days. For a specific diameter of 160 mm, they were grouped depending on the five curing time levels in order to investigate the curing time effect on the fracture toughness of the shotcrete.

During all the tests, specimens were loaded using the MTS 815 servo-controlled loading machine with a constant displacement rate of 0.0004 mm/s and 8Hz data acquisition frequency.

In all fracture toughness testing work, loading angle 2α of the specimens is kept nearly as 22° which corresponds to flattened end/radius ratio of L/R=0.19.

When the experiment started, load gradually increased up to a maximum point, P_{max} at which an unstable crack initiated at the center of the specimen. At this stage, a sudden drop in load from P_{max} to local minimum, P_{min} occurred. Local minimum point, P_{min} was the turning point between unstable and to stable crack propagation. Stable crack growth started at the P_{min}. At this load, experimental critical crack length (a_{ce}) was measured. Close-up photos were taken in order to measure the critical crack lengths through Adobe Photoshop Program. The purpose was the comparison between experimental and numeric critical crack lengths. Specimen dimensions, P_{max}, P_{min} and experimental critical crack length were recorded for each test. The average of the recorded P_{max} values of each testing group was used for the tensile strength computations from FBD geometry with the help of two researcher's approaches.

A typical force-displacement curve related the Mode I Fracture Toughness Test with Flattened Brazilian Disc geometry is shown Figure 5.1.

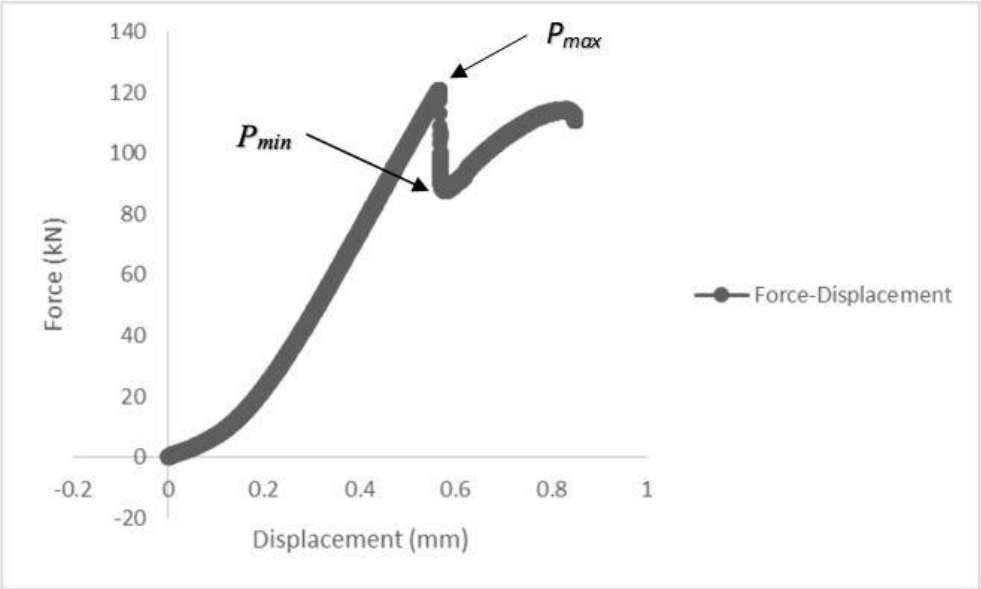

Figure 5.1. A typical Force-Displacement curve of a Flattened Brazilian Disc test

According to the Wang and Wu (2004), the last discussion was about the validity of a FBD test. To be valid, the failure must be caused by the development of the primary crack, not the secondary ones. In a typical force displacement graph of the test results, when the load reaches the maximum (P_{max}) at the end of elastic deformation, and local minimum load (P_{min}) is reached when the primary cracks propagate till its critical length. Second increase in load must be observed to progress up to a load level which is supposed to be lower than P_{max}. The load increase in the second rise should never be greater than the first one, (Figure 5.1). Otherwise, the secondary cracks would play role in the failure and disc may be split into more pieces than it should be. This criterion was taken into consideration in all the testing work here.

A typical experimental critical crack length measurement related the Mode I Fracture Toughness Test with Flattened Brazilian Disc geometry is shown Figure 5.2.

Figure 5.2. A typical experimental critical crack length measurement

5.2. Computation for Fracture Toughness

For determining the mode I fracture toughness value for FBD testing method was calculated by using the Eq. 5.1 (Wang and Xing, 1999).

$$K_{Ic} = \frac{Y_{Imax}\, P_{min}}{t\sqrt{R}} \tag{5.1}$$

Where,

K_{Ic} : Fracture toughness (MPa$\sqrt{m}$)

P_{min} : Minimum local load (kN)

R : Specimen Radius (mm)

t : Specimen thickness (mm)

Y_{Imax} : Maximum dimensionless stress intensity factor (SIF) which is determined from numerical modeling.

Özdoğan (2017) developed a formula based on numerical analysis for determination of the critical crack length and the maximum dimensionless stress intensity factor at the onset of stable crack propagation or at the local minimum points depending on the loading angle. The J-integral approach was used for K_I computation in ABAQUS models.

Özdoğan followed a procedure that numerical FBD models were developed based on different dimensionless crack lengths (*a/R*) for each loading angle in order to find K_I values. The K_I values obtained from these models were converted into Y_I values by using the equation described by Wang and Xing (1999) as follows;

$$Y_I = \frac{K_I\, t\, \sqrt{R}}{P} \tag{5.2}$$

Between the range of loading angles 2° to 50°, numerical models of FBD were created based on different dimensionless crack lengths (*a/R*) in order to find mode I stress intensity factor (K_I) values. K_I values from the ABAQUS were used to calculate dimensionless stress intensity factor Y_I by Wang's formula. For each loading angle, *a/R* depended Y_I values were fitted graphs and Y_{Imax} values were generated by using statistical program packages. There were two equations generated; one was for finding Y_{Imax} values for each loading angle, (Özdoğan,2017):

$$Y_{Imax} = e^{\frac{1.6897+1.4854*(2\alpha)-62.3324*(2\alpha)^2}{1+31.7876*(2\alpha)+4.3693*(2\alpha)^2-2.1703*(2\alpha)^3}} \tag{5.3}$$

In the Eq. (5.3), Y_{Imax} represents maximum mode I dimensionless stress intensity factor (SIF) and 2α is loading angle in radians.

The second equation fitted on a_{cn}/R vs loading angle (2α) plot and generated a formula given in Eq. (5.4), (Özdoğan,2017):

$$a_{cn}/_{R} = 0.9974 * e^{-0.844*(2\alpha)} \quad (5.4)$$

In Eq. (5.4), loading angle, 2α is in radians.

According to Özdoğan (2017), these equations are valid and reliable for loading angles (2α) between 2° to 50°. However, while working on the Brazilian test theoretically, experimentally and numerically the validity of such tests needed to be investigated by paying attention to the crack initiation location. In literature, there were many investigations of the stress analyses for crack initiation location on Brazilian disc such as studies of Wang and Xing (1999); Wang and Wu (2004); Wang et al. (2004a); Kaklis et al. (2005) and Keles and Tutluoglu (2011). By using boundary element method, critical 2α was found to be greater than 19.5° (Wang and Xing 1999). This angle was found to be equal to 20° and Wang and Wu (2004) and Wang et al. (2004a), reported that the upper limit for this angle should not be too large. It was 15° in Kaklis et al. (2005) while it was between 15° to 60° in Keles and Tutluoglu (2011) by finite element methods.

Considering the suggestions in the literature and practicality of constructing molds, loading angle 2α was selected as 22° in current work, so that crack is expected to initiate and develop along the central path.

According to the selected loading angle 2α=22° which was 0.384 in radians corresponding Y_{Imax} was calculated mathematically as 0.604 for all diameters.

After finding Y_{Imax} for tested specimens numerically, for determining the mode I fracture toughness value for FBD testing method was calculated by using the Eq. (5.5)

$$K_{Ic} = \frac{Y_{Imax} P_{min}}{t \sqrt{R}} \tag{5.5}$$

For loading angle of 22° (0.384 in radians), corresponding a_{cn}/R was calculated mathematically as 0.721. For each sample diameter, the measured critical crack length at the local minimum point and numerically computed critical crack length for 2α=22° loading angle were compared in proceeding sections.

5.3. Investigation of Size Effect on Mode I Fracture Toughness of Shotcrete

Size effect is an important characteristic of the fracture behavior in quasi brittle materials such as concretes, rocks and ceramics. The strength and toughness of specimens or structures made of these materials depends on their size thus especially in the field of engineering applications, using fracture mechanics is the most challenging concept to investigate.

The size effect was described as the geometrically similar structures have different nominal stress with respect to varying sizes. Perdikaris, Calomino and Chudnovsky (1986) indicated that the observed size effect on the fracture toughness in the static and fatigue tests suggested that G_{IC} and K_{IC} cannot be considered to be material parameters, (Perdikaris, 1986).

Bazant et al. (1991) conducted experimental studies to investigate the size effect on Brazilian concrete specimens and he deduced that up to a certain critical diameter, size effect existed and crack length expanded.

In this study while working with specimen size, loading angle kept constant at 22° in order to observe the effect of different diameters on mode I fracture toughness. Shotcrete-concrete FBD testing specimens were prepared according to six different diameters which are 100 mm, 120 mm, 140 mm, 160 mm, 180 mm, and 200 mm. A total of 30 experiments were performed to investigate the size effect on mode I fracture toughness; that is approximately 5 experiments of each diameter group.

Test specimens' name code was explained below Figure 5.3. Code includes type of specimen, sample diameter (*D*), and the number of testing specimen, (Figure 5.3).

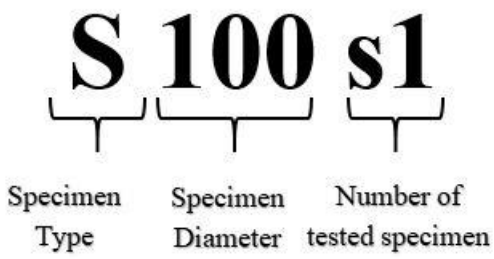

Figure 5.3. Name code of tested FBD specimens

A typical Flattened Brazilian Disc Test geometry with generalized dimensions was shown in Figure 5.4 .

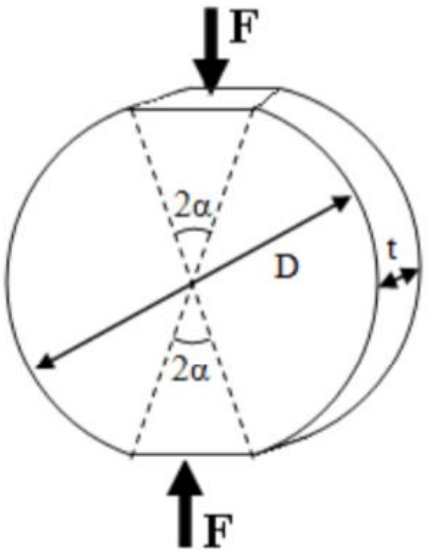

Figure 5.4. FBD specimen geometry

General geometric entities of the diameter-based specimen groups related to their codes are given in Table 5.1.

Table 5.1. *Dimensions of shotcrete specimens*

Name	*D (mm)*	*2L(mm)*	*t (mm)*
S100	100	19	67
S120	120	23	80
S140	140	27	84
S160	160	31	104
S180	180	34	122
S200	200	38	133

5.3.1. Tables for Individual Fracture Toughness Test Results

Individual test results are presented in Tables 5.2 to 5.7 for the seven day-cured samples of 100 mm, 120 mm, 140 mm, 160 mm, 180 mm and 200 mm diameter groups.

Table 5.2. *t, $2a_{ce}$, a_{ce}/R, P_{min}, and K_{IC} values of FBD specimens having 100 mm diameter*

Name	*t(mm)*	*$2a_{ce}$(mm)*	*a_{ce}/R*	*P_{min}(kN)*	$K_{IC}(MPa\sqrt{m})$
S100_s1	66.1	71.3	0.720	24.63	1.01
S100_s2	66.0	71.6	0.723	25.03	1.03
S100_s3	71.9	71.5	0.723	20.15	0.76
S100_s4	67.2	71.6	0.723	21.98	0.89
S100_s5	62.1	71.5	0.722	21.94	0.96
Average		71.5±0.12		22.75±2.05	0.93±0.11

Table 5.3. *t, $2a_{ce}$, a_{ce}/R, P_{min}, and K_{IC} values of FBD specimens having 120 mm diameter*

Name	*t(mm)*	*$2a_{ce}$(mm)*	*a_{ce}/R*	*P_{min}(kN)*	$K_{IC}(MPa\sqrt{m})$
S120_s1	80.5	84.4	0.712	32.34	1.00
S120_s2	81.7	84.8	0.716	32.64	0.99
S120_s3	79.2	85.1	0.716	28.13	0.88
S120_s4	79.1	86.3	0.730	34.43	1.08
S120_s5	79.1	86.5	0.730	27.40	0.86
S120_s6	77.7	86.3	0.730	33.71	1.08
Average		85.6±0.91		31.44±2.95	0.98±0.09

Table 5.4. *t, $2a_{ce}$, a_{ce}/R, P_{min}, and K_{IC} values of FBD specimens having 140 mm diameter*

Name	*t(mm)*	*$2a_{ce}$(mm)*	*a_{ce}/R*	*P_{min}(kN)*	$K_{IC}(MPa\sqrt{m})$
S140_s1	77.9	100.6	0.727	37.14	1.09
S140_s2	80.2	102.2	0.736	38.65	1.11
S140_s3	94.3	101.9	0.738	47.47	1.16
S140_s4	78.5	99.5	0.719	32.65	0.96
S140_s5	89.1	101.0	0.731	38.99	1.01
Average		101.0±1.08		38.98±5.38	1.06±0.08

Table 5.5. *t, $2a_{ce}$, a_{ce}/R, P_{min}, and K_{IC} values of FBD specimens having 160 mm diameter*

Name	*t(mm)*	*$2a_{ce}$(mm)*	*a_{ce}/R*	*P_{min}(kN)*	$K_{IC}(MPa\sqrt{m})$
S160_s1	104.3	114.1	0.722	57.85	1.19
S160_s2	105.4	115.7	0.732	57.04	1.16
S160_s3	104.9	114.4	0.722	56.28	1.15
S160_s4	102.0	116.0	0.734	57.96	1.22
S160_s5	102.8	115.5	0.729	56.54	1.18
Average		115.1±0.84		57.13±0.76	1.18±0.03

Table 5.6. *t, $2a_{ce}$, a_{ce}/R, P_{min}, and K_{IC} values of FBD specimens having 180 mm diameter*

Name	*t(mm)*	*$2a_{ce}$(mm)*	*a_{ce}/R*	*P_{min}(kN)*	$K_{IC}(MPa\sqrt{m})$
S180_s1	121.7	130.8	0.743	85.69	1.43
S180_s2	124.1	129.2	0.726	88.00	1.44
S180_s3	123.4	131.4	0.739	88.83	1.46
S180_s4	123.1	131.5	0.739	88.71	1.46
S180_s5	119.6	131.2	0.741	81.20	1.38
Average		130.8±0.94		86.49±3.21	1.43±0.03

Table 5.7. *t, $2a_{ce}$, a_{ce}/R, P_{min}, and K_{IC} values of FBD specimens having 200 mm diameter*

Name	*t(mm)*	*$2a_{ce}$(mm)*	*a_{ce}/R*	*P_{min}(kN)*	$K_{IC}(MPa\sqrt{m})$
S200_s1	136.7	150.4	0.760	114.11	1.60
S200_s2	132.0	147.8	0.748	97.18	1.42
S200_s3	131.9	149.3	0.756	95.81	1.40
S200_s4	132.0	148.4	0.751	99.28	1.45
Average		149.0±1.13		101.60±8.46	1.46±0.09

K_{IC} is seen to increase significantly with specimen size. The increase in K_{IC} is almost 57% from 100 mm to 200 mm.

5.4. Investigation of Curing Time on Mode I Fracture Toughness of Shotcrete/Concrete Type of Specimen

In order to investigate the effects of curing time on fracture toughness of shotcrete-concrete type of specimen, 1 day, 2 days, 3 days, 5 days and 7 days air-cured shotcrete specimens were tested. Diameter and the loading angle was kept constant at 160 mm and 22°, respectively. A total of 21 experiment results were investigated to analyze the effect of curing time on mode I fracture toughness of shotcrete specimens. For each curing time investigation group, four tests were conducted.

It can be discussed that the crack propagation mechanism developed for mature concrete can be applied to the early aged concrete (Hillerborg et al., 1976; Bazant, 2002). However, process of propagation cannot be fully explained by using this approach. (Dao, Dux, and Morris, 2014).

Test specimens' name code was explained below Figure 5.3. Code includes type of specimen, sample diameter (*D*), curing time (day) and the number of testing specimen, (Figure 5.5).

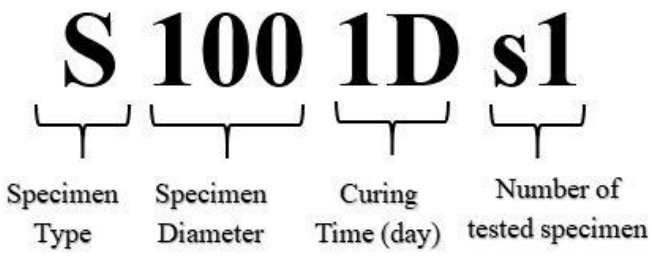

Figure 5.5. Name code of tested FBD specimens

5.4.1. Tables of Results for Curing Time Investigation

In Tables 5.8 to 5.12, K_{IC} values are listed for 1 day, 2 day, 3 day, 5 day and 7 day air-cured of 160 mm diameter samples. For seven-day cured 160 mm diameter group, additional result was available from the size effect study.

Table 5.8. *t, P_{min}, and K_{IC} values of FBD specimens having 160 mm diameter with 1 day cured*

Name	*t(mm)*	$P_{min}(kN)$	$K_{IC}(MPa\sqrt{m})$
S160-1D-s1	103.8	33.20	0.69
S160-1D-s2	104.7	29.42	0.60
S160-1D-s3	104.3	31.38	0.65
S1601-D-s5	104.0	33.29	0.69
Average		31.82±1.83	0.66±0.04

Table 5.9. *t, P_{min}, and K_{IC} values of FBD specimens having 160 mm diameter with 2 days cured*

Name	*t(mm)*	$P_{min}(kN)$	$K_{IC}(MPa\sqrt{m})$
S160-2D-s1	104.0	37.28	0.77
S160-2D-s2	105.0	42.28	0.87
S160-2D-s3	104.4	36.36	0.75
S160-2D-s4	103.0	38.85	0.81
Average		38.69±2.60	0.80±0.05

Table 5.10. *t, P_{min}, and K_{IC} values of FBD specimens having 160 mm diameter with 3 days cured*

Name	*t(mm)*	$P_{min}(kN)$	$K_{IC}(MPa\sqrt{m})$
S160-3D-s1	103.9	38.60	0.80
S160-3D-s2	104.5	39.94	0.82
S160-3D-s3	103.8	42.28	0.88
S160-3D-s4	104.0	40.80	0.84
Average		40.41±1.54	0.83±0.03

Table 5.11. *t, P_{min}, and K_{IC} values of FBD specimens having 160 mm diameter with 5 days cured*

Name	*t(mm)*	P_{min}*(kN)*	$K_{IC}(MPa\sqrt{m})$
S160-5D-s1	105.0	56.51	1.15
S160-5D-s2	104.8	55.83	1.14
S160-5D-s3	104.0	48.67	1.01
S160-5D-s3	104.0	51.12	1.06
Average		53.03±3.77	1.09±0.07

Table 5.12. *t, P_{min}, and K_{IC} values of FBD specimens having 160 mm diameter with 7 days cured*

Name	*t(mm)*	*Pmin(kN)*	$K_{IC}(MPa\sqrt{m})$
S160-7D-s1	104.3	57.85	1.19
S160-7D-s2	105.4	57.04	1.16
S160-7D-s3	104.9	56.28	1.15
S160-7D-s4	102.0	57.96	1.22
S160-7D-s5	102.8	56.54	1.18
Average		57.13±0.76	1.18±0.03

K_{IC} is seen to increase significantly with curing time, especially at early curing stages. The increase in K_{IC} is almost 100% from one day to seven-day curing states.

CHAPTER 6

EXPERIMENTAL RESULTS AND DISCUSSION

Tests with Flattened Brazilian Disc geometry were carried out to detect the presence of size effect on mode I fracture toughness. During the tests critical crack lengths at which a stable crack starts to propagate were measured.

30 shotcrete specimens, curing time of seven days, were subjected to mode I fracture toughness test with varying diameters between 100 mm and 200 mm. This was done to monitor the effect of changing diameter or in other words specimen size effect on mode I fracture toughness. For each diameter group around five tests were conducted and one average fracture toughness was evaluated. Loading angle was kept constant at 22°.

In the ground control system, shotcrete is used to provide temporary surface control for local stability before the primary support is installed. Because the shotcrete must become self-supporting before miners and equipment can work safely underneath, the curing characteristics of the shotcrete are critical to the speed of the mining cycle. Surface defects and cracks may already exist or may develop in shotcrete at ages from several hours after casting. These cracks may affect the service life of shotcrete by propagating or they can cause much damage either economically or even worst fatal. Therefore, it is important to understand the underlying fracture mechanism changing with curing time.

Early-age developed 21 shotcrete specimens with constant diameter D=160 mm and constant loading angle (2a=22°) with 1 day, 2 days, 3 days, 5 days and 7 days cured shotcrete specimens were subjected to mode I fracture toughness test in order to determine the effect of curing time on mode I fracture toughness. For each curing time group around four tests were conducted and one fracture toughness was evaluated.

6.1. Tables of Results for Size Effect Investigation

Seven-day air-cured shotcrete specimens with Uniaxial Compressive Strength (UCS) of 27 MPa, Elastic Modulus (E) of 21 GPa, and Poisson's Ratio ($\boldsymbol{v}$) of 0.18 results in fracture toughness values ranging between 0.93-1.46 MPa$\sqrt{m}$ for varying diameters. In Table5.1, diameter of specimens, average local minimum loads (P_{min}), average critical crack lengths ($2a_{ce}$) and mode I fracture toughness values (K_{IC}) were listed for 7 day cured shotcrete specimens. Overall test results are tabulated in Table 6.1 and individual group averages are presented in Table 6.2.

Table 6.1. *All test results for investigation of size effect on the fracture toughness*

Name	$P_{min}(kN)$	$2a_{ce}(mm)$	a_{ce}/R	$K_{IC}\,(MPa\sqrt{m})$
S100_s1	24.63	71.30	0.72	1.01
S100_s2	25.03	71.60	0.72	1.03
S100_s3	20.15	71.50	0.72	0.76
S100_s4	21.98	71.60	0.72	0.89
S100_s5	21.94	71.50	0.72	0.96
S120_s1	32.34	84.40	0.71	1.00
S120_s2	32.64	84.80	0.72	0.99
S120_s3	28.13	85.10	0.72	0.88
S120_s5	34.43	86.30	0.73	1.08
S120_s4	27.40	86.50	0.73	0.86
S120_s6	33.71	86.30	0.73	1.08
S140_s1	37.14	100.60	0.73	1.09
S140_s2	38.65	102.20	0.74	1.11
S140_s3	47.47	101.90	0.74	1.16
S140_s4	32.65	99.50	0.72	0.96
S140_s5	38.99	101.00	0.73	1.01
S160_s1	57.85	114.10	0.72	1.19
S160_s2	57.04	115.70	0.73	1.16
S160_s3	56.28	114.40	0.72	1.15
S160_s5	57.96	116.00	0.73	1.22
S160_s6	56.54	115.50	0.73	1.18
S180_s1	85.69	130.80	0.74	1.43
S180_s3	88.00	129.20	0.73	1.44
S180_s4	88.83	131.40	0.74	1.46
S180_s5	88.71	131.50	0.74	1.46
S180_s6	81.20	131.20	0.74	1.38
S200_s1	114.11	150.40	0.76	1.60
S200_s2	97.18	147.80	0.75	1.42
S200_s3	95.81	149.30	0.76	1.40
S200_s4	99.28	148.40	0.75	1.45
Average	54.06±28.70		0.73±0.01	1.16±0.22

Table 6.2. *Average fracture toughness results of FBD specimens with corresponding diameters*

D(mm)	$P_{min\ ave}$ *(kN)*	$2a_{ce\ ave}$*(mm)*	$a_{ce\ ave}/R$	K_{ICavg}+*STD(MPa*$\sqrt{m}$*)*
100	22.75	71.50	0.72	0.93±0.11
120	31.44	85.57	0.72	0.98±0.11
140	38.98	101.04	0.73	1.06±0.09
160	57.13	115.14	0.73	1.18±0.07
180	86.49	130.82	0.74	1.43±0.04
200	101.60	148.98	0.75	1.46±0.09
Average	56.40±31.65		0.73±0.01	1.18±0.23

For a better visualization, K_{IC} values and $K_{IC\ avg}$ values of FBD specimens having constant loading angle ($2\alpha = 22°$) and various diameters are represented in Figure 6.1. Red dots symbolize average values related to specimen diameter whereas the blue dots stand for individual results, (Figure 6.1). Curve is fitted to the average results of each diameter group. Fracture toughness increases with sample size following a fitted third degree polynomial. The lowest 0.93 MPa$\sqrt{m}$ for 100 mm size group and the highest is 1.46 MPa$\sqrt{m}$ for the 200 mm group. The average fracture toughness increase is about 57% according to the average of the diameter group.

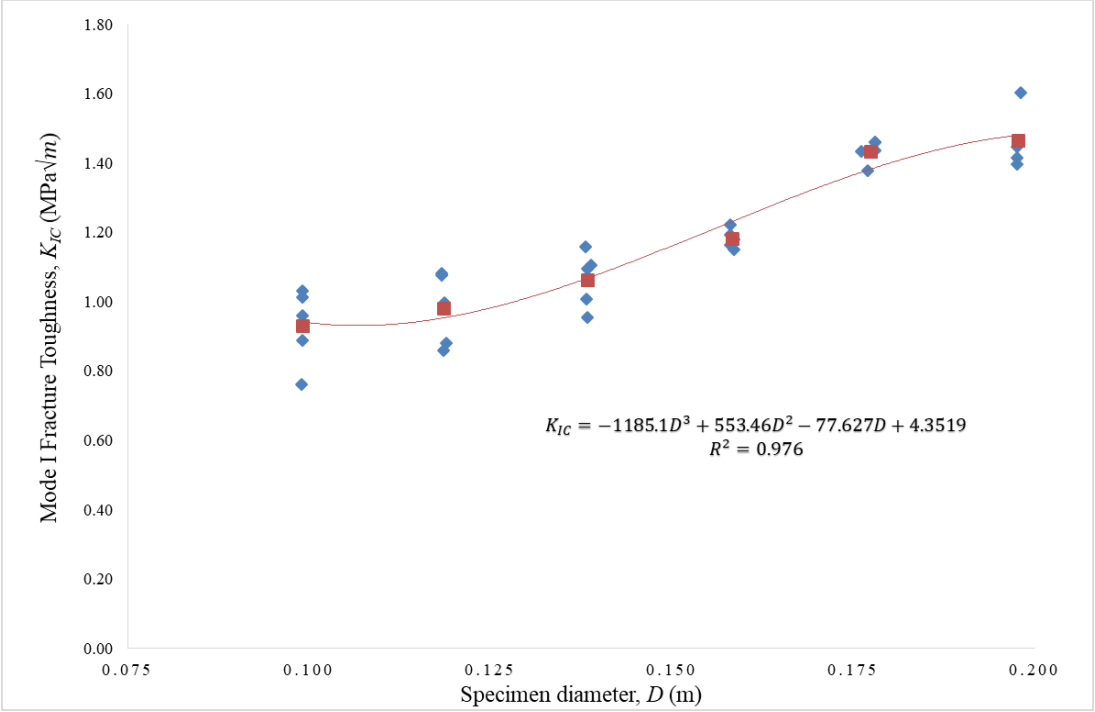

Figure 6.1. K_{IC} values of FBD tested specimens having various diameters

A third-degree polynomial functional fit to the ratios in Figure 6.1 is the best fit and this fitted function gives an estimated minimum at D=0.107 m as K_{IC}=0.93 MPa$\sqrt{m}$ and maximum at D=0.205 m as K_{IC}=1.49 MPa$\sqrt{m}$. According to the extreme points of the equation, it is predicted that after the diameter increases up to around 205 mm, the increase in fracture toughness would not continue.

The size effect phenomenon can be clearly observed from Figure 6.1. Mode I fracture toughness values increase with the specimen diameter. $K_{IC\,avg}$ for the largest diameter group (D=200 mm) is about 1.57 times higher than the $K_{IC\,avg}$ of the smallest diameter group (D=100 mm). As the specimen gets larger, the crack tip gets further from the compressively loaded area. In this case, the size of the fracture process zone is relatively small compared to the specimen dimension, this can explain the reason behind the higher fracture toughness values at higher diameters. Moreover, another possible factor that lead to this increase can be explained as confining effect.

Shotcrete is heterogeneous material; if a crack is forced to follow a strict path for a large enough path in a large size disc, crack tip may be forced to break through both binder and rather strong aggregate grains, resulting in a higher K_{IC}.

During test, cracks initiated at the center of the specimens and propagated toward the loaded flat ends. A graphical representation of critical dimensionless crack lengths determined from experimental results for all thirty FBD shotcrete specimens and their average values for various diameters are shown Figure 6.2. Red dots symbolize average values calculated related to specimen diameter whereas the blue dots stand for individual results. Curve fitted to the each diameter group. Dimensionless critical crack length increases with sample size following a fitted third degree polynomial. The lowest 0.72 MPa$\sqrt{m}$ for 100 mm size group and the highest is 0.75 MPa$\sqrt{m}$ for the 200 mm group.

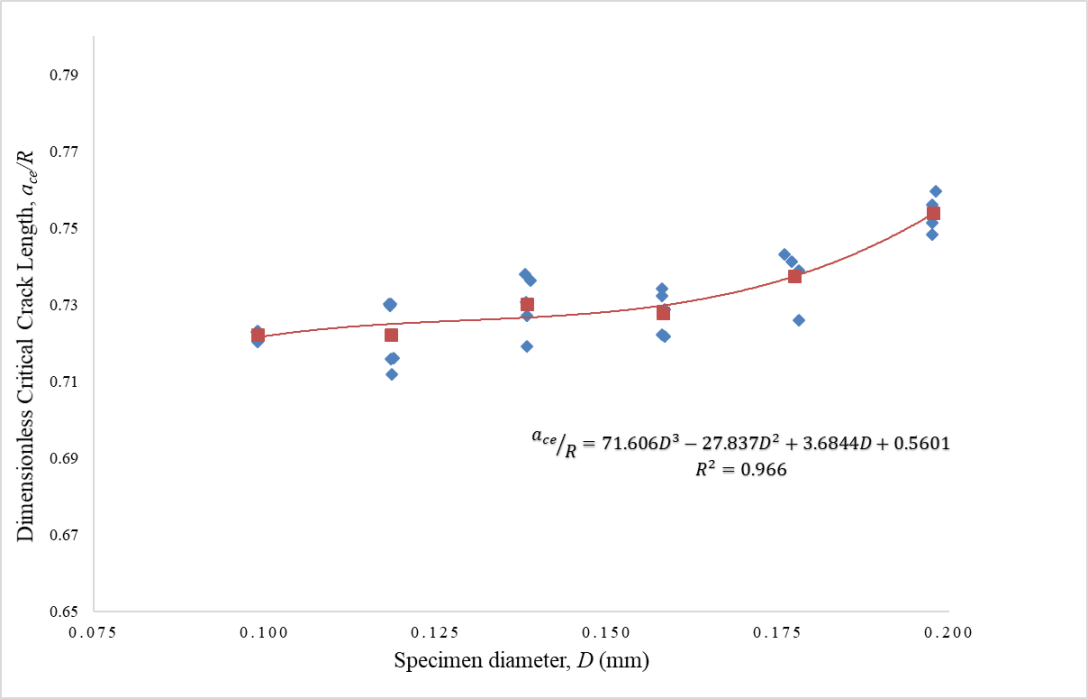

Figure 6.2. Dimensionless critical crack length of FBD tested specimens

The a_{ce}/R ratio increases in specimen diameter. The amount of increase is about 4%. Normally, a_{ce}/R must remain constant at the numerically computed a_{ce}/R. This increase is attributed to the size effect issue in the sense that inertia of unstably moving crack is greater in a large size sample.

Another observation was that cracks were seen more prominently and clearly as the specimen diameters grew.

6.2. Effect of Curing Time on the Fracture Toughness

Early-age developed-which designated in this study the period between 1 and 7 days after casting- 21 shotcrete specimens with constant diameter D=160 mm and constant loading angle (2a=22°) with 1 day, 2 days, 3 days, 5 days and 7 days cured shotcrete specimens were subjected to mode I fracture toughness test in order to determine the effect of curing time on mode I fracture toughness. Again, during all tests, cracks initiated at the center of the tested specimen and propagated through the flattened ends.

All test results are tabulated in Table 6.3. The averages of each curing time group are provided in Table 6.4.

Table 6.3. *All test results for investigation of curing time on the fracture toughness*

Name	*CuringTime(day)*	$P_{min}(kN)$	$K_{IC}(MPa\sqrt{m})$
S160-1D-s1	1	33.20	0.69
S160-1D-s2	1	29.42	0.60
S160-1D-s3	1	31.38	0.65
S160-1D-s4	1	33.29	0.69
S160-2D-s1	2	37.28	0.77
S160-2D-s2	2	42.28	0.87
S160-2D-s3	2	36.36	0.75
S160-2D-s4	2	38.85	0.81
S160-3D-s1	3	38.60	0.80
S160-3D-s2	3	39.94	0.82
S160-3D-s3	3	42.28	0.88
S160-3D-s4	3	40.80	0.84
S160-5D-s1	5	56.51	1.15
S160-5D-s2	5	55.83	1.14
S160-5D-s3	5	48.67	1.01
S160-5D-s4	5	51.12	1.06
S160-7D-s1	7	57.85	1.19
S160-7D-s2	7	57.04	1.16
S160-7D-s3	7	56.28	1.15
S160-7D-s4	7	57.96	1.22
S160-7D-s5	7	56.54	1.18
Average		44.83±10.04	0.92±0.21

Table 6.4. *Average FBD test results according to the changing curing time*

Curing Time (day)	$P_{min\ ave}$ (kN)	K_{ICavg} ($MPa\sqrt{m}$)
1	31.82	0.66
2	38.69	0.80
3	40.41	0.83
5	53.03	1.09
7	57.13	1.18
Average	44.22±10.53	0.91±0.22

The average mode I fracture toughness value for 1 day cured shotcrete specimens was calculated as 0.66 MPa$\sqrt{m}$, for 2 days cured shotcrete specimens it was 0.80 MPa$\sqrt{m}$, 0.83 MPa$\sqrt{m}$ for 3 days cured, 1.09 MPa$\sqrt{m}$ for 5 days cured and for 7 day cured shotcrete specimens it was calculated as 1.18 MPa$\sqrt{m}$. Results showed that the average mode I fracture toughness values of early aged shotcrete specimens were changing between 0.66-1.18 MPa$\sqrt{m}$, (Table 6.4).

Based on the test results, determined fracture toughness of two day cured shotcrete specimens increased approximately by 21% in comparison with the average of 1 day cured results. The average fracture toughness value for seven day cured shotcrete specimens increased dramatically from around 21% to 78% in comparison with the average of 1 day cured test results.

Effect of curing time on mode I fracture toughness can be clearly observed from Figure 6.5. Curve fitted to the each curing time group. Fracture toughness increases with increasing curing time following a fitted third degree polynomial.

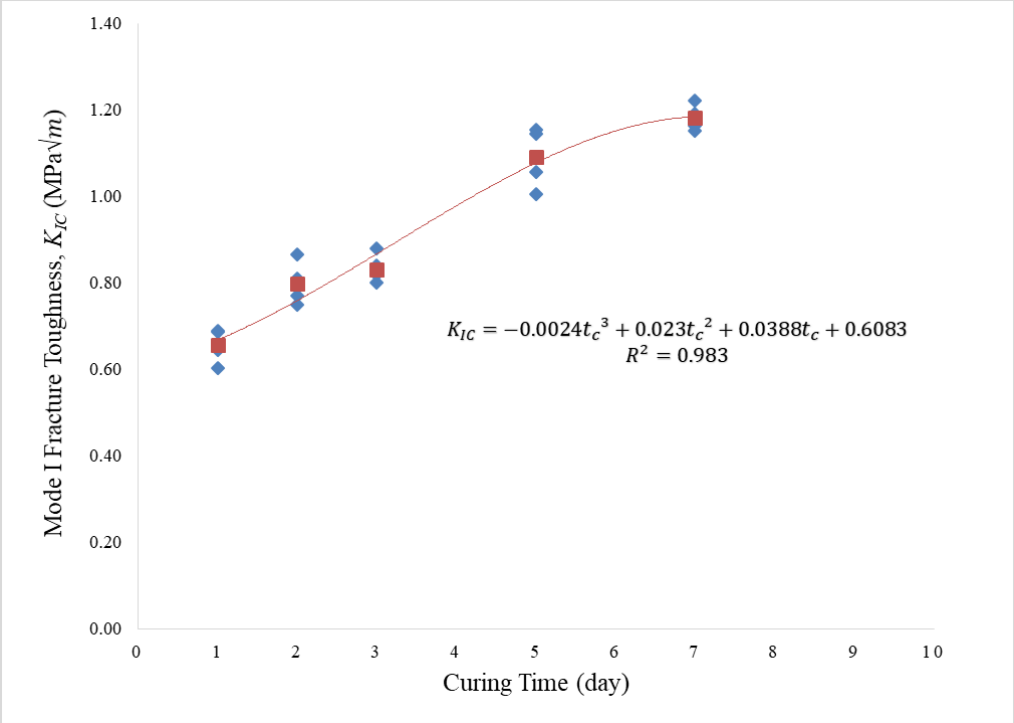

Figure 6.3. Average K_{IC} values changing with the curing time of shotcrete

Fracture Toughness increases with curing time following a fitted third degree polynomial. The lowest 0.66 MPa$\sqrt{m}$ for 1 day-cured group and the highest is 1.18 MPa$\sqrt{m}$ for 7 day-cured group. $K_{IC\ avg}$ for the seven day-cured group is about 1.78 times higher than the $K_{IC\ avg}$ of the one day-cured group. The average fracture toughness increase of about 79% according to the average of the curing time group.

6.3. Tensile Strength - Fracture Toughness Investigation

In below Table 6.5, mode I fracture toughness values for corresponding diameters from 100 mm to 200 mm and tensile strength results, $\sigma_{t,W}$, which was calculated using Wang's correction coefficient and relevant FBD test results and tensile strength results, $\sigma_{t,K\,T}$, which was calculated using Keles' correction coefficient and relevant test results were tabulated, (Table 6.5).

Table 6.5. *Tensile strength calculation from Wang's correction coefficient*

Name	t_{ave} (mm)	$P_{max\ ave}$ (kN)	$\sigma_{t\,W}$ (MPa)	$\sigma_{t\,K\,T}$ (MPa)	K_{ICavg}+STD ($MPa\sqrt{m}$)
S10022	66.62	24.98	2.30	2.33	0.93±0.11
S12022	79.55	37.31	2.40	2.43	0.98±0.11
S14022	83.99	45.77	2.39	2.42	1.06±0.09
S16022	103.86	67.68	2.50	2.53	1.18±0.07
S18022	122.38	102.92	2.87	2.91	1.43±0.04
S20022	133.16	127.14	2.93	2.97	1.46±0.09

$*\ \sigma_{t\,W}$ represents calculated tensile strength by using Wang's approach and $\sigma_{t\,K\,T}$ represents calculated tensile strength by using Keles and Tutluoglu's approach.

It is possible to correlate between the mode I fracture toughness values and the tensile strength. Since in an opening mode, specimen splitting is due to the tensile stress. To this extent, existence of the same relationship in shotcrete specimen was investigated in Figure 6.4 and Figure 6.5.

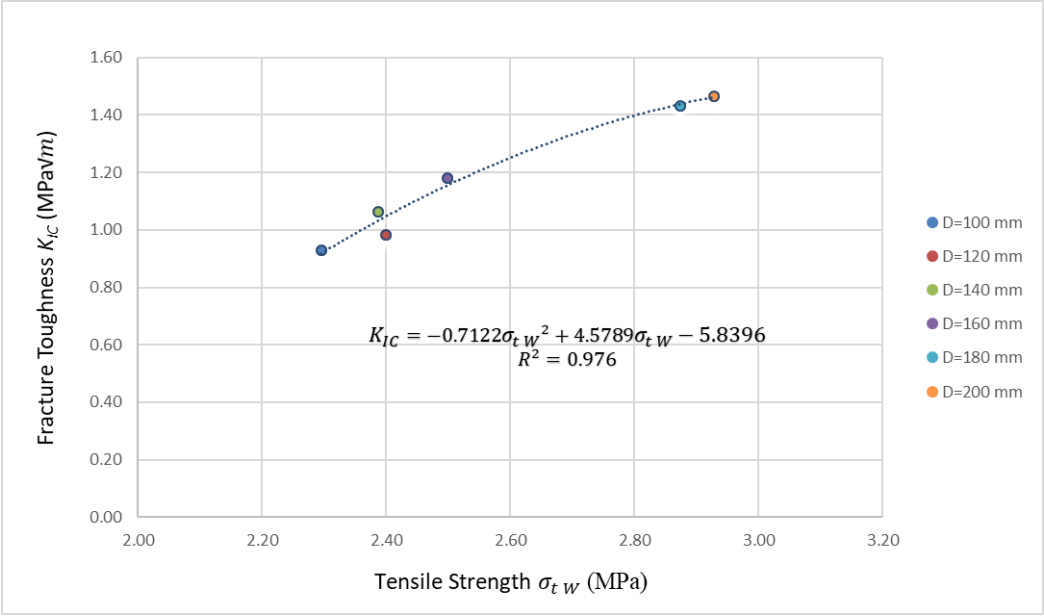

Figure 6.4. The relation between $\sigma_{t\,W}$ and K_{IC}

Both average tensile strength that computed from the Wang's approach and fracture toughness increase with sample size following a fitted second-degree polynomial.

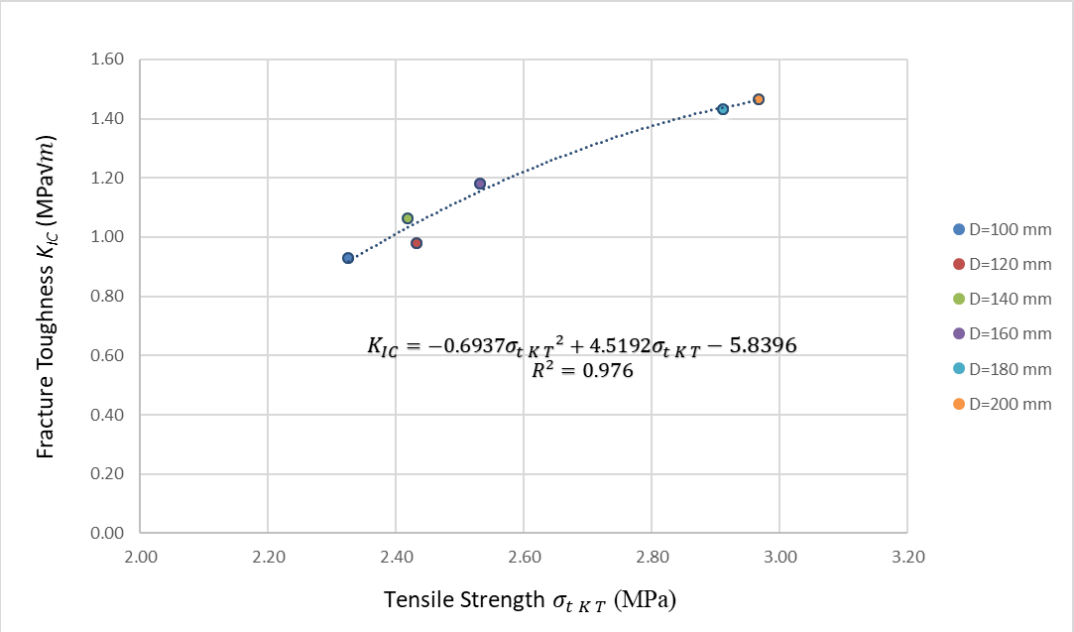

Figure 6.5. The relation between $\sigma_{t,K\,T}$ and K_{IC}

Both average tensile strength that computed from the Keles and Tutluoglu's approach and fracture toughness increase with sample size following a fitted second-degree polynomial.

A second-degree polynomial functional fit to the results in Figure 6.5 is the best fit and this fitted function gives an estimated maximum at σ_t =3.26 MPa as K_{IC}=1.52 MPa$\sqrt{m}$.

These graphs show that calculated tensile strength from the Flattened Brazilian Disc test is increasing while fracture toughness of the sample is increasing with changing diameters between 100 mm to 200 mm. The rate of increase of fracture toughness with tensile strength decreases for larger diameter groups. For shotcrete, size-independent

ratio between the fracture toughness and tensile strength is estimated as K_{IC}/σ_t=1.52/3.26=0.47 for the first time compared to the related literature.

Advancing this study, dimensionless fracture toughness over tensile strength ratio changing with specimen size was investigated with tensile strength calculated using Keles and Tutluoglu's approach, which is a more recent study, in Figure 6.6.

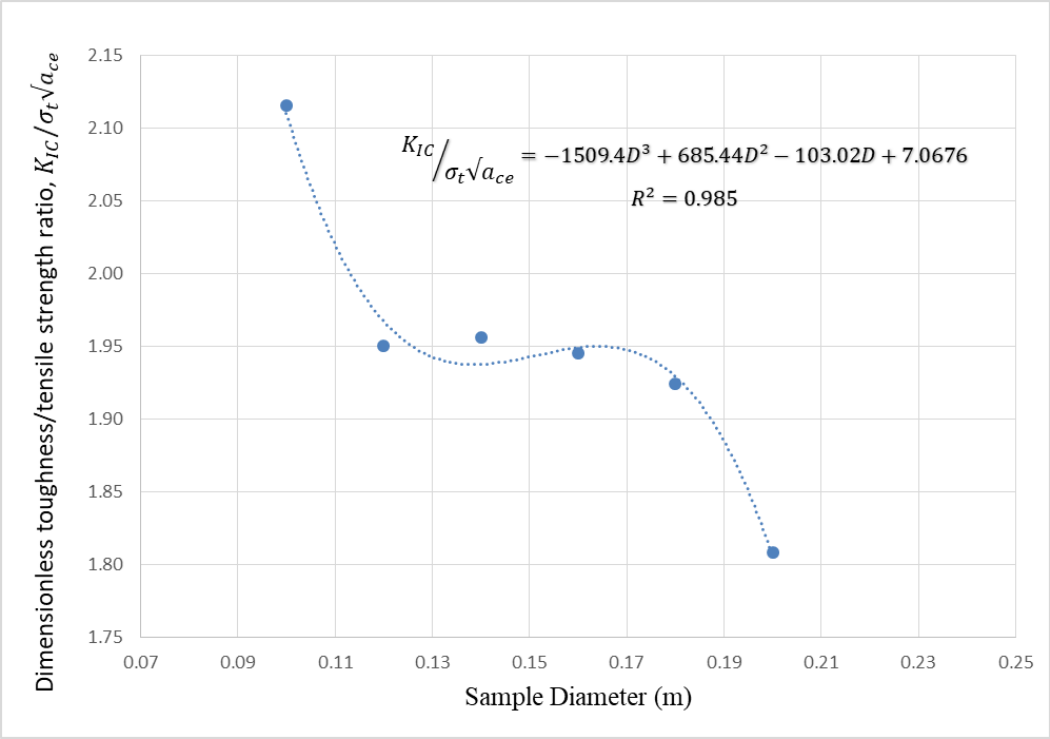

Figure 6.6. Dimensionless toughness over tensile strength ratio

This polynomial function of degree three becomes zero at D=0.26 m meaning that size independent fracture toughness and tensile strength is best measured for a diameter range between 120-180 mm (best D=160 mm) tensile strength; after the tensile strength increases too rapidly compared to fracture toughness taking curve down to zero at 0.26 m diameter.

CHAPTER 7

CONCLUSION AND RECOMMENDATIONS

FBD geometry is used here for measuring the tensile strength and the tensile mode fracture toughness of the molded shotcrete samples. For the FBD geometry, compressive load at the flat ends results tension in the center, and crack is forced to initiate at the center and propagate towards the loaded flattened ends. 3D printing technology provides great advantages in terms of the accurate sample preparation geometry for the desired diameter range of testing samples.

Size effect was clearly observed in results of seven day cured FBD testing work. According to the American Shotcrete Association; concrete, when applied using the shotcrete process, or cast-in-place, needs to cure for 7 days (American Shotcrete Association, n.d.). Moreover, according to the American Concrete Institute (ACI) often specified seven-day curing is recommend as a minimum curing period for Type I cement in standards ASTM C 150. (Zemajtis, n.d.). Mode I fracture toughness values at constant loading angle (*22*°) were increasing with the specimen diameter. The average mode I fracture toughness, $K_{IC\ avg}$ for the largest diameter group (D=200 mm) is about 1.57 times higher than the average mode I fracture toughness, $K_{IC\ avg}$ of the smallest diameter group (D=100 mm). As the specimen gets larger, the crack tip gets further from the compressively loaded area. In this case, the size of the fracture process zone is relatively small compared to the specimen dimension, this can explain the reason behind the higher fracture toughness values at higher diameters. Moreover, another possible factor that lead to this increase can be explained as confining effect. Shotcrete is a heterogeneous material; if a crack is forced to follow a strict path for a large enough path in a large size disc, crack tip may be forced to break through both binder and rather strong aggregate grains, resulting in a higher fracture toughness K_{IC}.

According to the extreme points of the equation, it was predicted that after the diameter increases up to around 205 mm, the increase in fracture toughness would not continue.

In the size effect investigation, numerically computed and experimentally observed crack lengths were compared. Shotcrete samples with rather large diameters showed clearer local minimum load drops in the related load-displacement plots. Compared to the numerically computed crack length/radius ratio a_{cn}/R of constant 0.72, a_{ce}/R ratio increases with specimen diameter. The amount of increase is about 4%. This increase is attributed to the size effect issue in the sense that inertia of unstably moving crack is greater in a large size sample.

Considering the fact that shotcrete support unit provides temporary surface control of underground openings, the effect of curing time on fracture toughness can be a significant contribution. The early aged mixture design was used for the investigation of curing time effect on the fracture toughness for specimens having diameter of 160 mm; K_{IC} values increased about 79% with the curing time varying 1 day to 7 days.

In order to study the relation between fracture toughness and tensile strength, the comparisons were made. After the results of several experimental works, it was concluded that, up to a certain point tensile strength and the fracture toughness increases proportionally.

The difference between the tensile strength obtained from the regular Brazilian Disc test and the Flattened Brazilian Disc test can be explained by two reasons. The first possible reason is the loading angle of the jaw used in the regular Brazilian Disc Test is lower than the loading angle of the Flattened Brazilian Disc test. As the loading angle decreases, fracture toughness is believed to increase, and thus tensile strength increases too, since as found in this work, fracture toughness and tensile strength increase proportionally. The second possible reason can be the loading differences. While regular Brazilian Disc specimen is under an arc type loading because of the

steel jaws, the Flattened Brazilian Disc specimen is under the uniform diametrical compression.

The Size effect phenomenon is effective on tensile strength obtained from the Flattened Brazilian Disc test. With using two different approaches, Wang's approach and Keles & Tutluoglu's approach, to obtain tensile strength from Flattened Brazilian Disc tests results, tensile strength is found to increase with increasing diameter from 100 mm to 200 mm. There was a threshold diameter after which strength increased with increasing disc size. Threshold diameter was around 200 mm.

In this study, for the shotcrete specimens that have 0.5 water/cement ratio, the size effect on tensile strength was observed between 100 mm diameter and 200 mm. As a result of fitted third degree polynomial function between the dimensionless fracture toughness/tensile strength ratio and specimen diameter, the size-independent values can be calculated in a diameter range between 120-180 mm (the best at 160 mm).

Tensile strength from FBD tests increased with increasing size. Explanation can be in terms of crack tip stress field and a 3D yield criterion in terms of all principal stresses (σ_1, σ_2, σ_3). As diameter increases and specimen gets thicker, in-plane minimum principal stresses and out of plane principal stresses change and perhaps increase in compression. Use of a single yield criterion based on tensile strength and minimum principal stress may not be the right approach to characterize the cracking failure for this geometry. A yield criterion in terms of all principal stresses may be the choice for describing the tensile cracking and surrounding stress distributions which are to be inserted to 3-dimensional yield criteria.

For future work, it is suggested to use a stronger mold material to be used in the 3D printer, since some molds broke before the tests are completed successfully. Another recommendation is to extend this testing work for specimen sizes larger than the ones used here. Also curing time work may involve more data points in the early ages of curing, since this aging process is an important issue in carrying the expected loads in a temporary support unit.

REFERENCES

Alexander M.G., Heiyantuduwa R. (2009). *A Rewiew of Shotcrete Materials, Mix Design and Applications*. Shotcrete for Africa Conference.

Akbardoost, M. R. A. J. (2014). *Size and Geometry Effects on Rock Fracture Toughness: Mode I Fracture.* Rock Mechanics and Rock Engineering, 677–687. https://doi.org/10.1007/s00603-013-0430-7

American Shotcrete Association. (n.d.). Retrieved from https://www.shotcrete.org/pages/products-services/technical-questions-archive.htm

Anderson, T. L. (2005). *Fracture mechanics: fundamentals and applications.* CRC Press.

Antolovich, S. D., Saxena, A., & Gerberich, W. W. (2018). *Fracture mechanics – An interpretive technical history.* Mechanics Research Communications, 91, 46–86. https://doi.org/10.1016/j.mechrescom.2018.03.003

Aydan, O., Sezaki, M. & Kawamoto, T. (1992), *Mechanical and numerical modelling of shotcrete*, in Pande & Pietruszczak, eds, 'Numerical Models in Geomechanics', pp. 757– 764.

Bazant, Z. P. (1976). *Instability, Ductility and Size Effect in Strain-Softening Concrete*, Journal of the Engineering Mechanics Division, ASCE, Vol. 102, pp. 331-344.

Bazant, Z. P., & Kazemi, M. (1991). *Size effect on diagonal shear failure of concrete beams without stirrups*. ACI Structural Journal 88(3), 268-276.

Bazant, Z. P., Kazemi,M.T, Hasegawa, T., Mazars, J. (1991). *Size Effect in Brazilian Split-Cylinder Tests: Measurements and Fracture Analysis*. ACI Materials Journal, 88.

Byfors, J. (1980), *Plain concrete at early ages*, Technical report, Swedish Cement and Concrete Research Institute.

Carpinteri, A. (1984). *Stability of Fracturing Process in RC Beams*. Journal of Structural Engineering, 110(3), 544–558. doi: 10.1061/(asce)0733-9445(1984)110:3(544)

Ceriolo, L., & Di Tommaso, A. (1998). *Fracture mechanics of brittle materials: An historical point of view*. Proceedings - 2nd International PhD Symposium in Civil Engineering, (May), 207–214.

Chang, Y. (1994), Tunnel support with shotcrete in weak rock - A rock mechanics study, PhD thesis, Royal Institute of Technology, Stockholm, Sweden.

Chong, K.P. and Kuruppu, M. D. (1984). *New Specimen for Fracture Toughness Determination*

Cotterell, B. (2002*). The past, present, and future of fracture mechanics*. Engineering Fracture Mechanics, 69(5), 533–553. https://doi.org/10.1016/S0013-7944(01)00101-1

Dao, V., Dux, P., & Morris, P. H. (2014). *Crack propagation in concrete at very early ages.* Magazine of Concrete Research, s. 643-651.

EN 206:2013+A1 Concrete - Specification, performance, production and conformity standard.

Erdoğan, T.Y. (2013). *Beton*. Metu Press.

Fowell, R.J., *"ISRM Commission on Testing Methods: Suggested Method for Determining Mode I Fracture Toughness Using Cracked Chevron Notched Brazilian Disc (CCNBD) Specimens",* Int. J. Rock Mech. Min. Sci. and Geomech. Abstr.. Vol. 32, No. 1, pp. 57-64, 1995.

Griffith, A. A. (1921). The Phenomena of Rupture and Flow in Solids. Philosophical Transactions of the Royal Society A: Mathematical, Physical and Engineering Sciences, 221(582-593), 163–198. doi: 10.1098/rsta.1921.0006

Griffith, A.A. (1924). *The Theory of Rupture*, Proc. of First Int. Cong. Appl. Mech., pp. 53-64.

Gross, D. (2014). Some Remarks on the History of Fracture Mechanics. *The History of Theoretical, Material and Computational Mechanics - Mathematics Meets Mechanics and Engineering Lecture Notes in Applied Mathematics and Mechanics*, 195–209. doi: 10.1007/978-3-642-39905-3_12

Guo, H., Aziz, N. I., & Schmidt, L. C. (1993). *Rock fracture-toughness determination by the Brazilian test.* Engineering Geology, 33(3), 177–188. https://doi.org/10.1016/0013-7952(93)90056-I

Hillerborg, A. (1985). *The theoretical basis of a method to determine the fracture energy G F of concrete.* Materials and Structures, 18(4), 291–296. https://doi.org/10.1007/BF02472919

Hillerborg, A., Modeer, M., & Petersson, P. (1976). *Analysis of crack formation and growth in concrete be means of fracture mechanics and finite elements*. Cement & Concrete Research Vol.6, 773-782.

Irwin, G. (1958). *Fracture*. Handbuch der Physik (s. 551-590). içinde Berlin: Springer.

ISRM. (1979). *Suggested Methods for Determining the Uniaxial Compressive Strength*. Int. J. Rock Mech. Min. Sci. & Geomech, 135-140.

Japaridze, L. (2015). Stress-deformed state of cylindrical specimens during indirect tensile strength testing. *Journal of Rock Mechanics and Geotechnical Engineering*, *7*(5), 509–518. doi: 10.1016/j.jrmge.2015.06.006

Jenq, Y., & Shah, S. P. (1985). *Two Parameter Fracture Model for Concrete*. Journal of Engineering Mechanics, 111(10), 1227–1241. doi: 10.1061/(asce)0733-9399(1985)111:10(1227)

Kaklis, K. N., Agioutantis, Z., Sarris, E., & Pateli, A. (2005). *A theoretical and numerical study of discs with flat edges under diametral compression (flat Brazilian test).* 5th GRACM International Congress on Computational Mechanics, 29(June 2017).

Kaplan, M. (1961). *Crack propagation and the fracture of concrete*. Journal of ACI Vol.58, 591-610.

Karihaloo, B., & Nallathambi, P. (1989). *An improved effective crack model for the determination of fracture toughness of concrete*. Cement and Concrete Research, 19(4), 603–610. doi: 10.1016/0008-8846(89)90012-4

Keles, C., & Tutluoglu, L. (2011). *Investigation of proper specimen geometry for mode I fracture toughness testing with flattened Brazilian disc method.* Int. J. Frac. , 61-75.

Kesler, C., Naus, D., & Lott, J. (1971*). Fracture mechanics its applicability to concrete.* The Society of Material Science Vol.4, 113-124.

Key to Metals Database, http://steel.keytometals.com, last visited on 24th March 2010.

Kuruppu, M. D., Obara, Y., Ayatollahi, M.R., Chong, K.P., & Funatsu, T. (2015*) ISRM- suggested method for determining the mode I static fracture toughness using semi- circular bend specimen.* In the ISRM Suggested Methods for Rock Characterization, Testing and Monitoring: 2007-2014, 107-114. Springer International Publishing

Liang, P., & Tao, J. (2014). *The Contrast of Concrete Brazilian and Flattened Brazilian Disc.* Applied Mechanics and Materials , s. 263-268.

Mahanta, B., Sirdesai, N., Singh, T. N., & Ranjith, P. G. (2017). *Experimental Study of Strain Rate Sensitivity to Fracture Toughness of Rock using Flattened Brazilian Disc.* In Procedia Engineering (Vol. 191, pp. 256–262). The Author(s). https://doi.org/10.1016/j.proeng.2017.05.179

McClintock, F.A. and J.B. Walsh (1962). *Friction of Griffith cracks in rock under pressure.* Proc. Fourth U.S. Congr. Appl. Mech. 1015-21. Berkeley: American Society of Mechanical Engineers.

Miner, G. M. (1973). *Use of shotcrete from the standpoint of the owner. Use of Shotcrete for Underground Structural Support.* South Berwick: American Society of Civil Engineers and American Concrete Institute.

Nallathambi, P., & Karihaloo, B. (1986). *Determination of the specimen size independent fracture toughness of plain concrete.* Magazine of Concrete Research Vol. 38, 67-76.

Neville, A. (1981), *Properties of concrete*, Longman Scientific & Technical.

Ouchterlony, F., *"ISRM Commission on Testing methods; Suggested Methods for determining fracture toughness of rock"*, Int. J. Rock Mech. Min. Sci. & Geomech. Abstr., Vol. 25, pp. 71-96, 1988.

Özdoğan, C. (2017). *Pure tensile fracture modelling and toughness measurements on brazilian discs of andesite and marble*. Ankara.

Perdikaris, P. C., Calomino, A. M., & Chudnovsky, A. (1986, August). *Effect of Fatigue on Fracture Toughness of Concrete*. Journal of Engineering Mechanics, s. 776-791.

Rossmanith, H. (1983). *Rock Fracture Mechanics (Cilt 68).* (I. C. Sciences, Dü.) Wien-New York: Springer-Verlag.

Shah, S. P. (1995). *Fracture Mechanics of Concrete, Applications of Fracture Mechanics to Concrete, Rock and Other Quasi-Brittle Materials.* NY: A Wiley-Interscience Publication.

Sheity, D. K., Rosenfield, A. R., & Duckworth, W. H. (1985). *Fracture Toughness of Ceramics Measured by a Chevron-Notch Diametral-Compression Test. Journal of the American Ceramic Society*, 68(12). doi:10.1111/j.1151-2916.1985.tb10135.x

SIKA. (2001). SIKA ViscoCrete Hi-Tech.

Timoshenko, S.P. and Goodier, J.N. (1970). *Theory of Elasticity*. 3rd Edition, Mc Graw-Hill, New York.

Ulusay, R., & Hudson, J. A. (2007). *The Complete ISRM Suggested Methods for Rock Characterization*, Testing and Monitoring: 1974-2006. Ankara.

Walsh, P. F. (1979). *Fracture of Plain Concrete*, The Indian Concrete Journal, Vol. 46, No. 11, pp. 469-470, and 476.

Wang, Q.Z., Jia, X.M., Kou, S.Q., Zhang, Z.X. and Lindqvist, P.A. (2004). *The Flattened Brazilian Disc Specimen Used for Testing Elastic Modulus, Tensile*

Strength and Fracture Toughness of Brittle Rocks: Analytical and Numerical Results. Int. J. of Rock Mech. Min. Sci., Vol. 41, pp. 245-253.

Wang, Q. Z., & Wu, L. Z. (2004). *The flattened Brazilian disc specimen used for determining elastic modulus, tensile strength and fracture toughness of brittle rocks: Experimental results.* International Journal of Rock Mechanics and Mining Sciences, 41(SUPPL. 1), 1–5. https://doi.org/10.1016/j.ijrmms.2004.03.015

Wang, Q. Z., & Xing, L. (1999). *Determination of fracture toughness KIc by ussing the flattened Brazilian dics specimen for rocks.* Engineering Fracture Mechanics (64), 193-201.

Zemajtis, J. Z. (n.d.). PCA: *Portland Cement Association. Role of Concrete Curing*: Retrieved from https://www.cement.org/learn/concrete-technology/concrete-construction/curing-in-construction

Zhao, X. L., Fowell, R. J., Roegiers, J. C., & Xu, C. (1994). *Rock fracture-toughness determination by the Brazilian test*, by H. Guo, N.I. Aziz, L.C. Schmidt. Engineering Geology, 38(1–2), 181–184. https://doi.org/10.1016/0013-7952(94)90033-7

APPENDICES

A. Static Deformability and Brazilian Disc Test Graphs

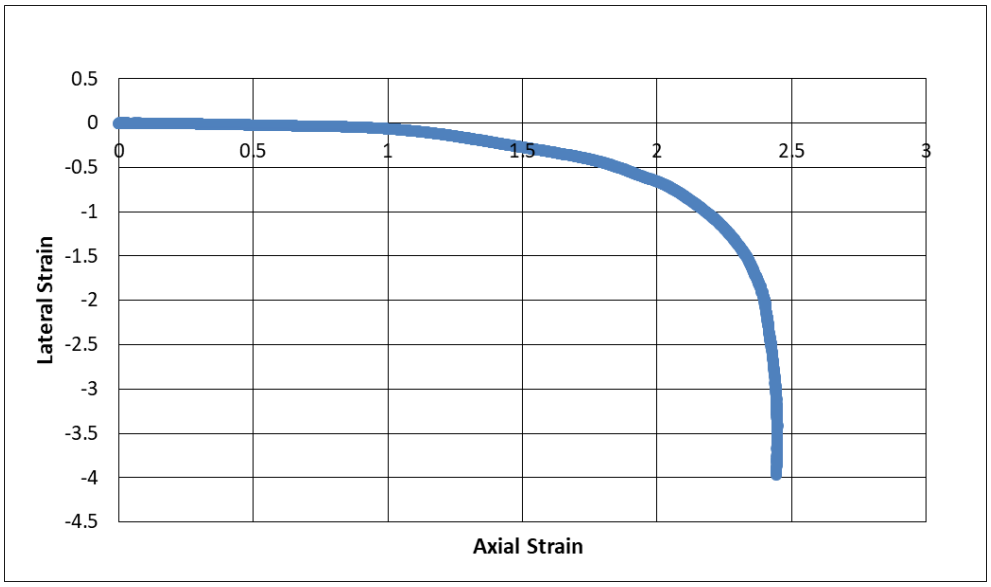

Figure 0.1. Static deformability test graph of S_SD_1

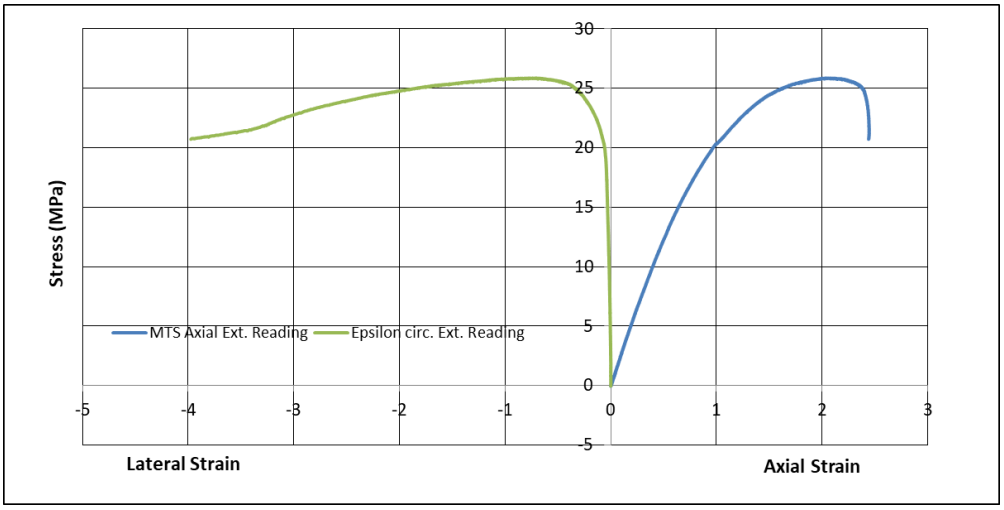

Figure 0.2. Static deformability test graph of S_SD_1

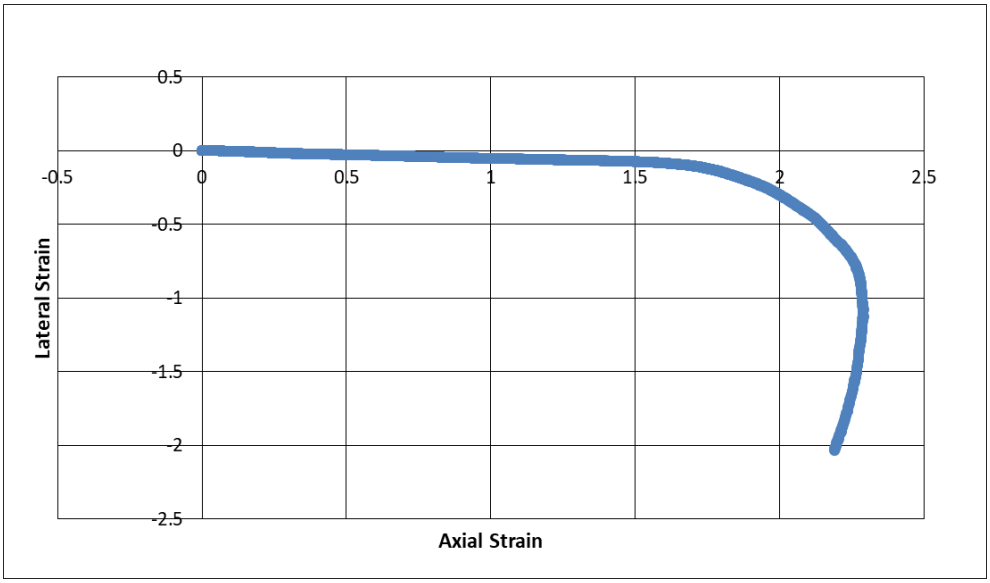

Figure 0.3. Static deformability test graph of S_SD_2

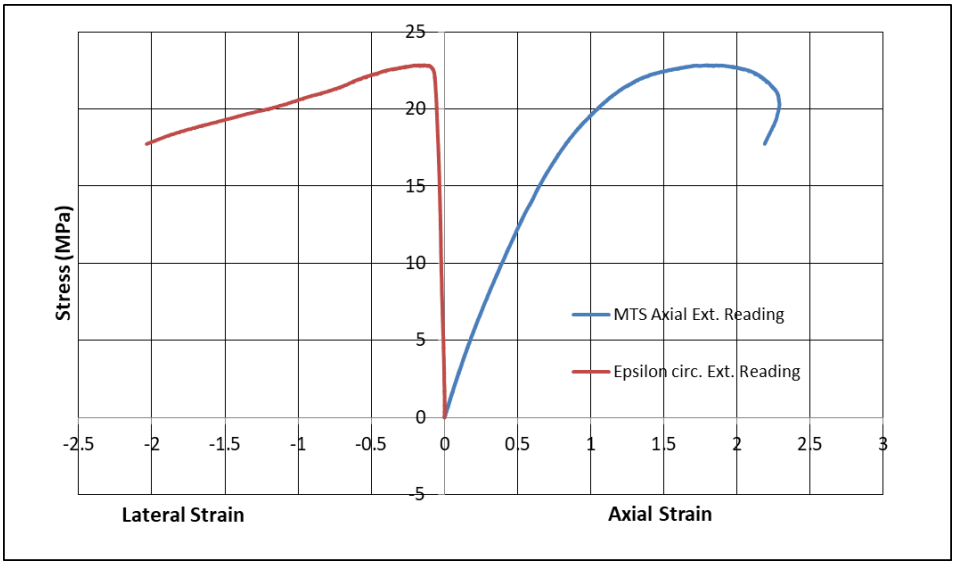

Figure 0.4. Static deformability test graph of S_SD_2

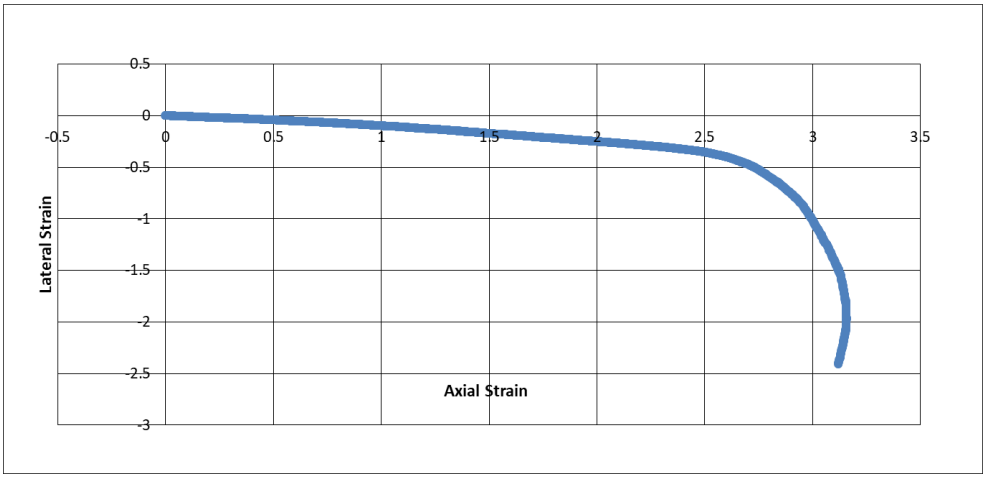

Figure 0.5. Static deformability test graph of S_SD_3

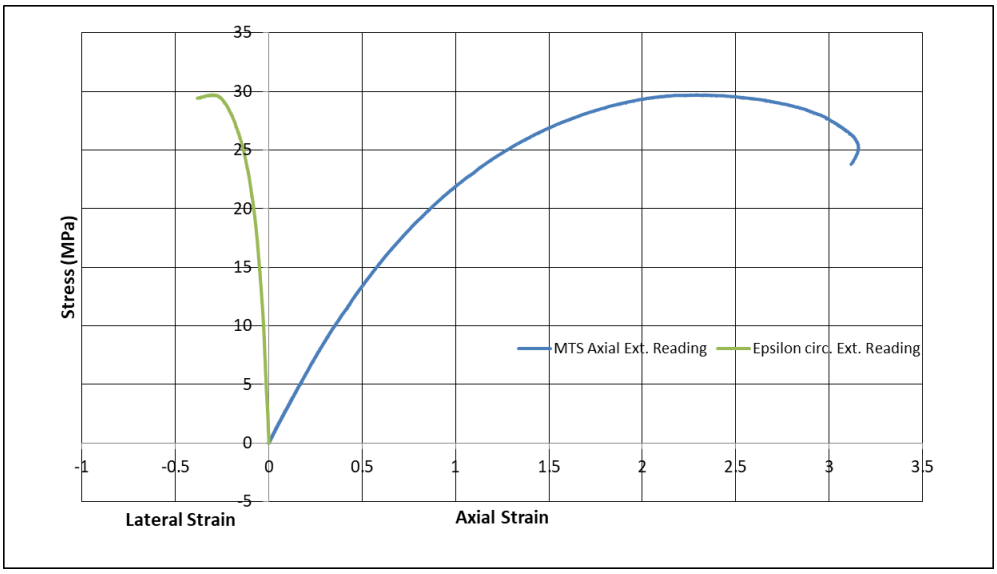

Figure 0.6. Static deformability test graph of S_SD_3

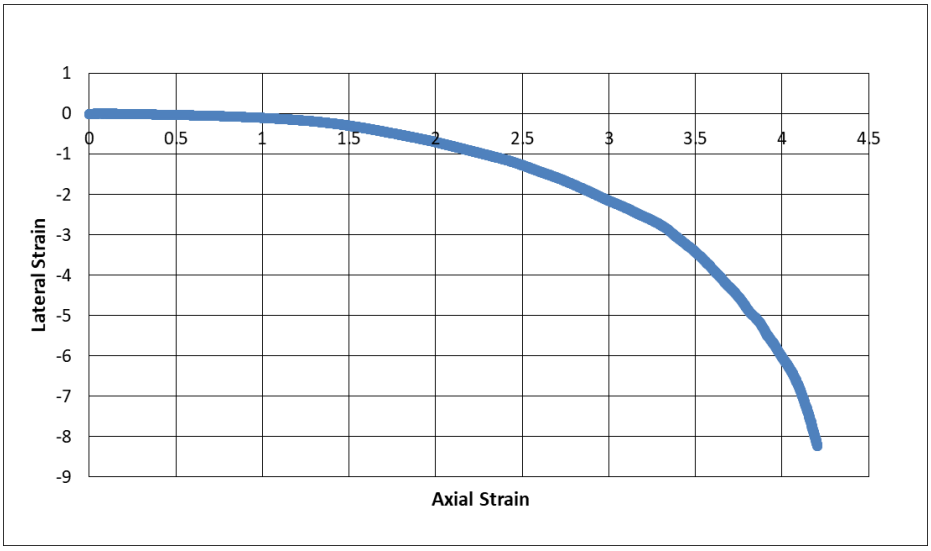

Figure 0.7. Static deformability test graph of S_SD_4

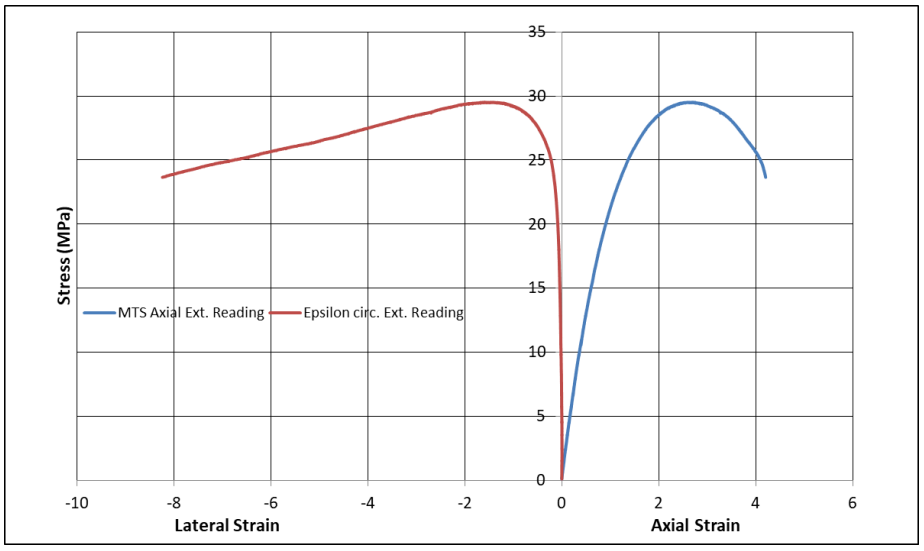

Figure 0.8. Static deformability test graph of S_SD_4

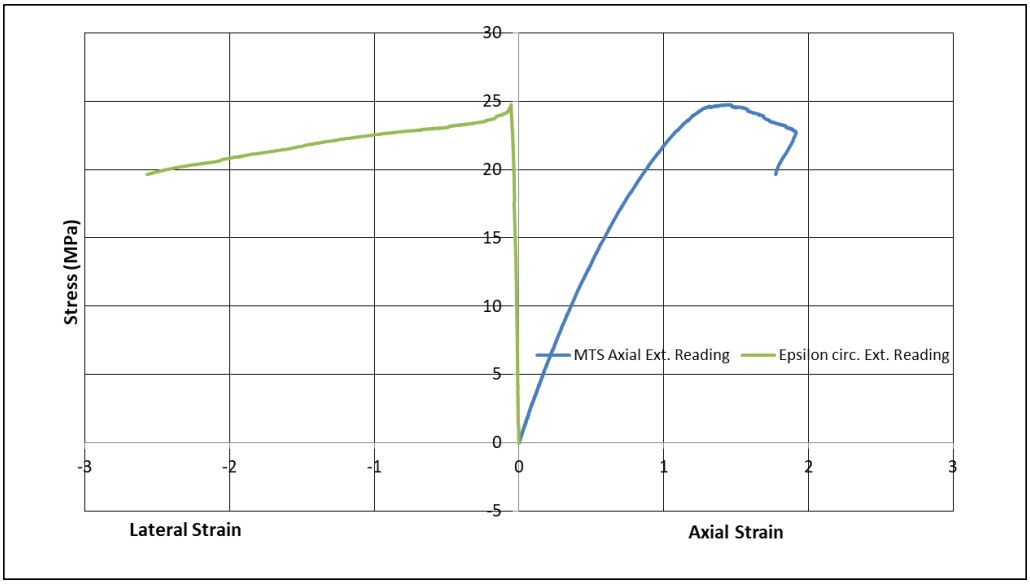

Figure 0.9. Static deformability test graph of S_SD_5

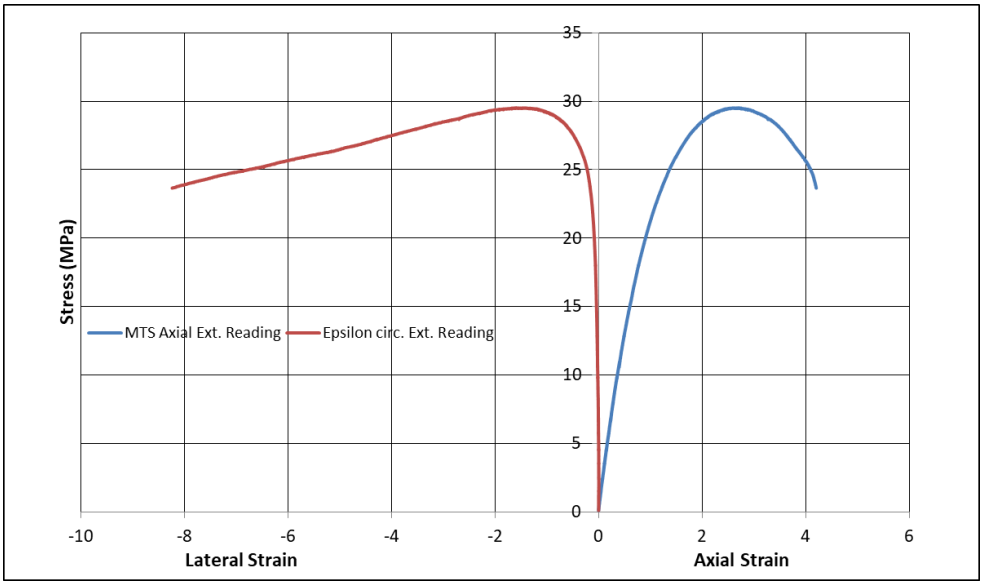

Figure 0.10. Static deformability test graph of S_SD_5

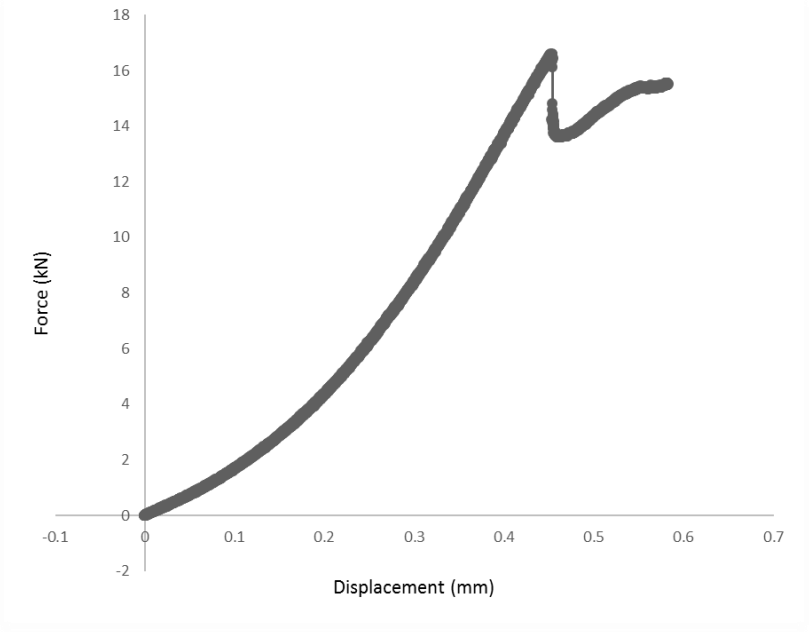

Figure 0.11. Brazilian Disc test graph of S_BD_1

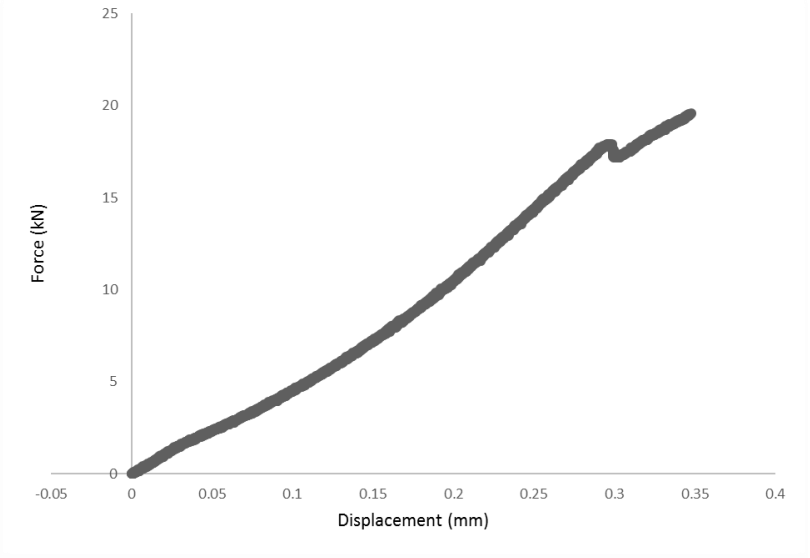

Figure 0.12. Brazilian Disc test graph of S_BD_2

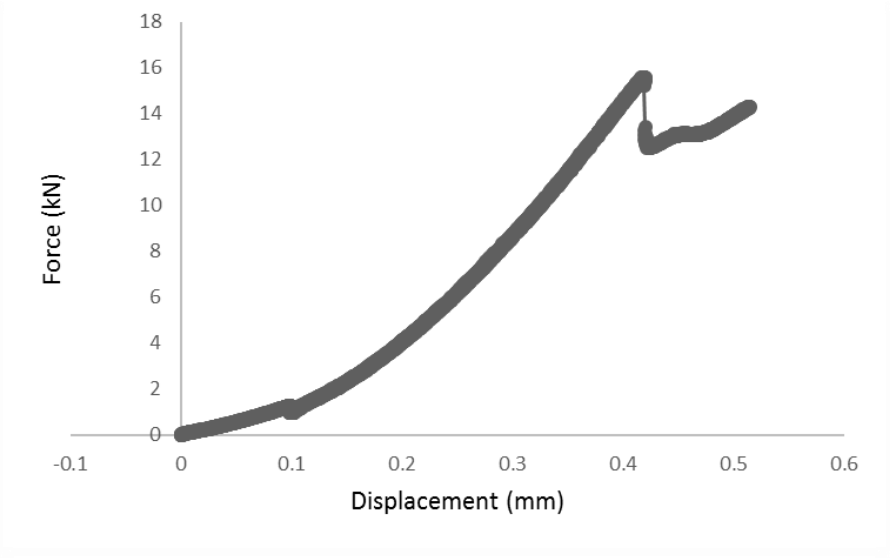

Figure 0.13. Brazilian Disc test graph of S_BD_3

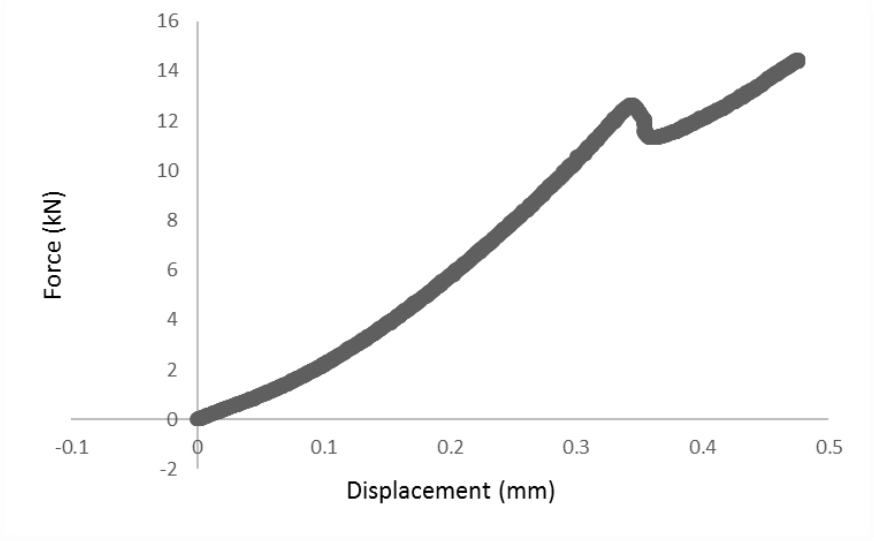

Figure 0.14. Brazilian Disc test graph of S_BD_4

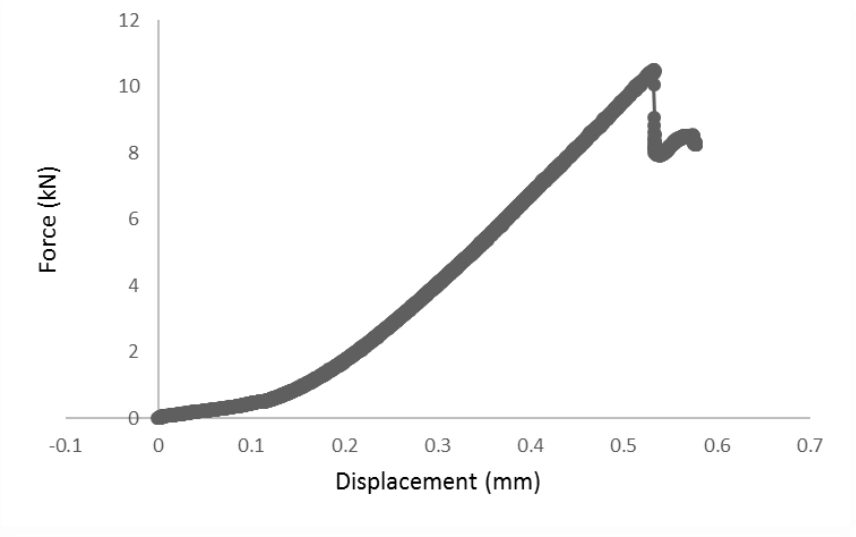

Figure 0.15. Brazilian Disc test graph of S_BD_5

B. Mode I Fracture Toughness Test Graphs

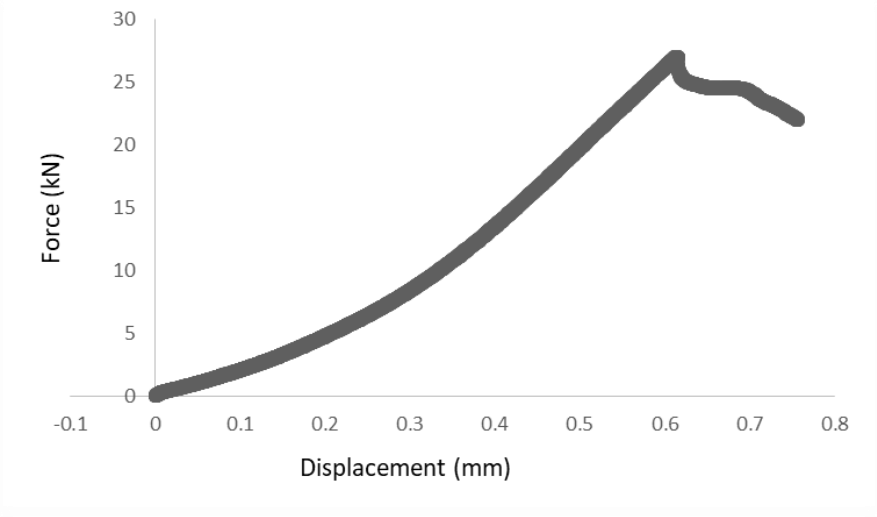

Figure 0.16. Flattened Brazilian Disc test graph of S100_s1

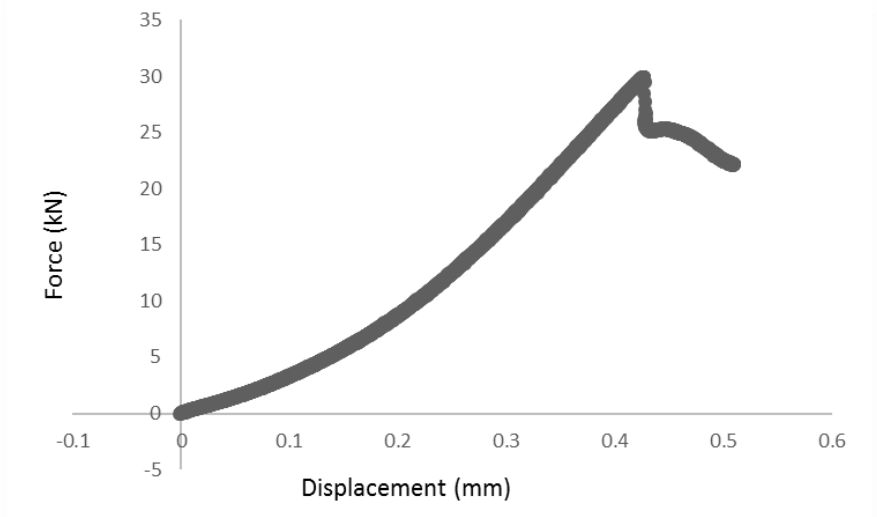

Figure 0.17. Flattened Brazilian Disc test graph of S100_s2

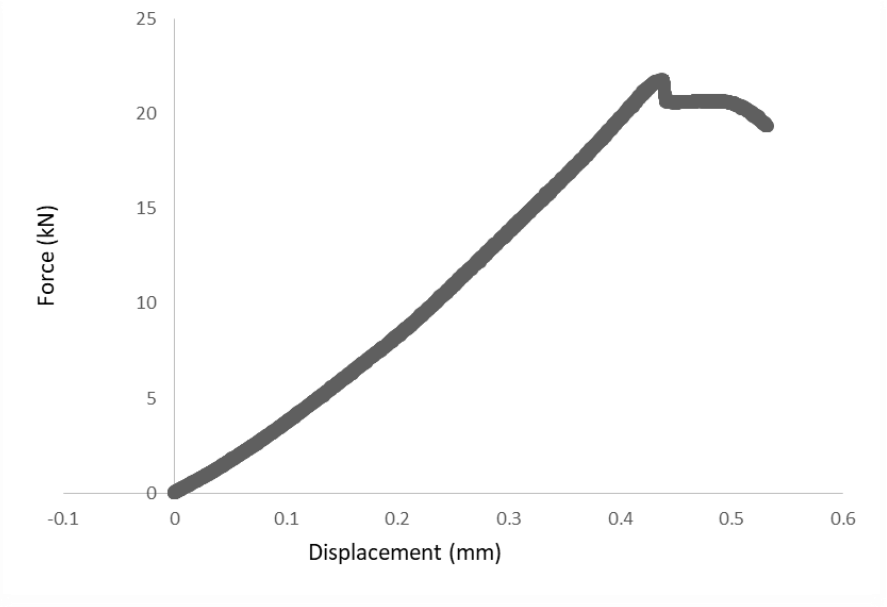

Figure 0.18. Flattened Brazilian Disc test graph of S100_s3

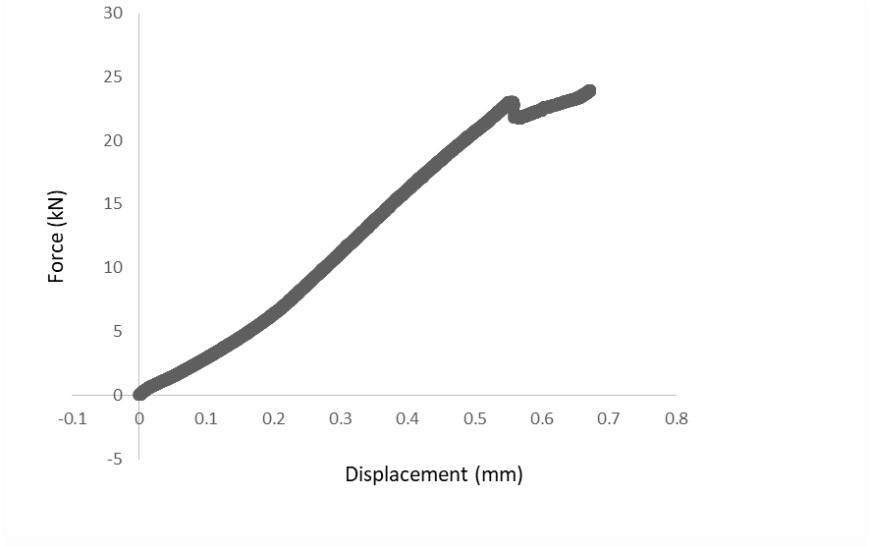

Figure 0.19. Flattened Brazilian Disc test graph of S100_s4

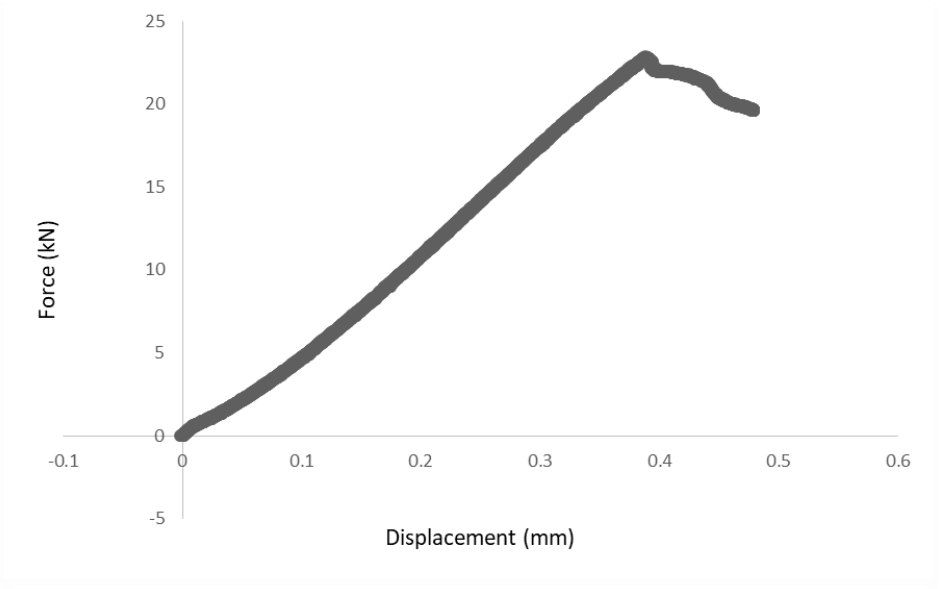

Figure 0.20. Flattened Brazilian Disc test graph of S100_s5

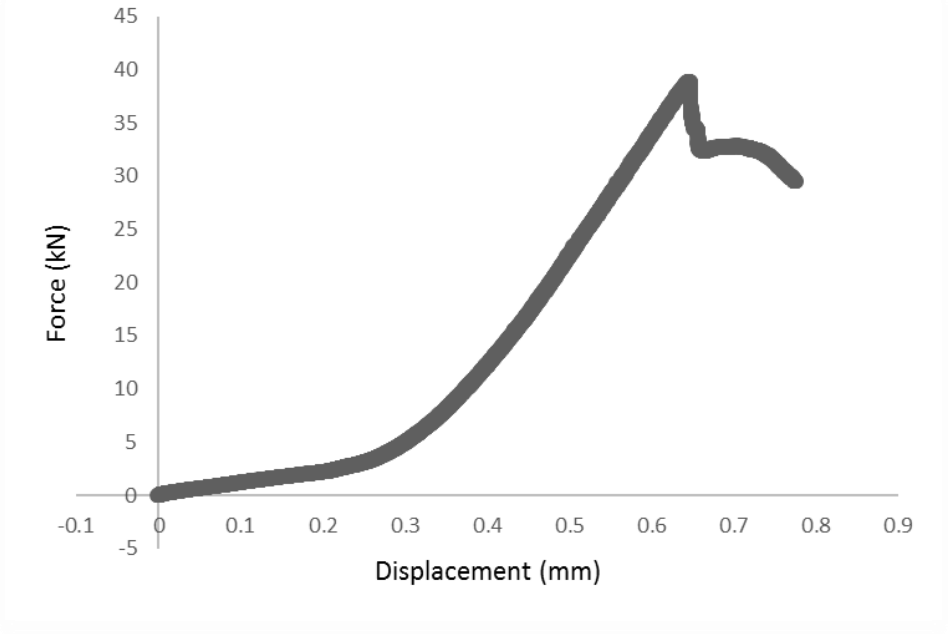

Figure 0.21. Flattened Brazilian Disc test graph of S120_s1

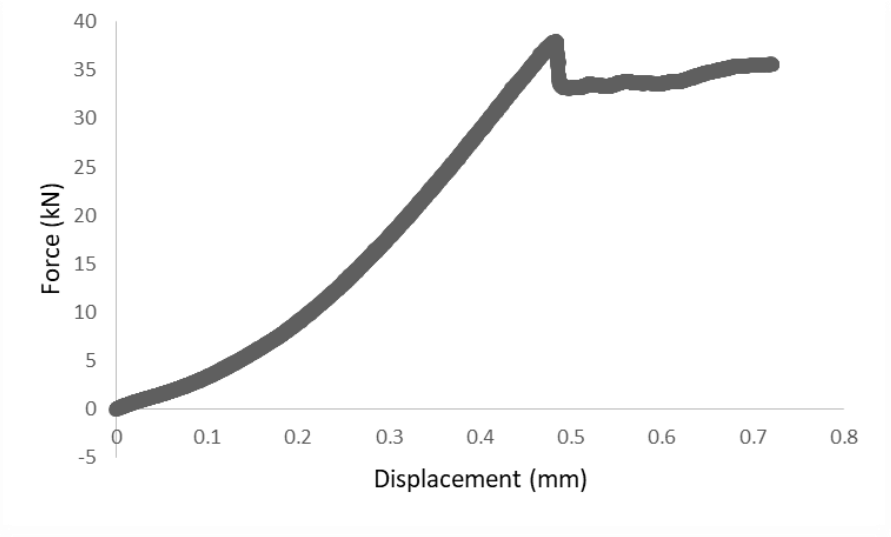

Figure 0.22. Flattened Brazilian Disc test graph of S120_s2

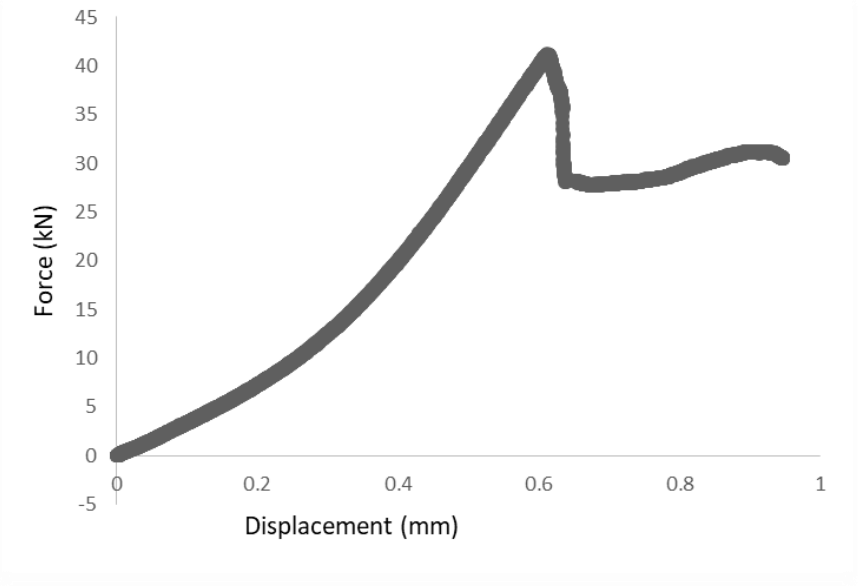

Figure 0.23. Flattened Brazilian Disc test graph of S120_s3

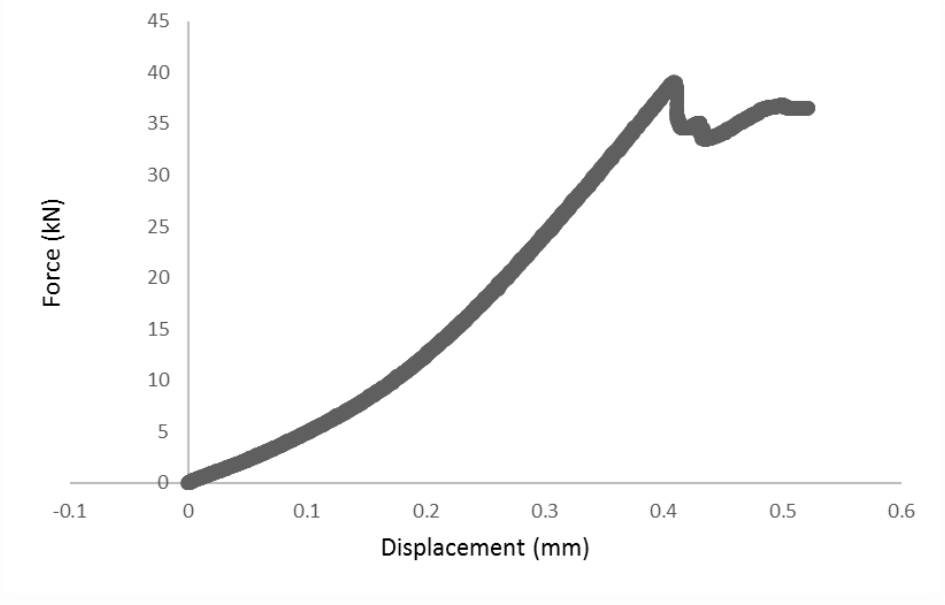

Figure 0.24. Flattened Brazilian Disc test graph of S120_s4

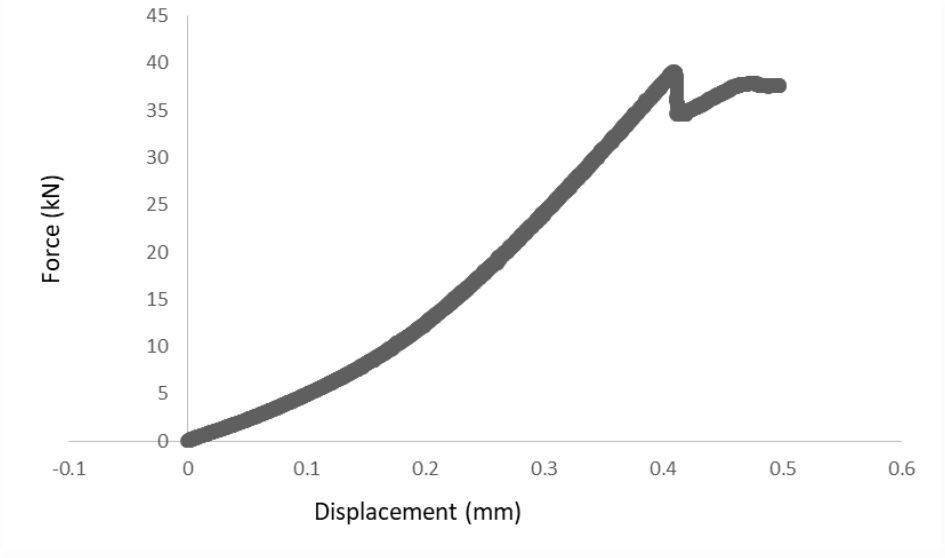

Figure 0.25. Flattened Brazilian Disc test graph of S120_s5

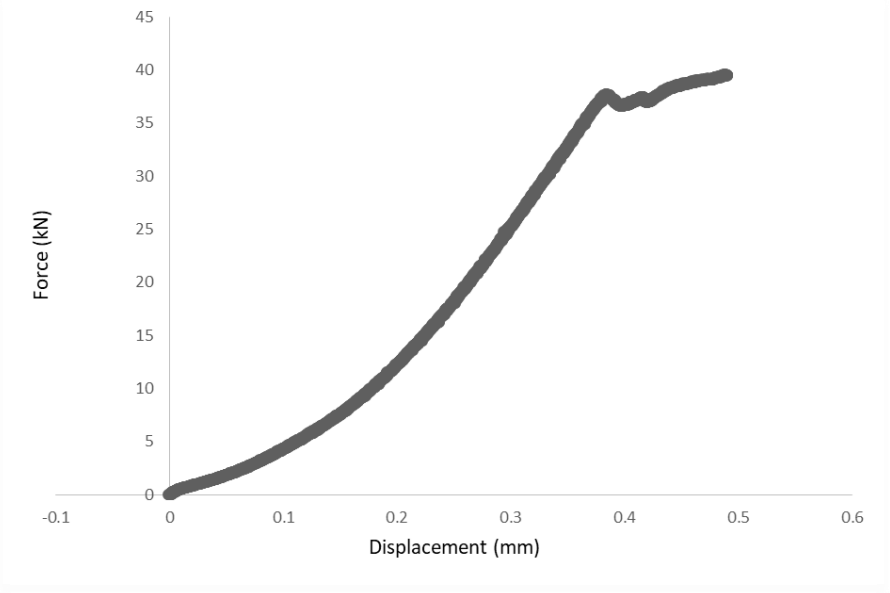

Figure 0.26. Flattened Brazilian Disc test graph of S120_s6

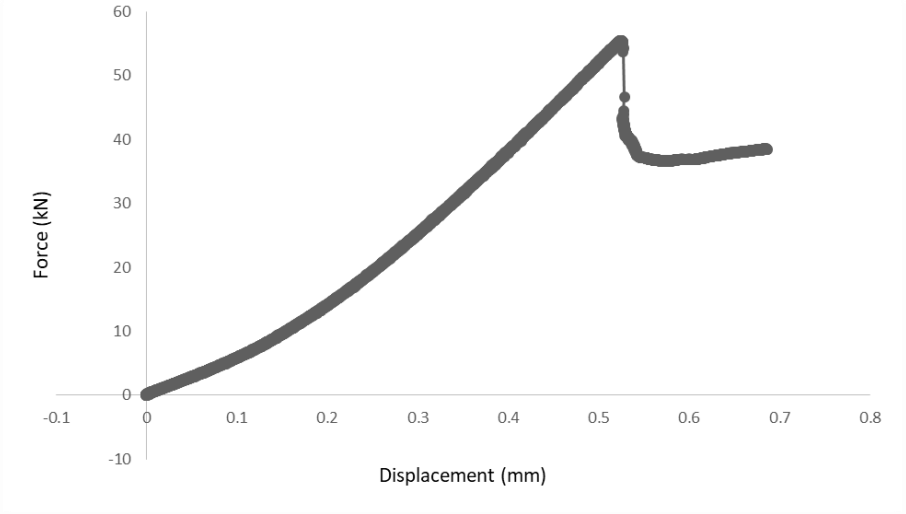

Figure 0.27. Flattened Brazilian Disc test graph of S140_s1

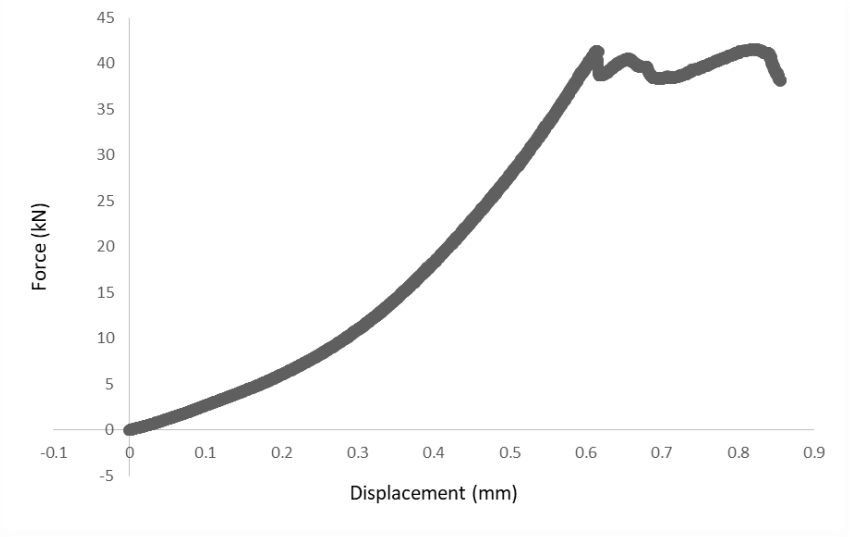

Figure 0.28. Flattened Brazilian Disc test graph of S140_s2

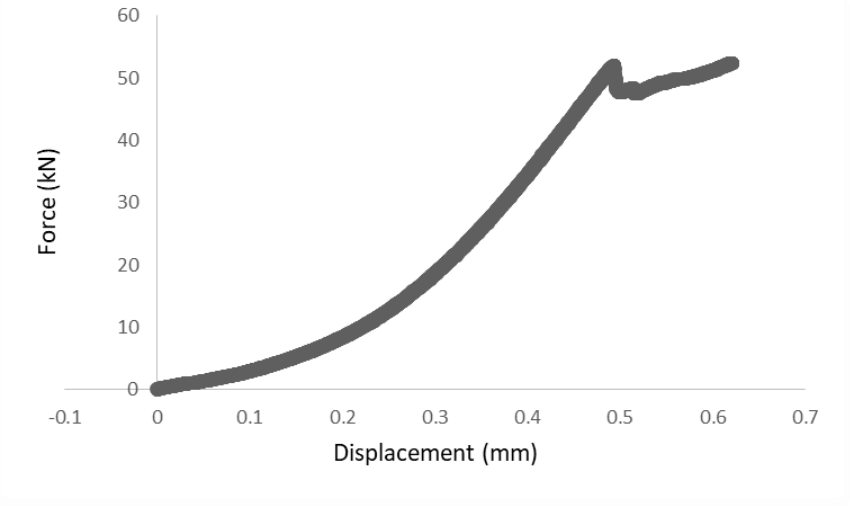

Figure 0.29. Flattened Brazilian Disc test graph of S140_s3

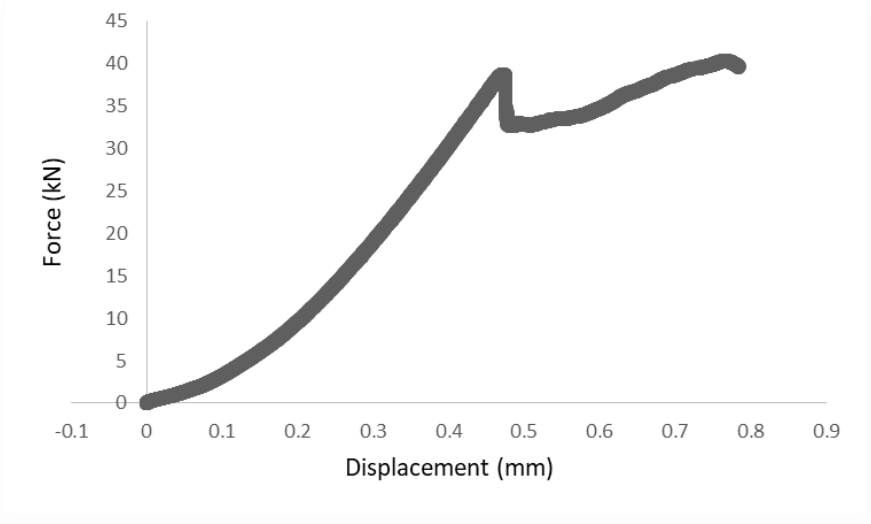

Figure 0.30. Flattened Brazilian Disc test graph of S140_s4

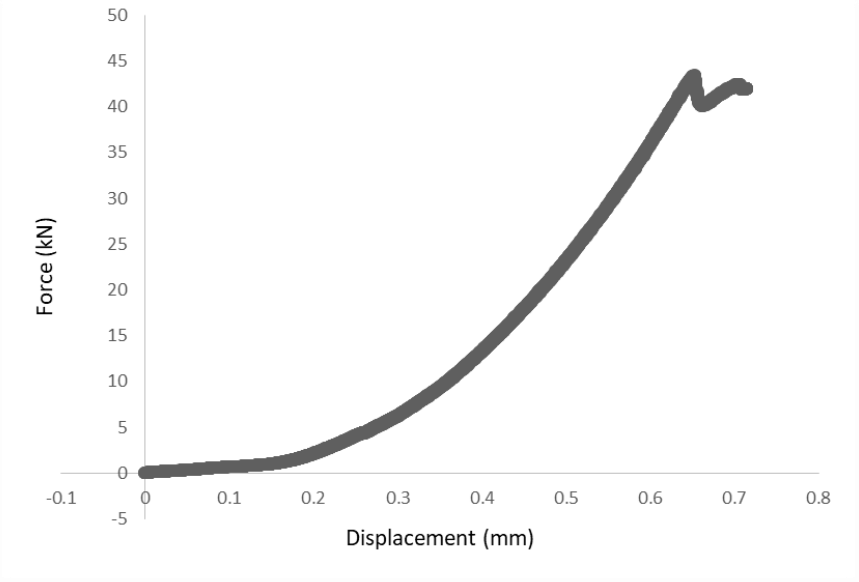

Figure 0.31. Flattened Brazilian Disc test graph of S140_s5

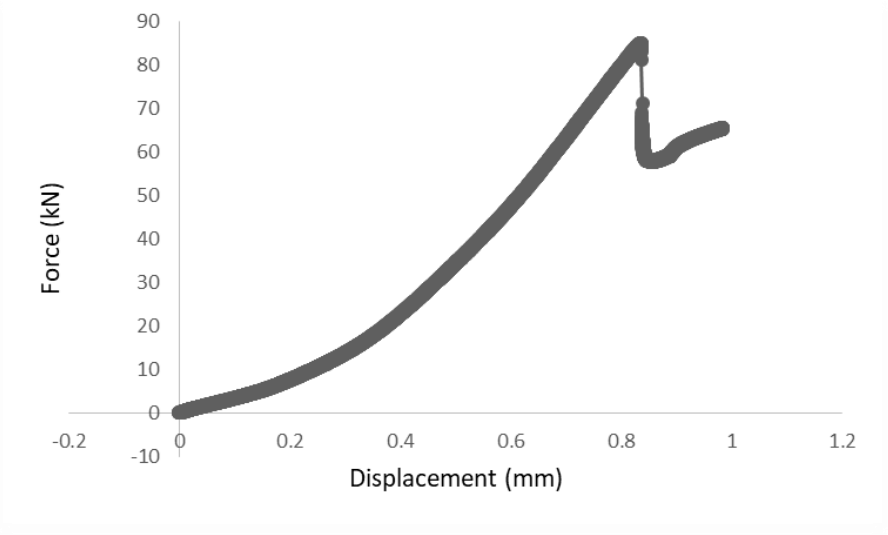

Figure 0.32. Flattened Brazilian Disc test graph of S160_s1

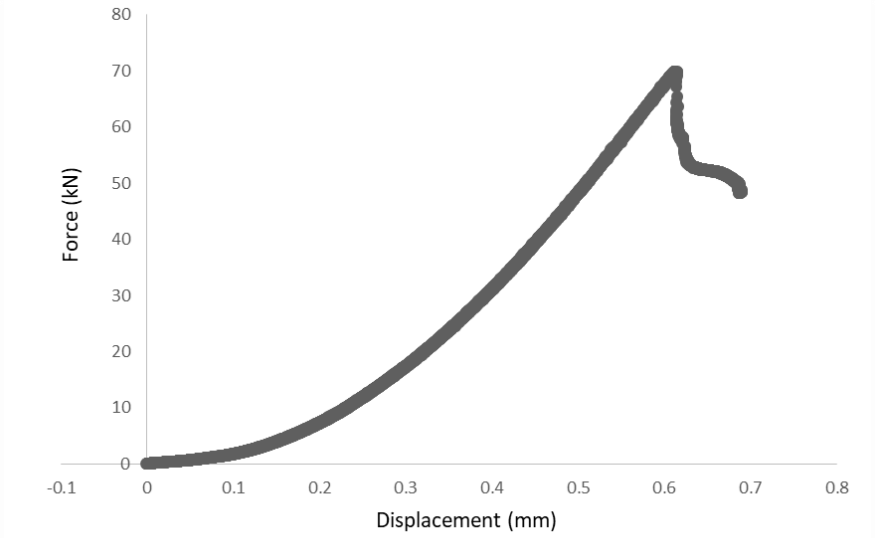

Figure 0.33. Flattened Brazilian Disc test graph of S160_s2

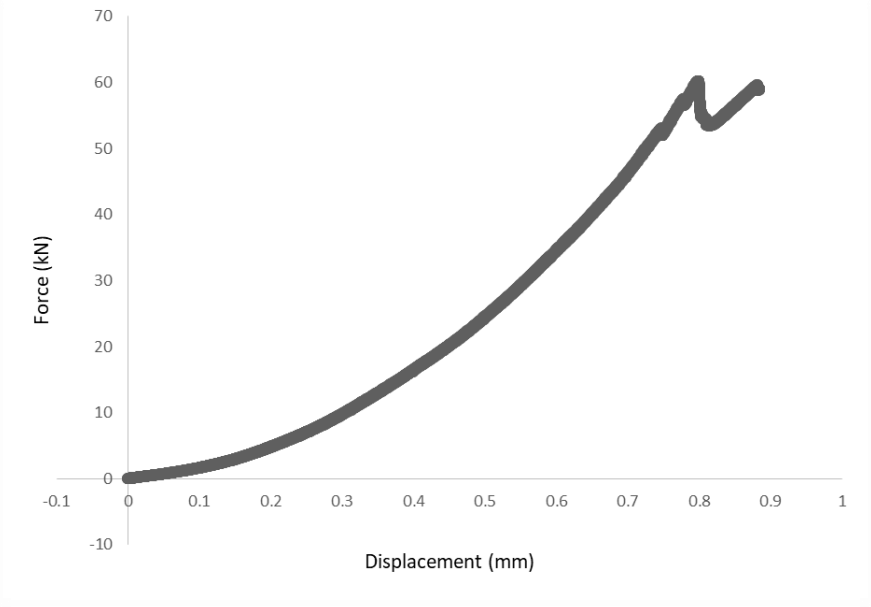

Figure 0.34. Flattened Brazilian Disc test graph of S160_s3

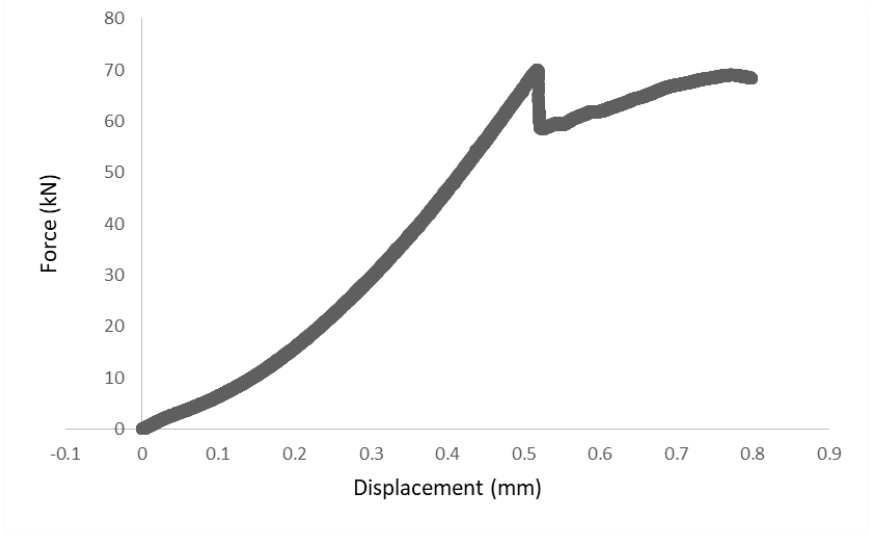

Figure 0.35. Flattened Brazilian Disc test graph of S160_s4

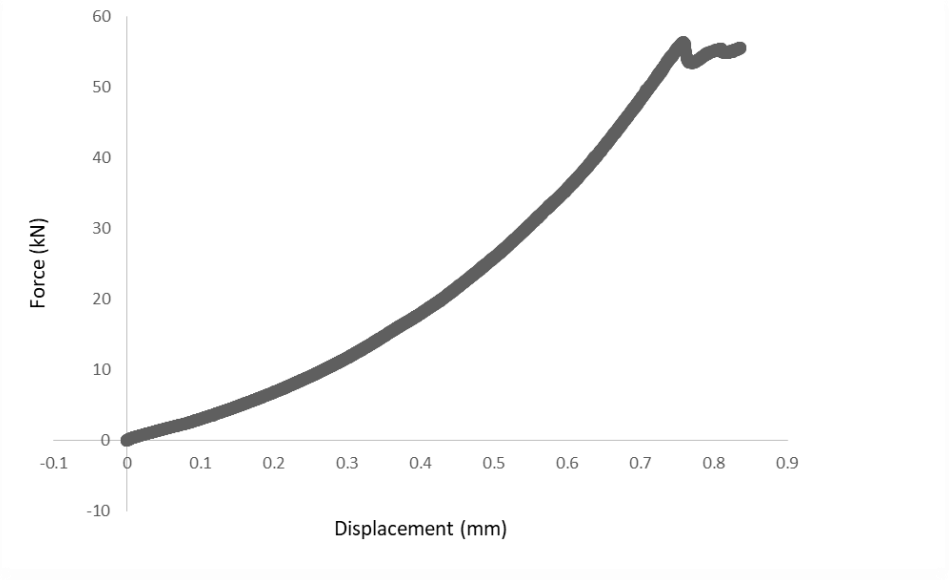

Figure 0.36. Flattened Brazilian Disc test graph of S160_s5

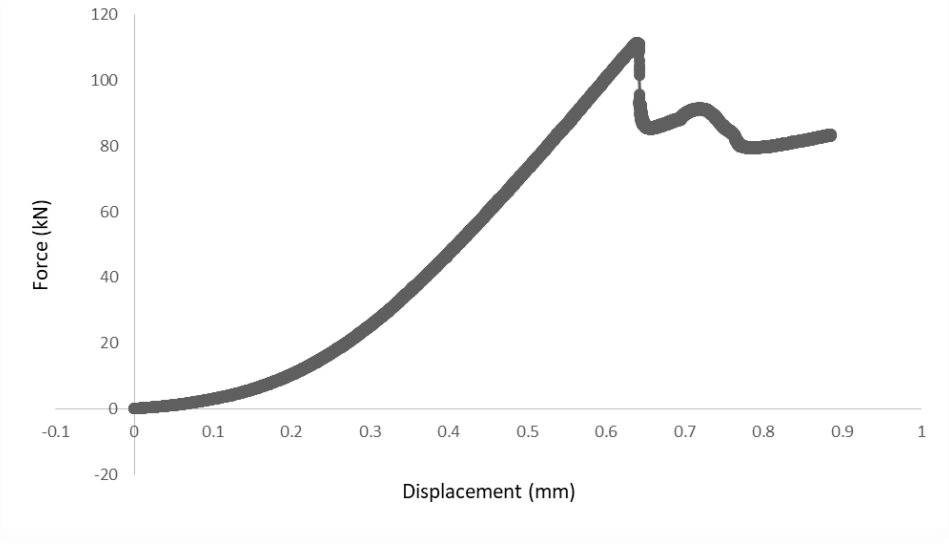

Figure 0.37. Flattened Brazilian Disc test graph of S180_s1

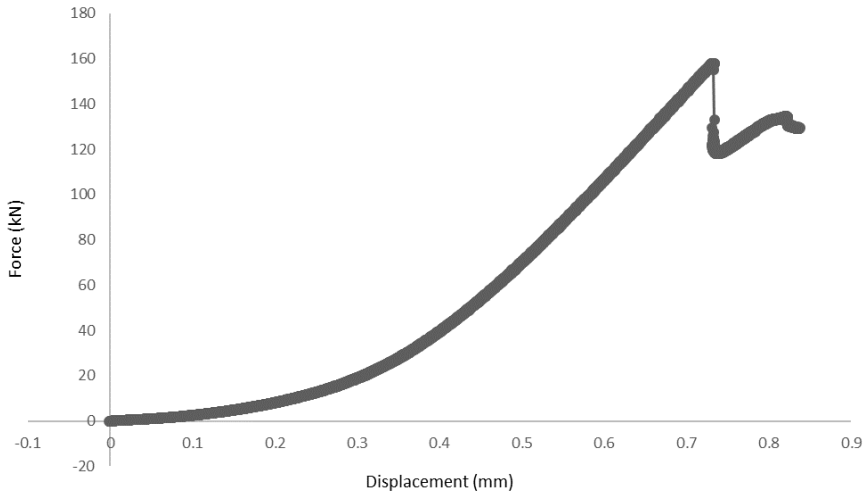

Figure 0.38. Flattened Brazilian Disc test graph of S180_s2

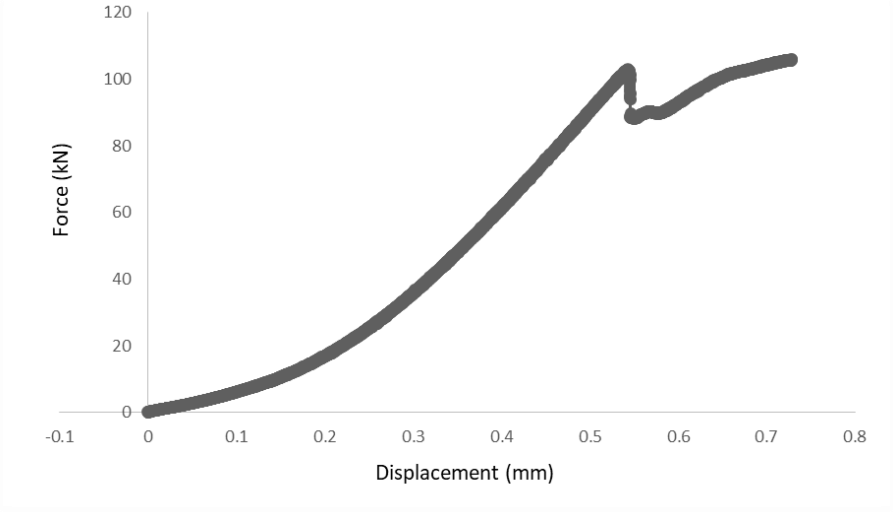

Figure 0.39. Flattened Brazilian Disc test graph of S180_s3

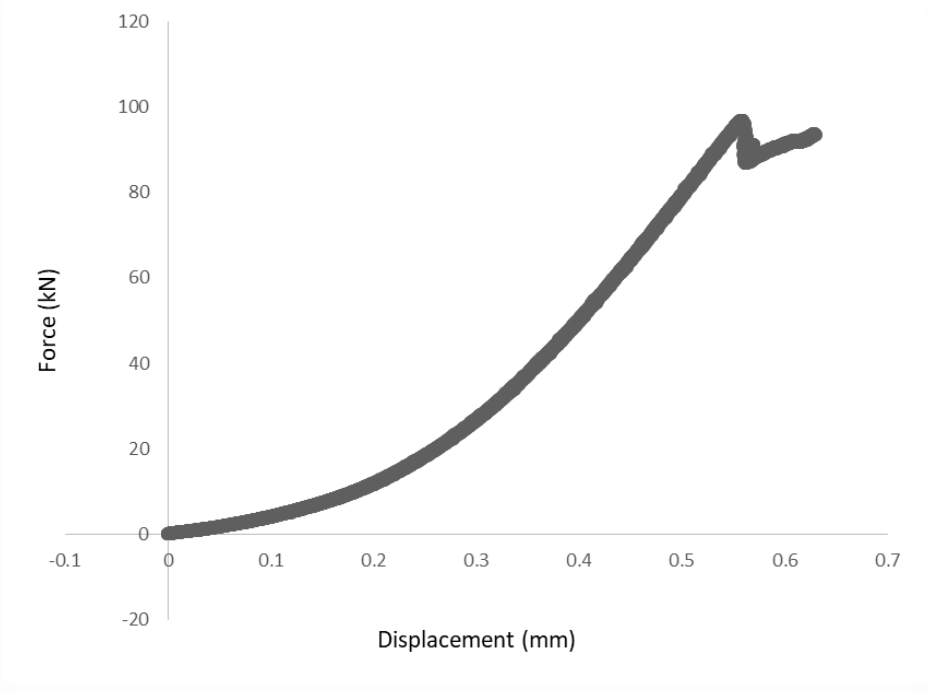

Figure 0.40. Flattened Brazilian Disc test graph of S180_s4

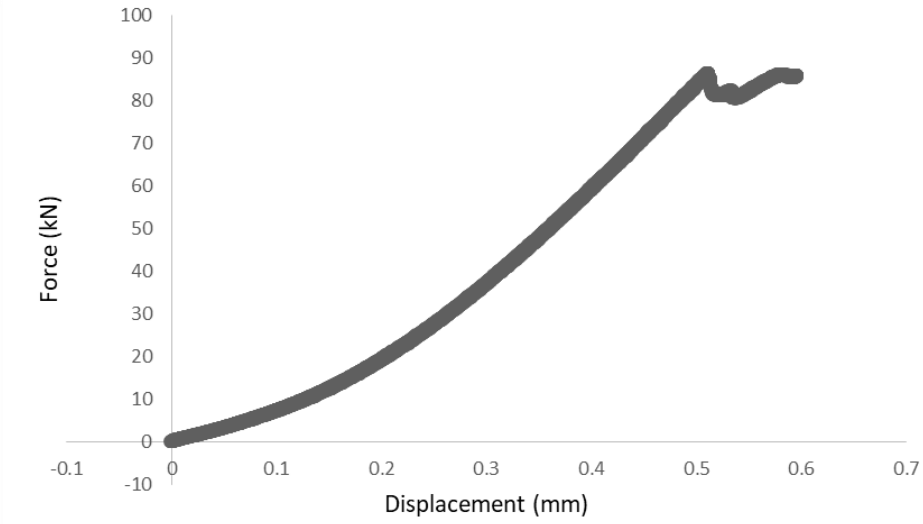

Figure 0.41. Flattened Brazilian Disc test graph of S180_s5

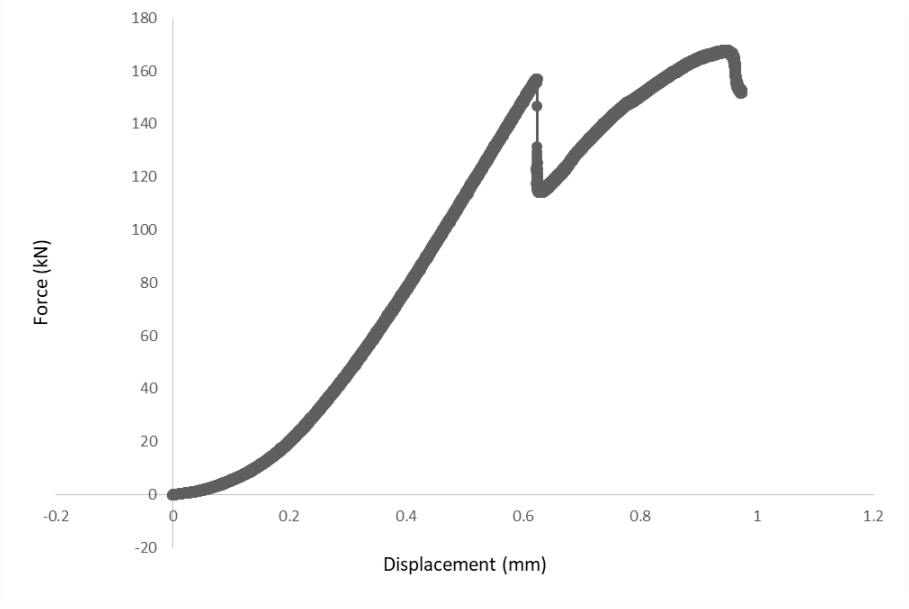

Figure 0.42. Flattened Brazilian Disc test graph of S200_s1

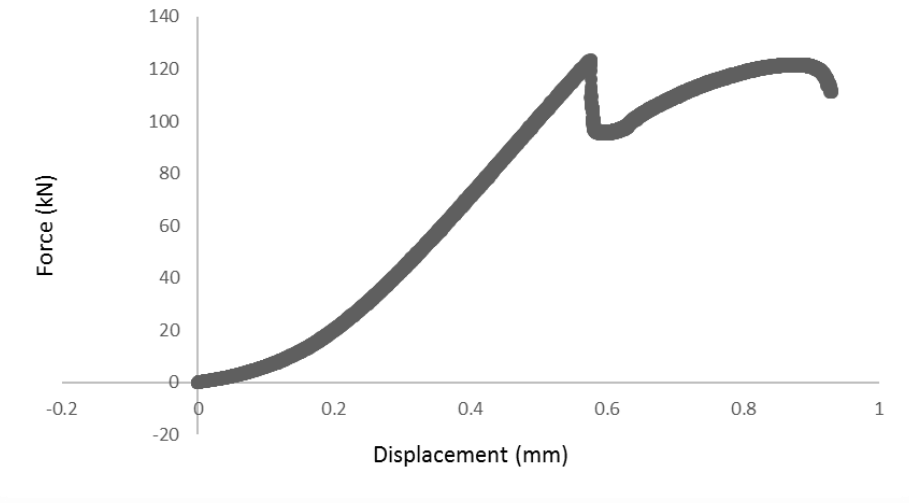

Figure 0.43. Flattened Brazilian Disc test graph of S200_s2

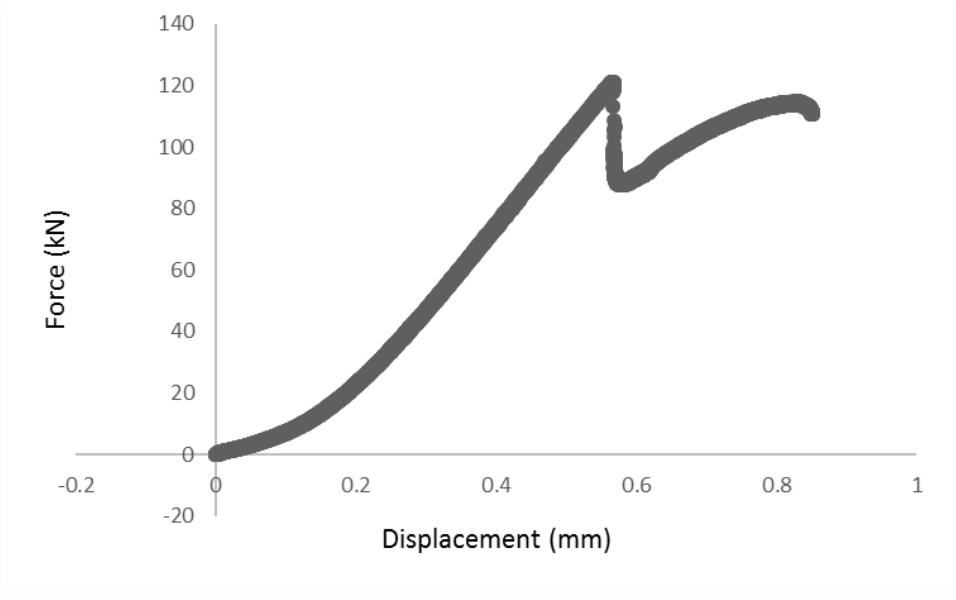

Figure 0.44. Flattened Brazilian Disc test graph of S200_s3

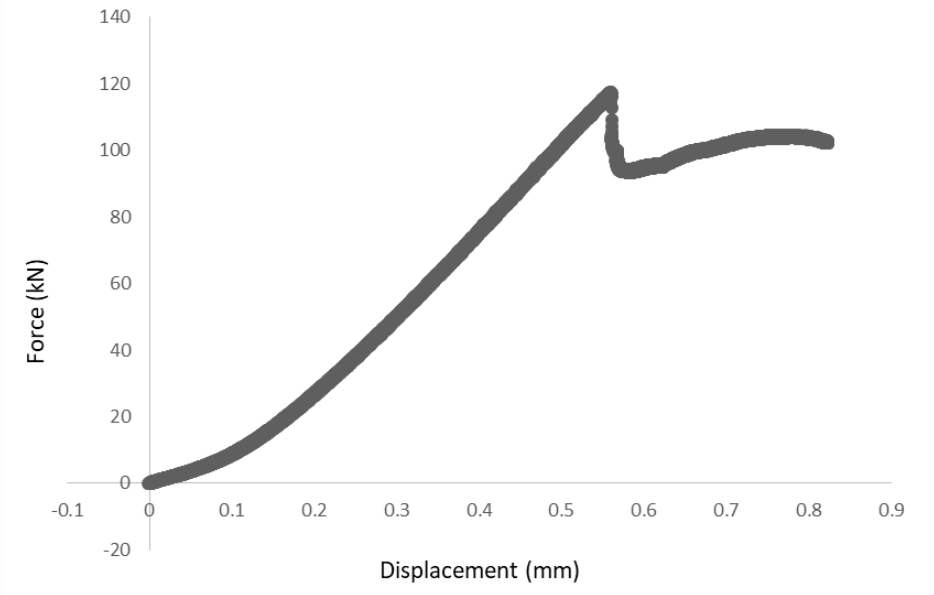

Figure 0.45. Flattened Brazilian Disc test graph of S200_s4

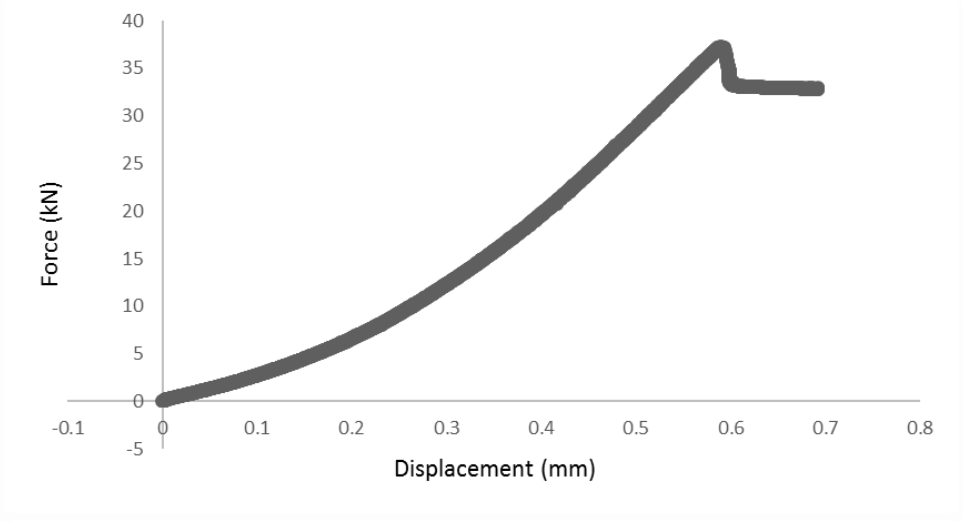

Figure 0.46. Flattened Brazilian Disc test graph of S160-1D-s1

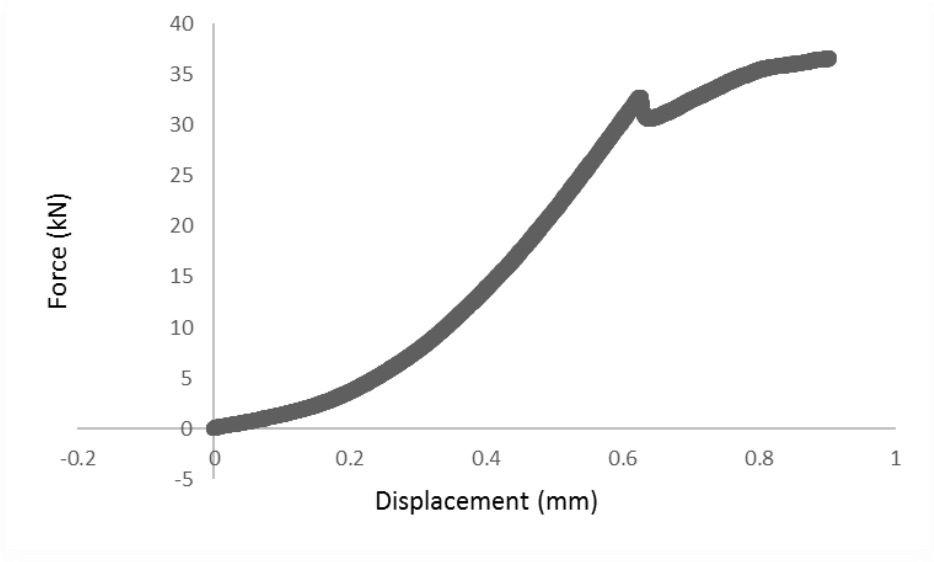

Figure 0.47. Flattened Brazilian Disc test graph of S160-1D-s2

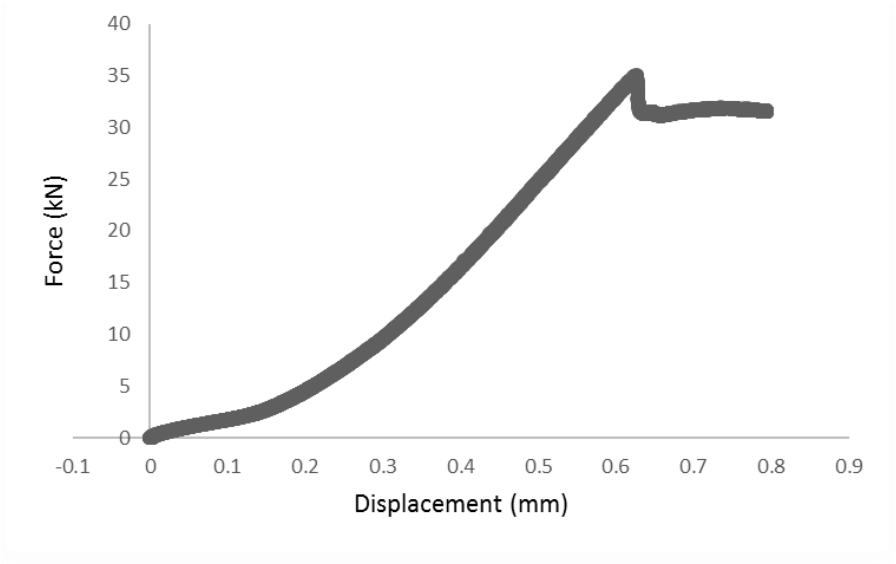

Figure 0.48. Flattened Brazilian Disc test graph of S160-1D-s3

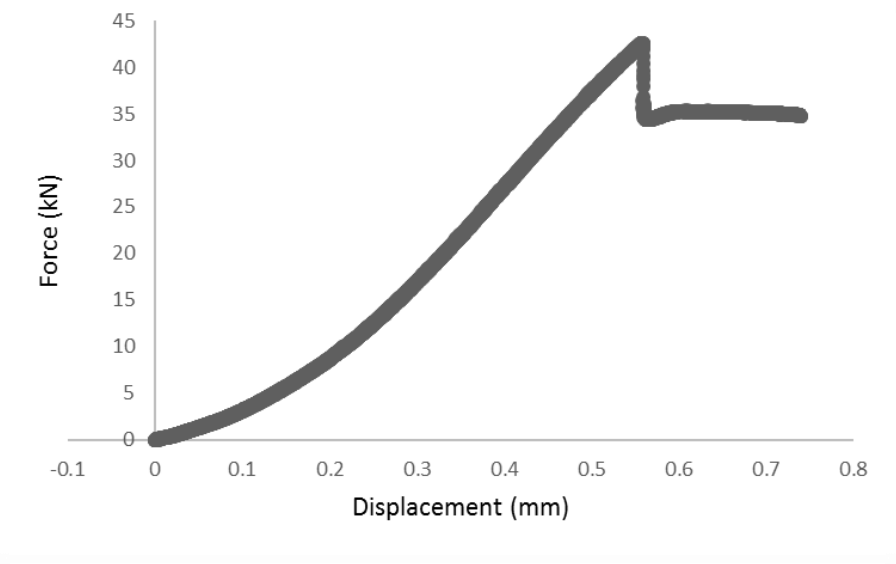

Figure 0.49. Flattened Brazilian Disc test graph of S160-1D-s4

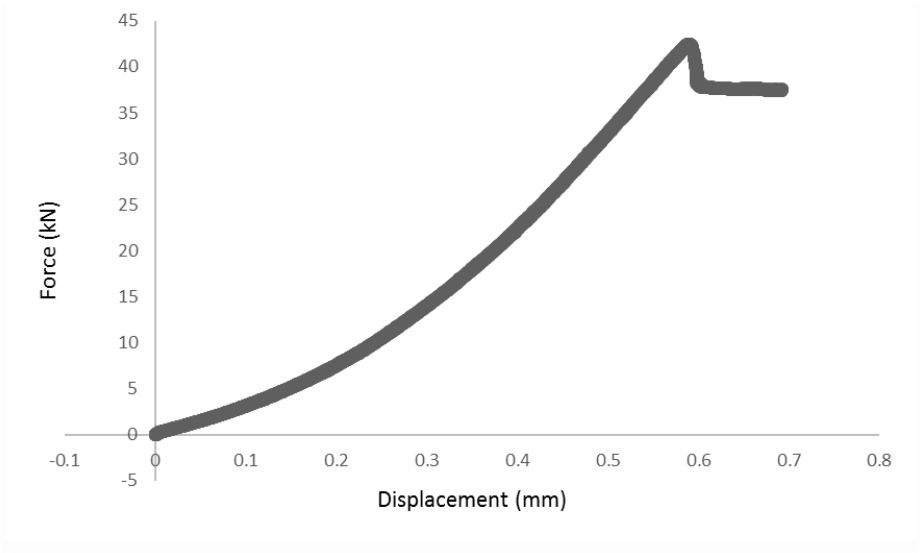

Figure 0.50. Flattened Brazilian Disc test graph of S160-2D-s1

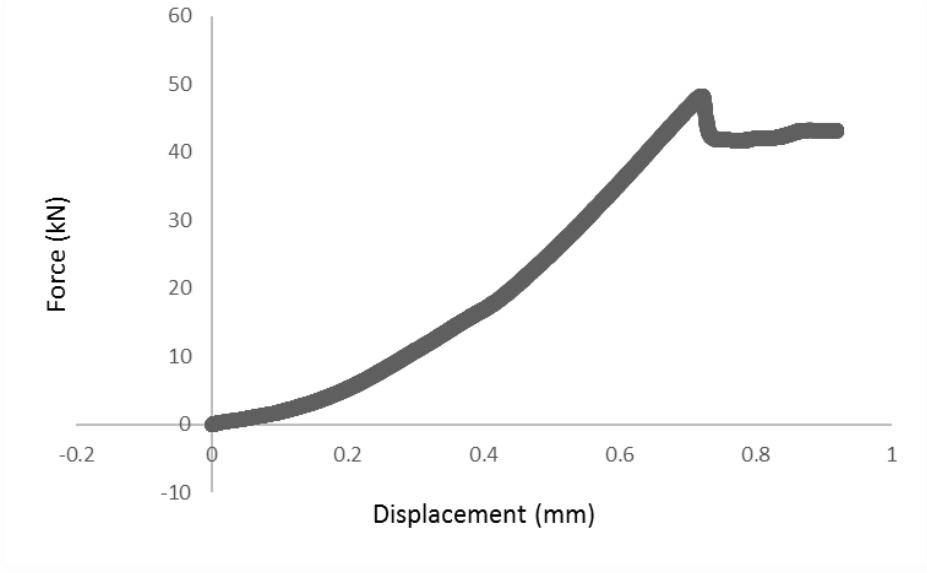

Figure 0.51. Flattened Brazilian Disc test graph of S160-2D-s2

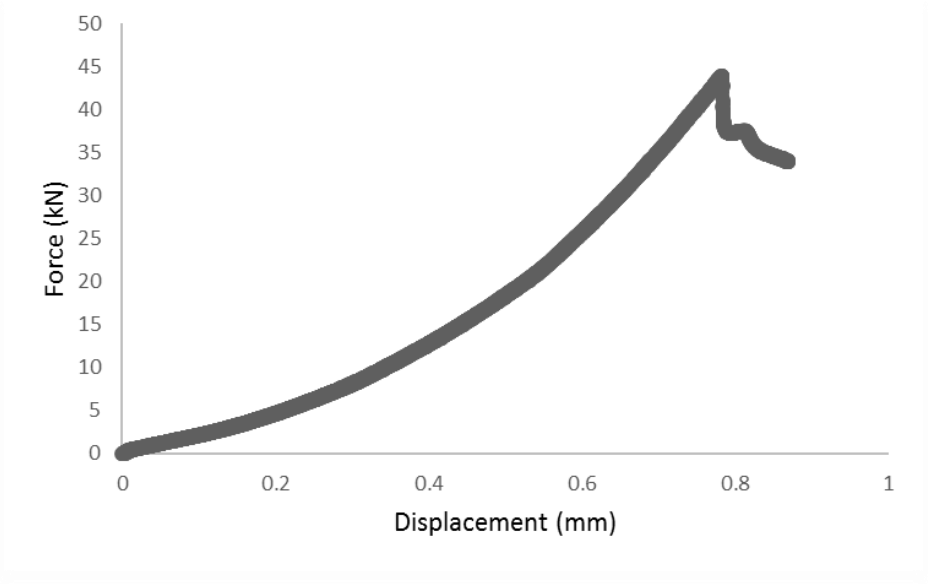

Figure 0.52. Flattened Brazilian Disc test graph of S160-2D-s3

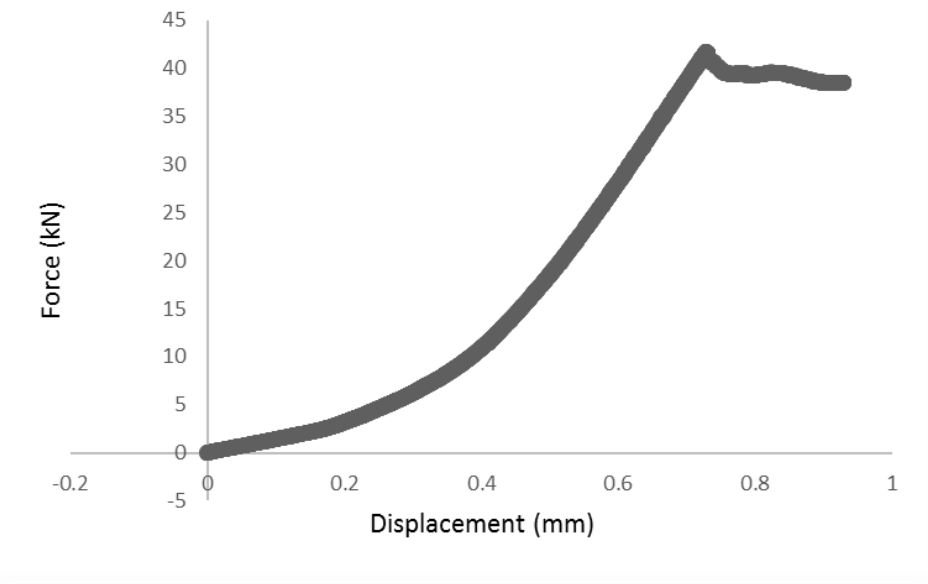

Figure 0.53. Flattened Brazilian Disc test graph of S160-2D-s4

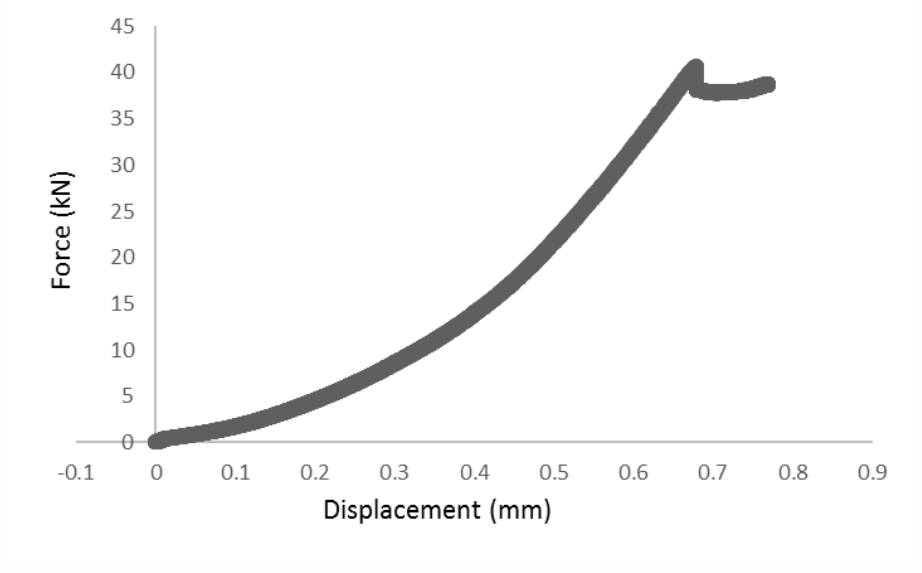

Figure 0.54. Flattened Brazilian Disc test graph of S160-3D-s1

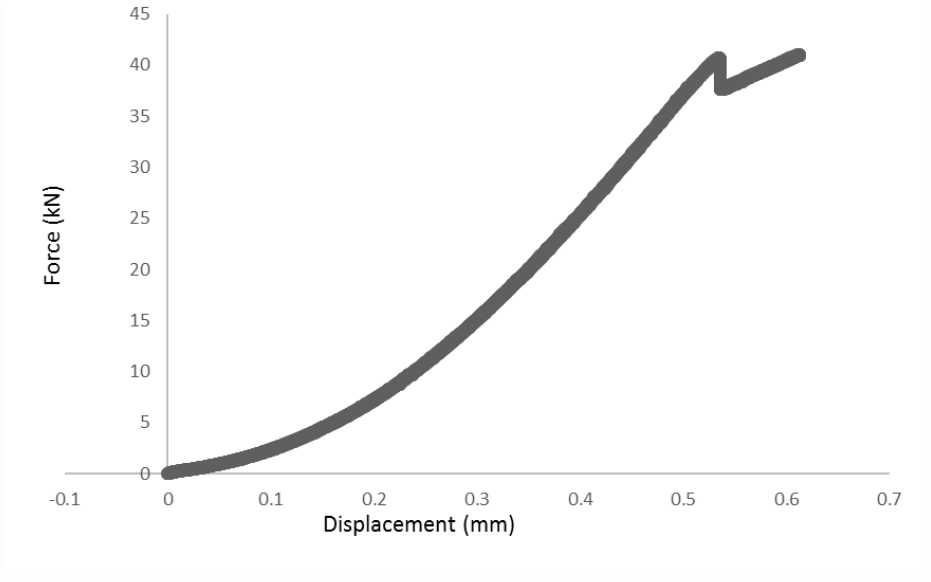

Figure 0.55. Flattened Brazilian Disc test graph of S160-3D-s2

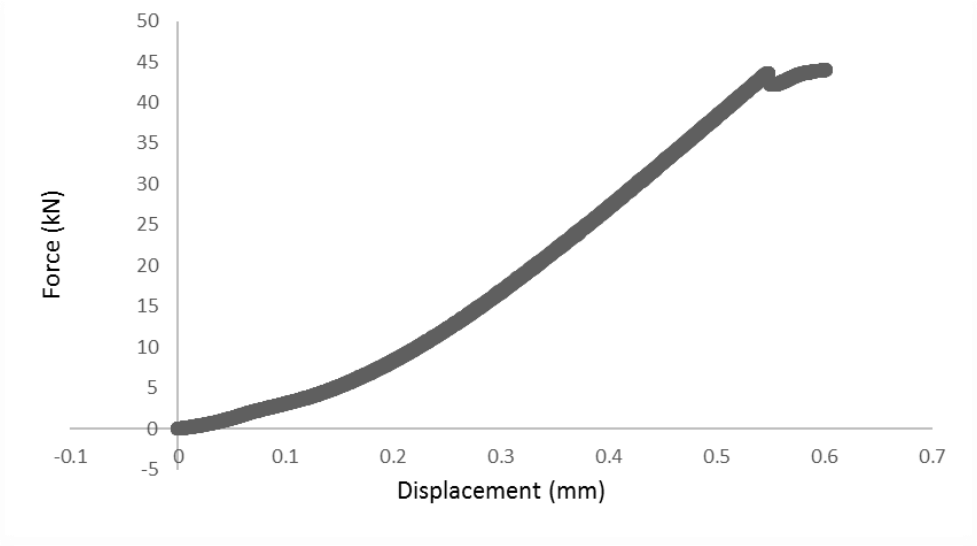

Figure 0.56. Flattened Brazilian Disc test graph of S160-3D-s3

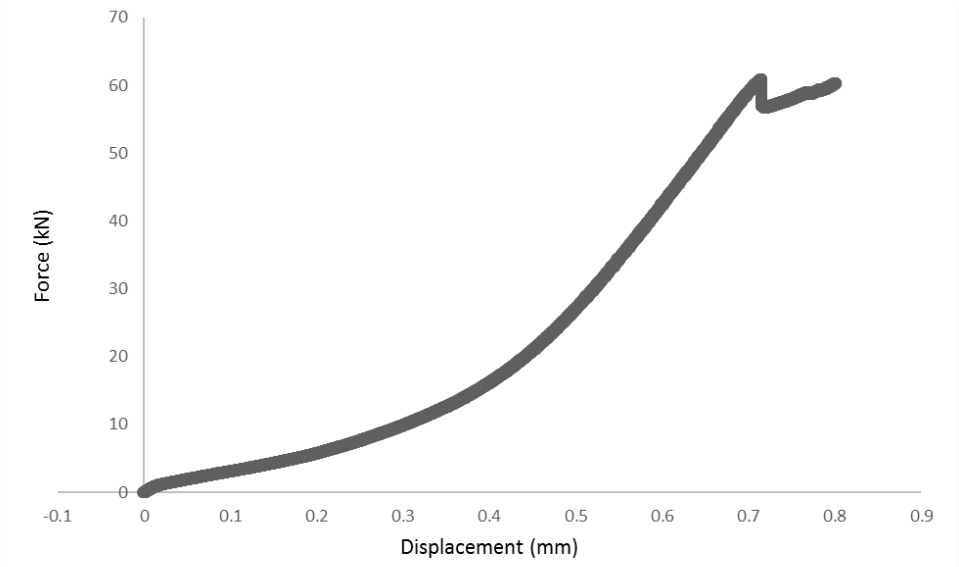

Figure 0.57. Flattened Brazilian Disc test graph of S160-5D-s1

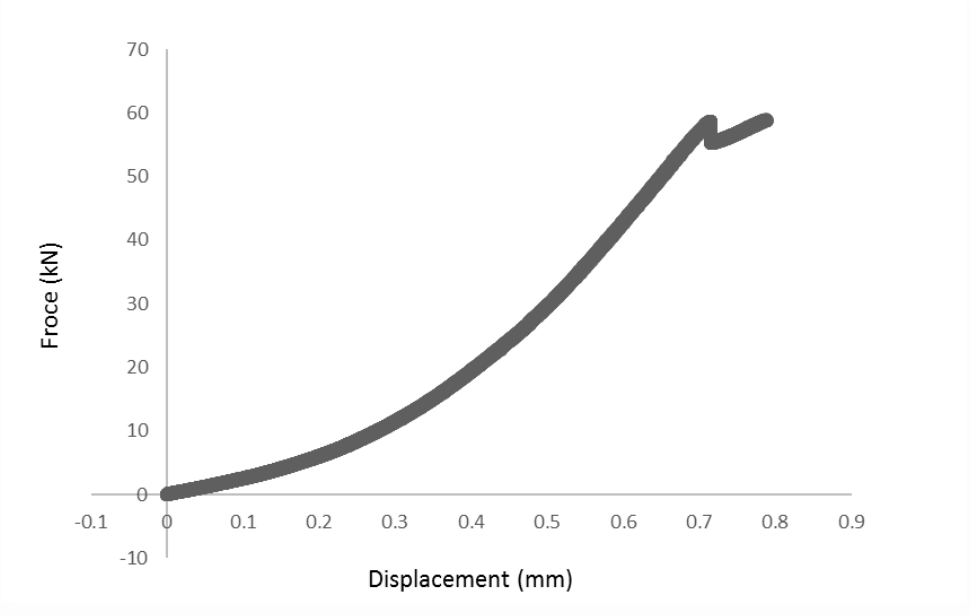

Figure 0.58. Flattened Brazilian Disc test graph of S160-5D-s2

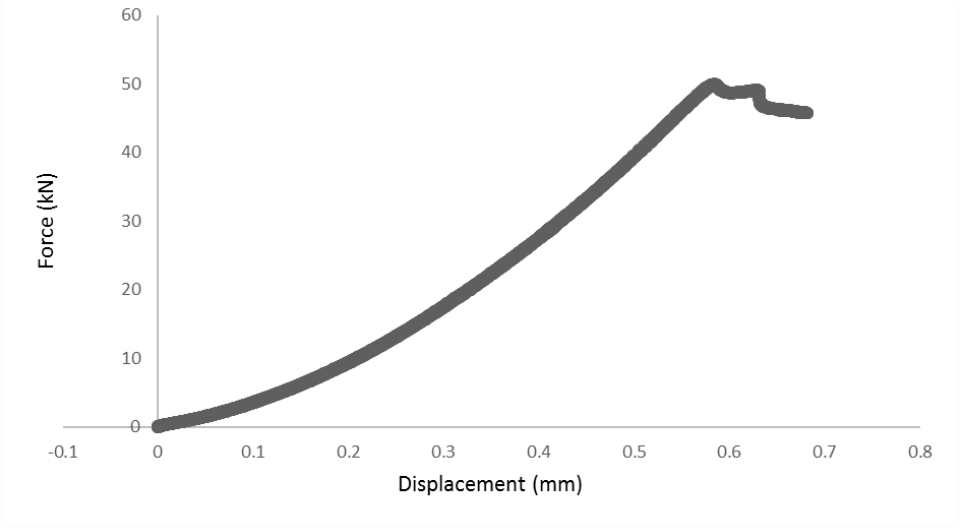

Figure 0.59. Flattened Brazilian Disc test graph of S160-5D-s3

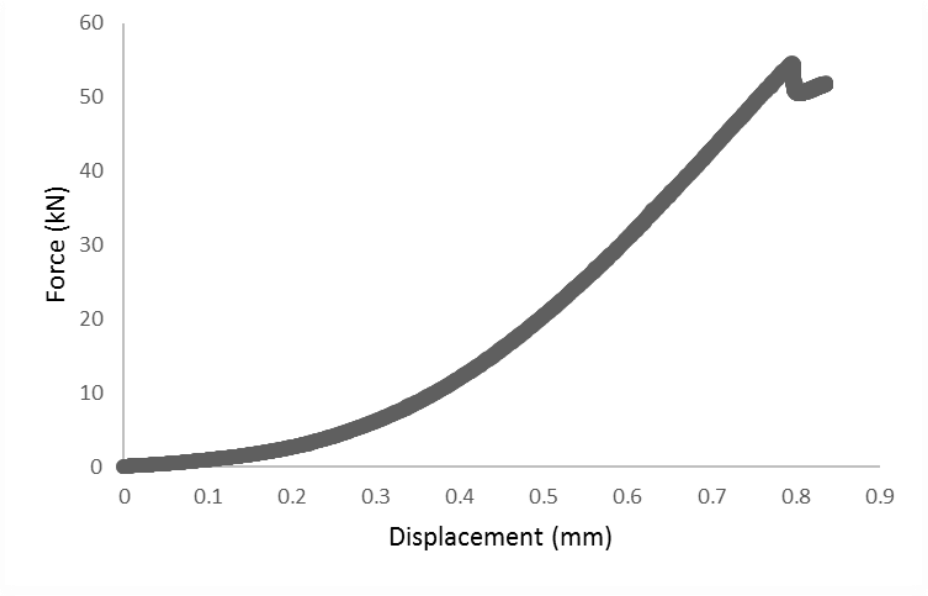

Figure 0.60. Flattened Brazilian Disc test graph of S160-5D-s4

C. Crack Length Measurement of Mode I Fracture Toughness Test Samples

Figure 0.61. FBD test crack measurement of the sample S100_s1

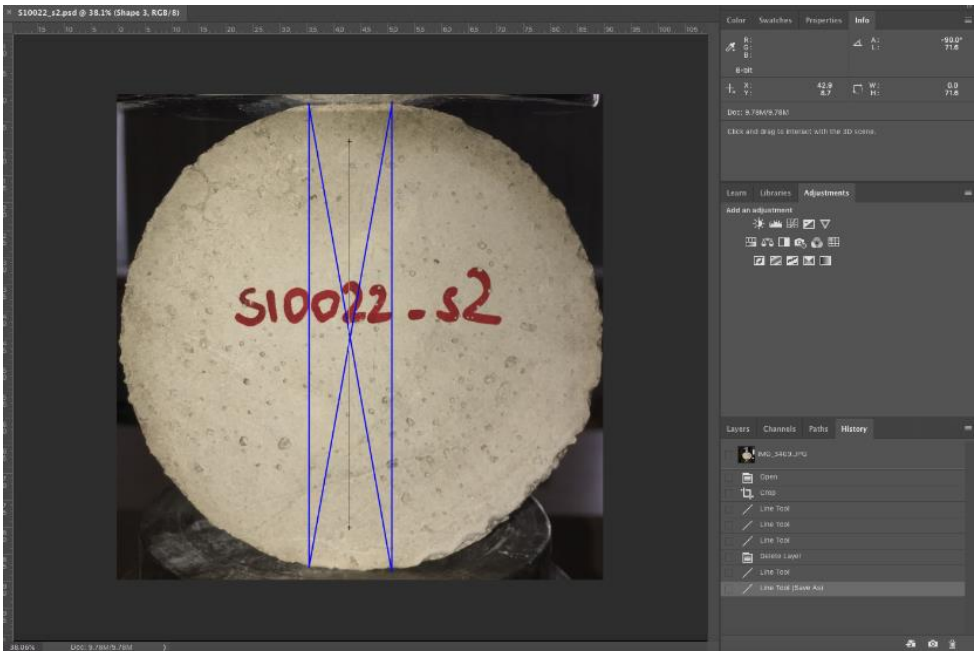

Figure 0.62. FBD test crack measurement of the sample S100_s2

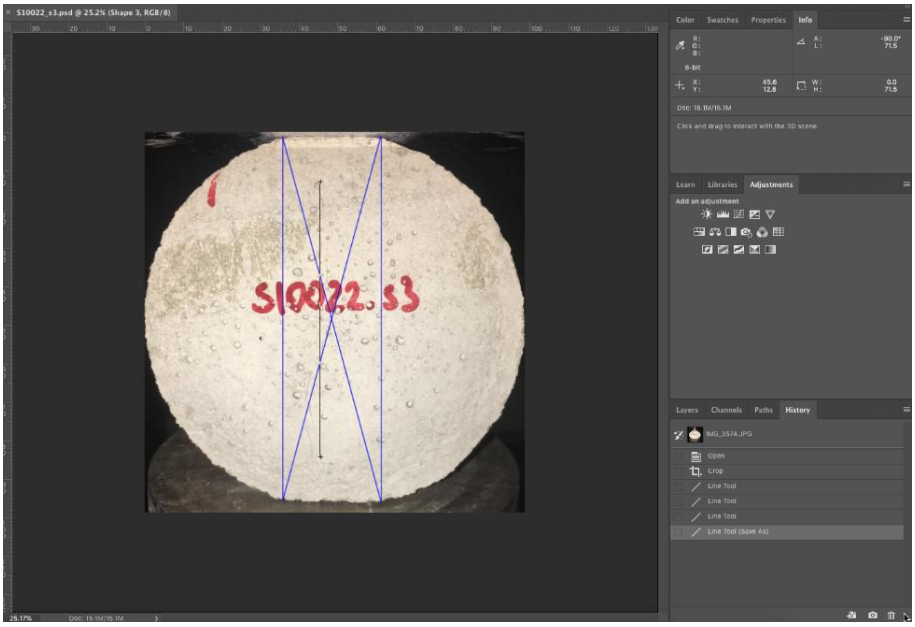

Figure 0.63. FBD test crack measurement of the sample S100_s3

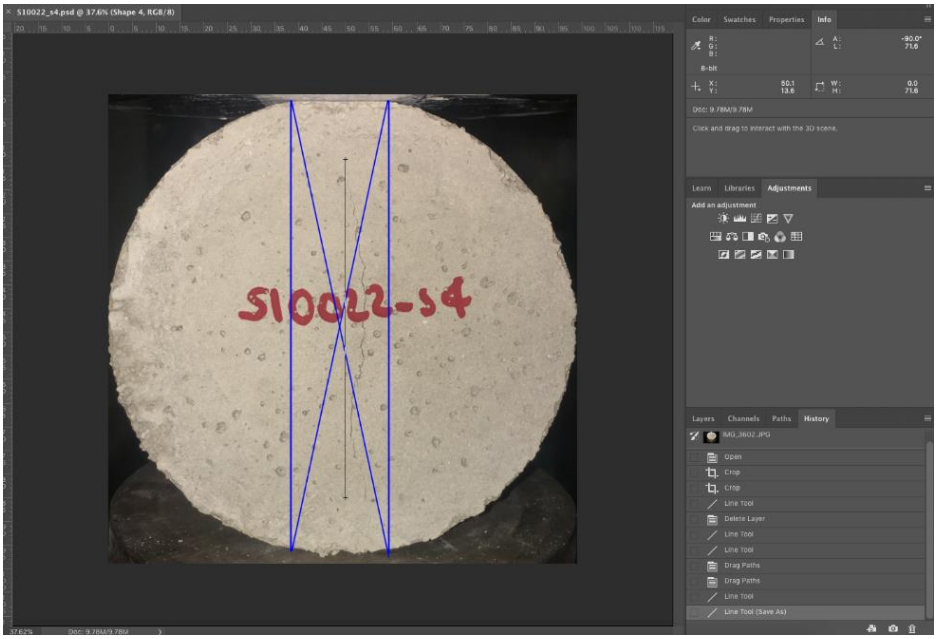

Figure 0.64. FBD test crack measurement of the sample S100_s4

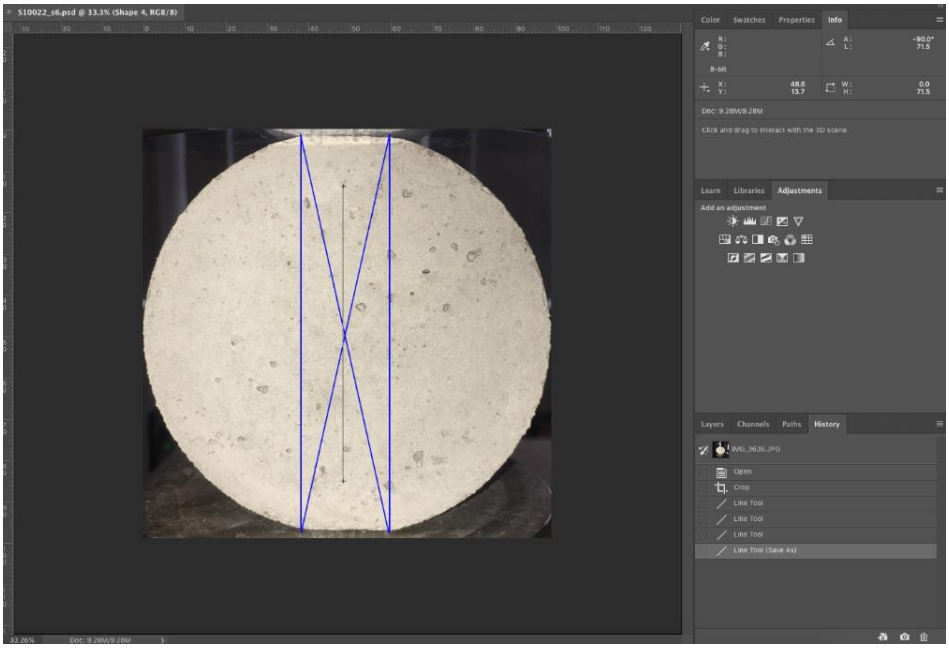

Figure 0.65. FBD test crack measurement of the sample S100_s5

Figure 0.66. FBD test crack measurement of the sample S120_s1

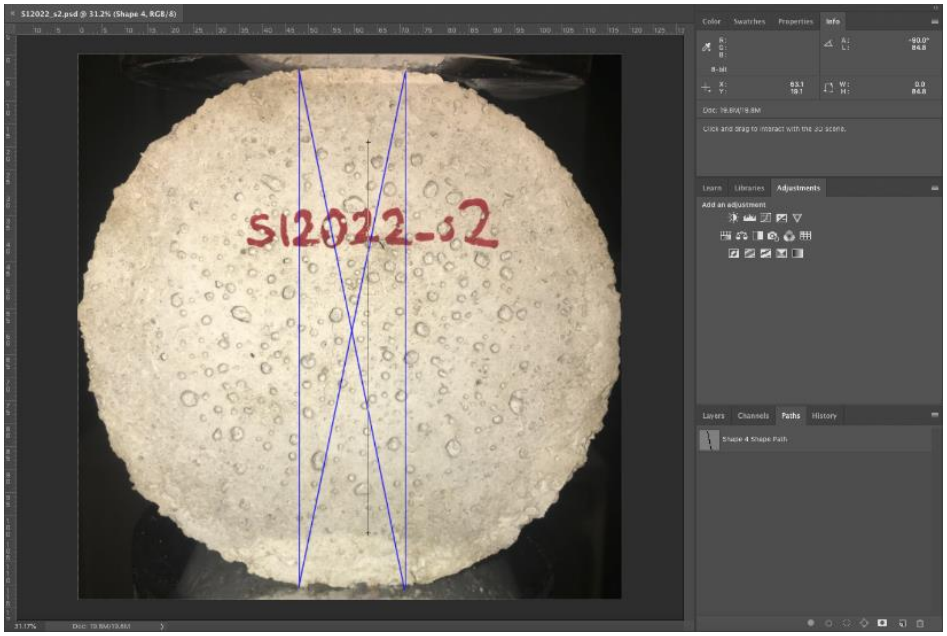

Figure 0.67. FBD test crack measurement of the sample S120_s2

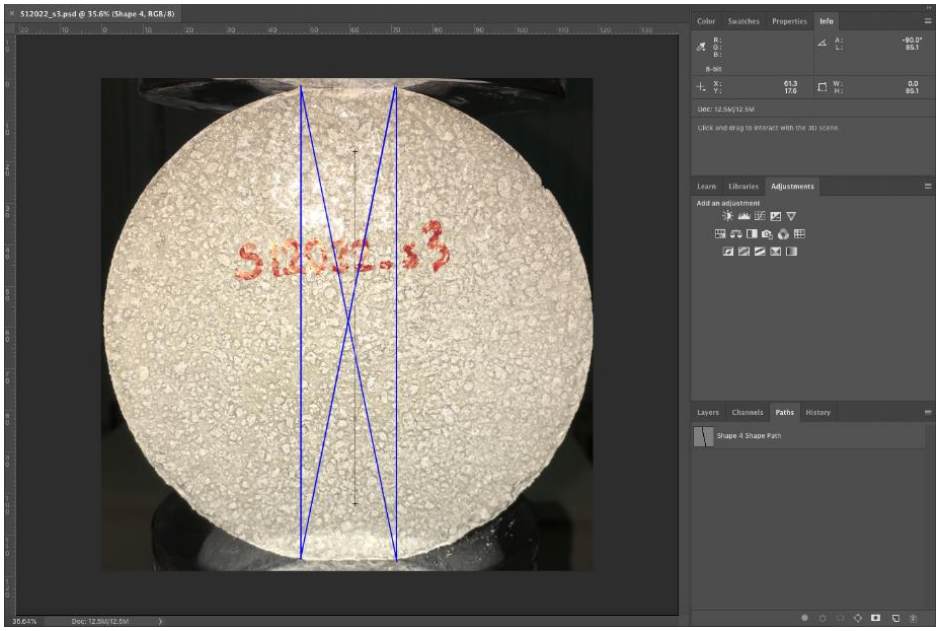

Figure 0.68. FBD test crack measurement of the sample S120_s3

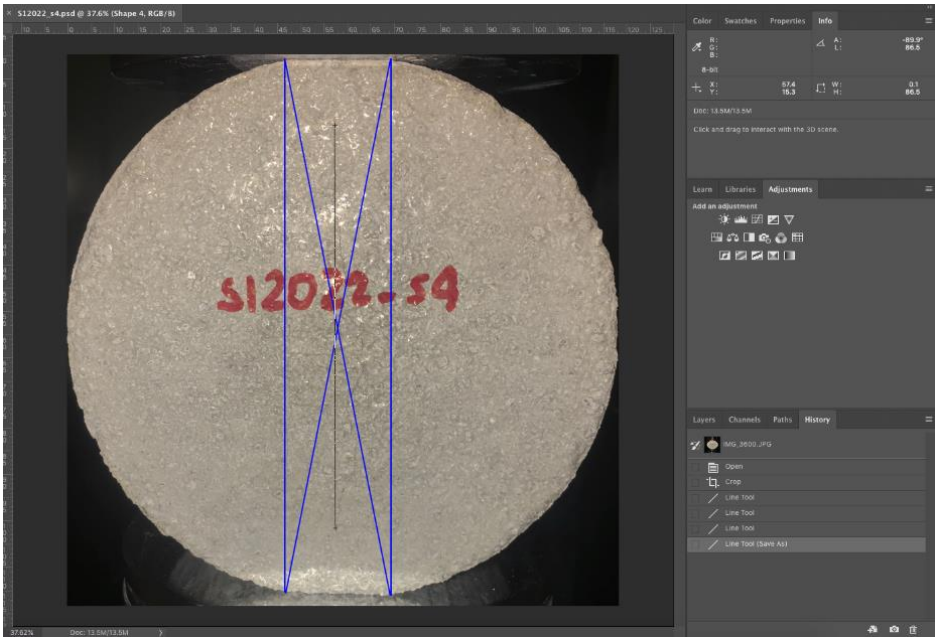

Figure 0.69. FBD test crack measurement of the sample S120_s4

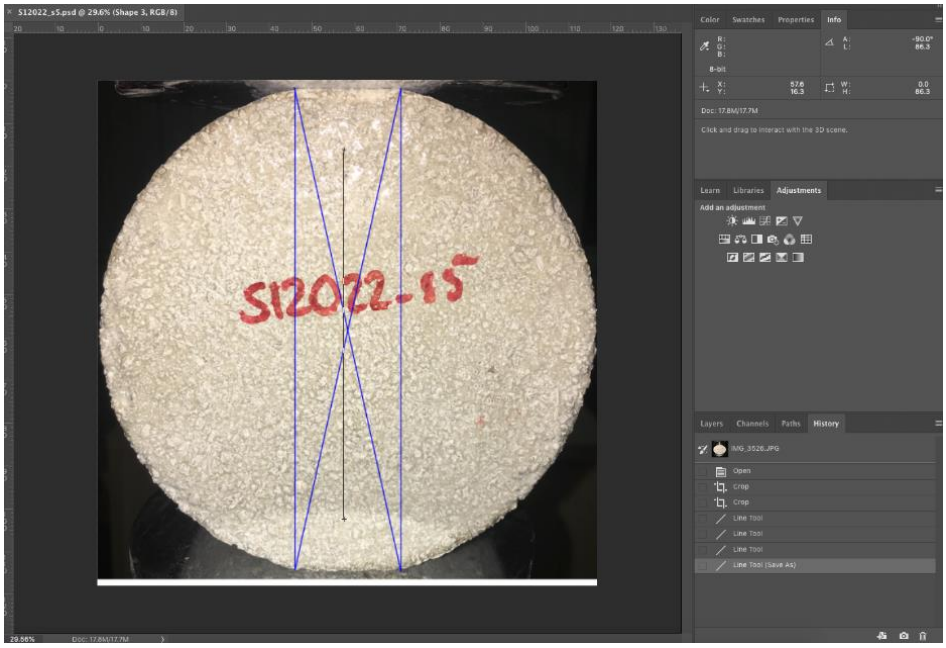

Figure 0.70. FBD test crack measurement of the sample S120_s5

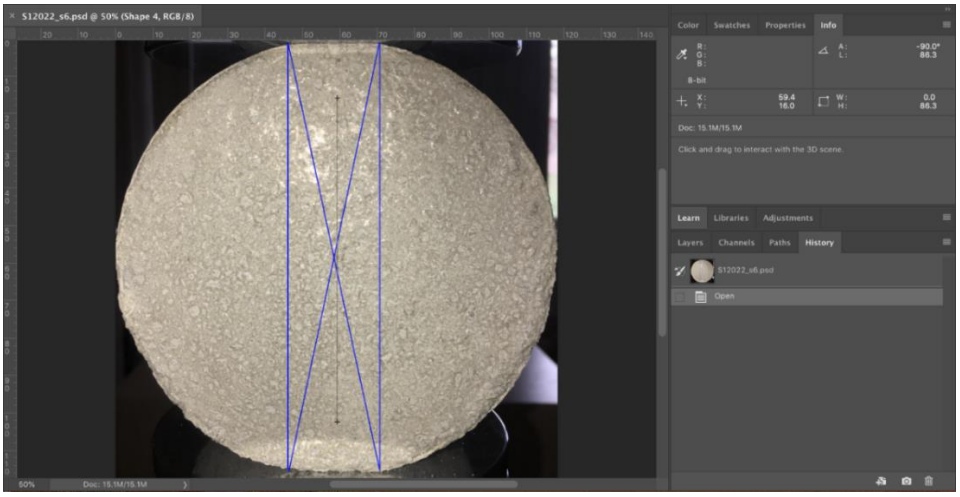

Figure 0.71. FBD test crack measurement of the sample S120_s6

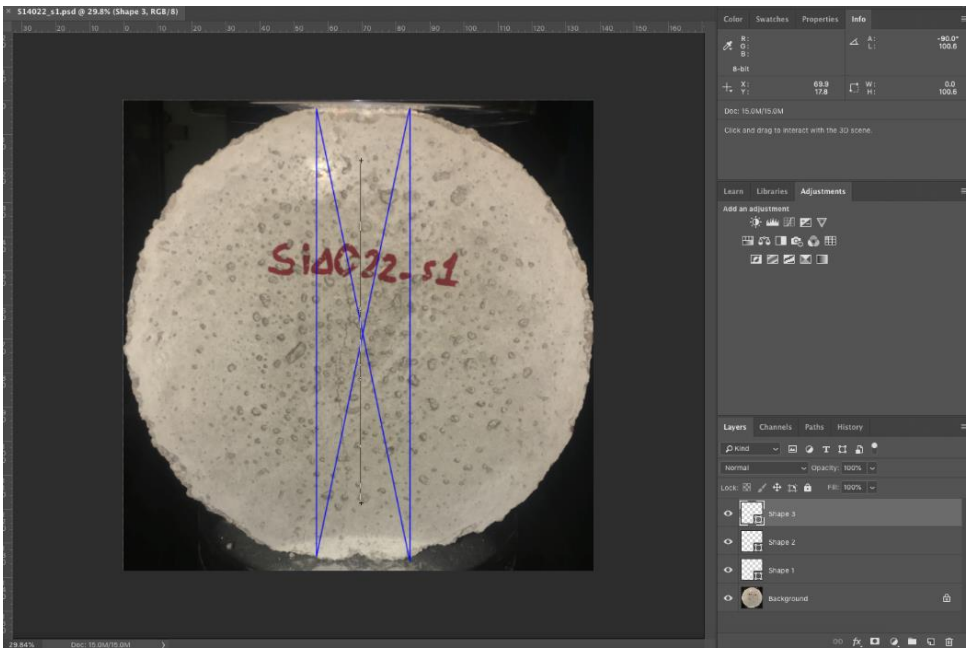

Figure 0.72. FBD test crack measurement of the sample S140_s1

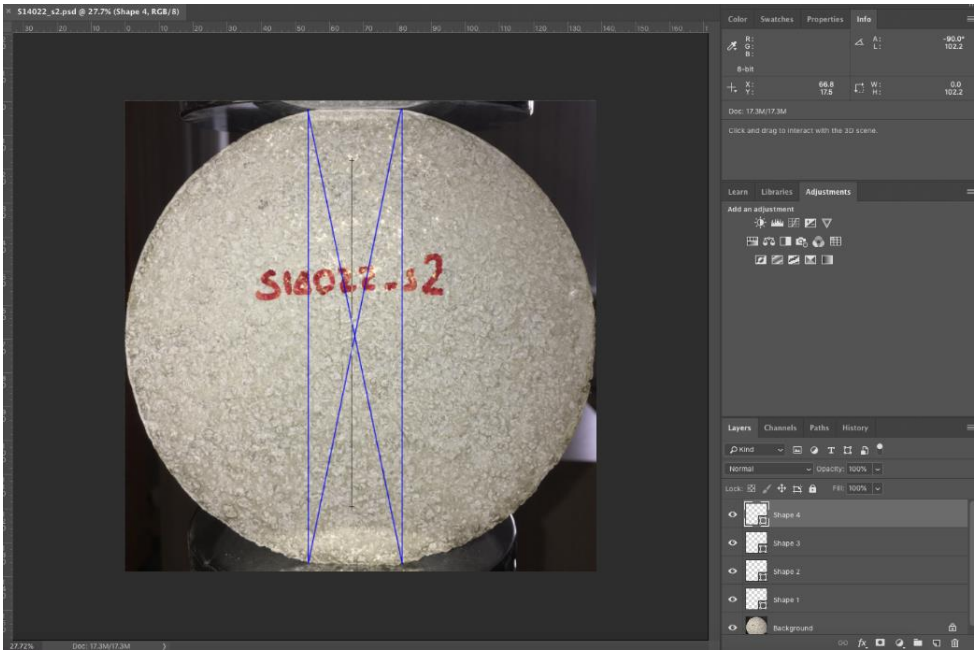

Figure 0.73. FBD test crack measurement of the sample S140_s2

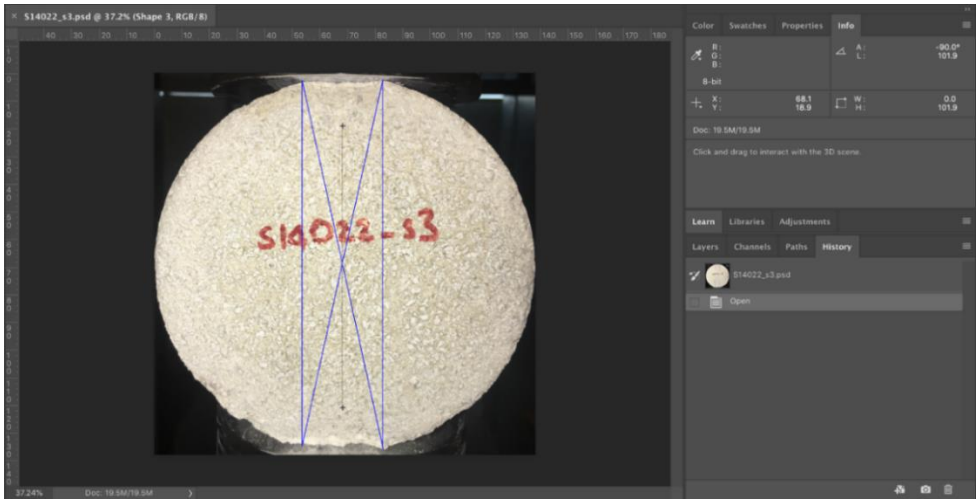

Figure 0.74. FBD test crack measurement of the sample S140_s3

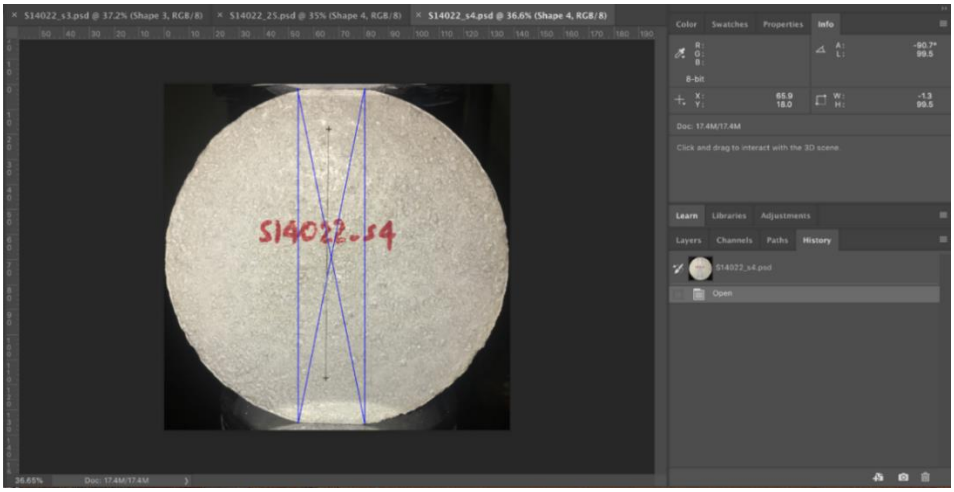

Figure 0.75. FBD test crack measurement of the sample S140_s4

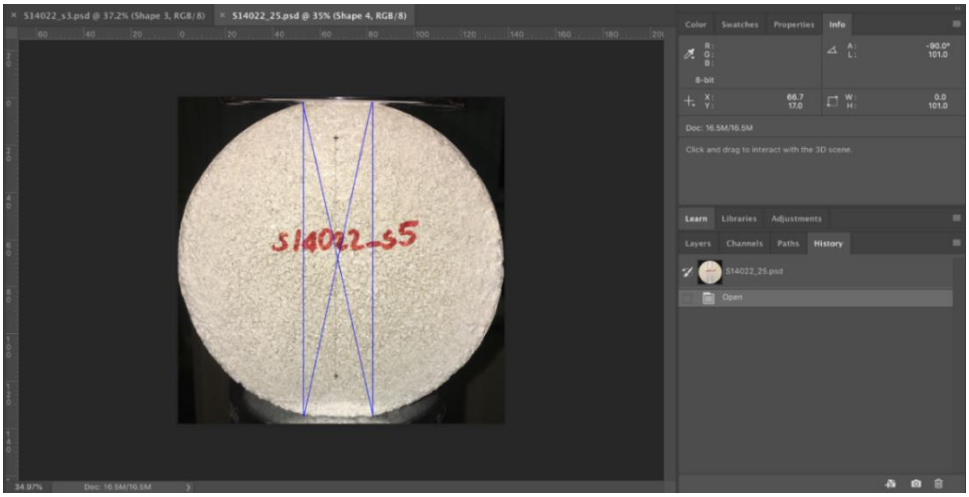

Figure 0.76. FBD test crack measurement of the sample S140_s5

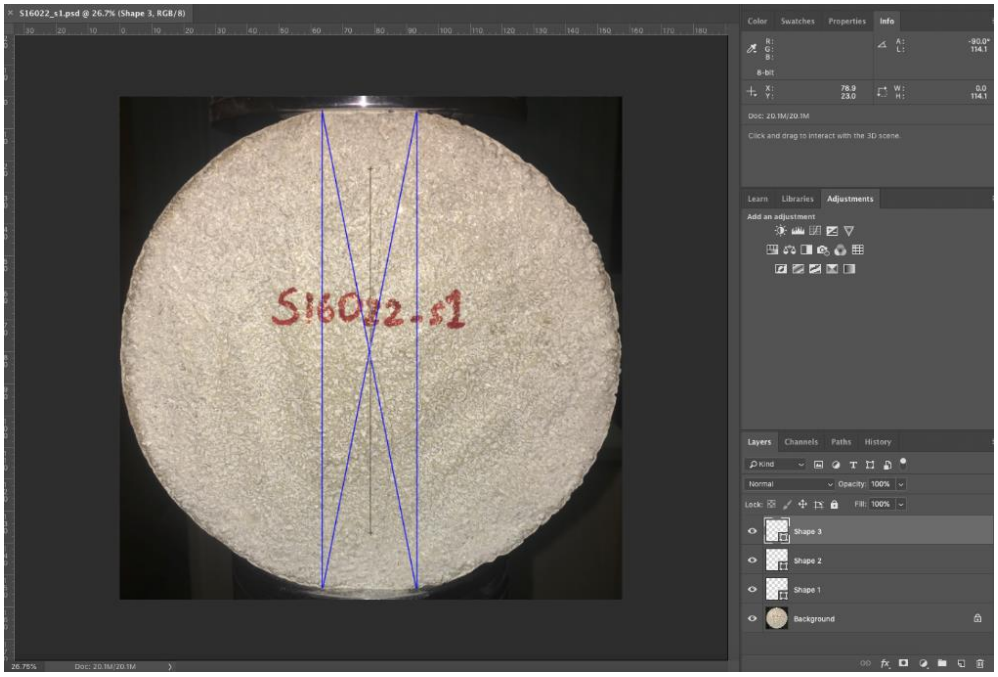

Figure 0.77. FBD test crack measurement of the sample S160_s1

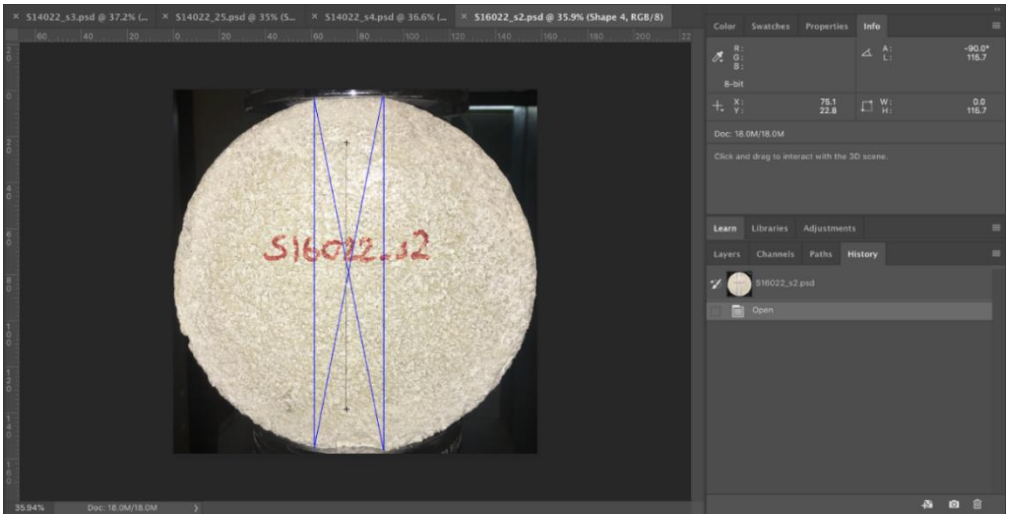

Figure 0.78. FBD test crack measurement of the sample S160_s2

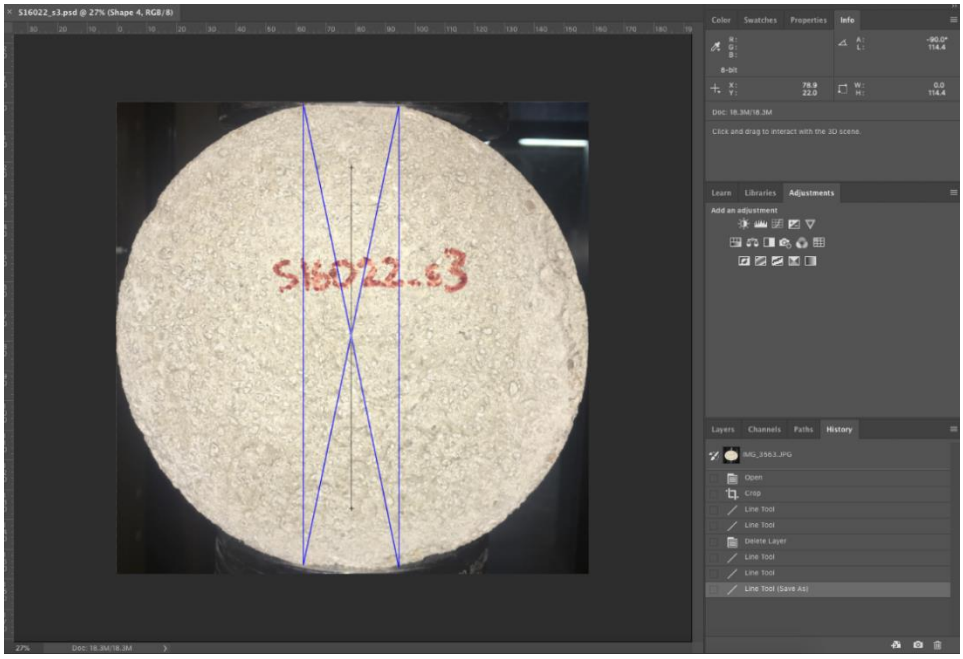

Figure 0.79. FBD test crack measurement of the sample S160_s3

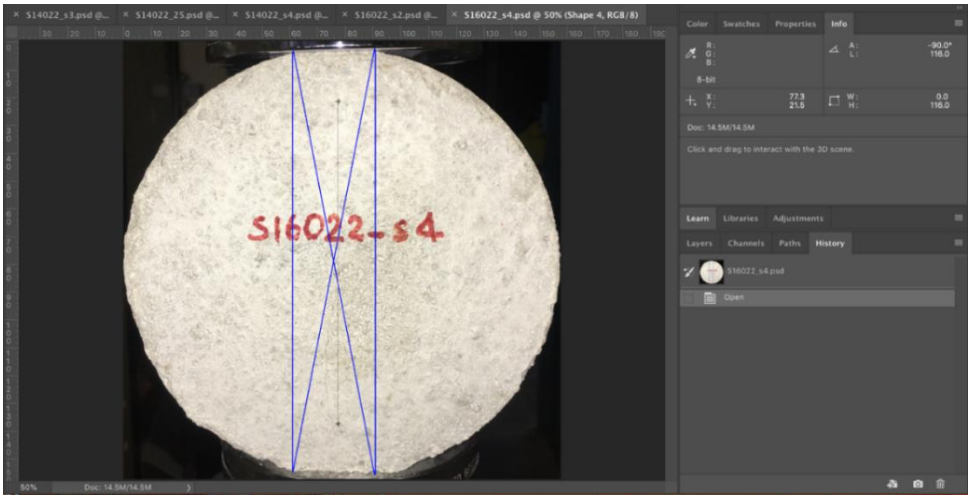

Figure 0.80. FBD test crack measurement of the sample S160_s4

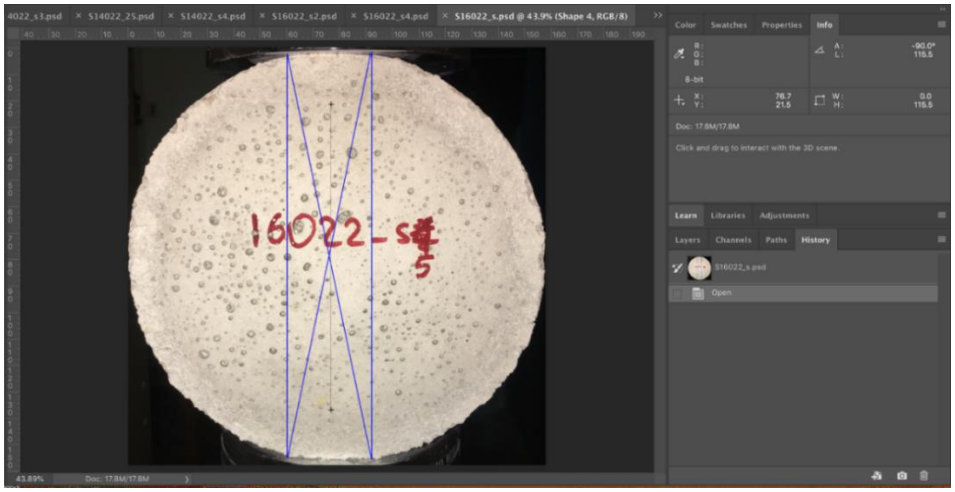

Figure 0.81. FBD test crack measurement of the sample S160_s5

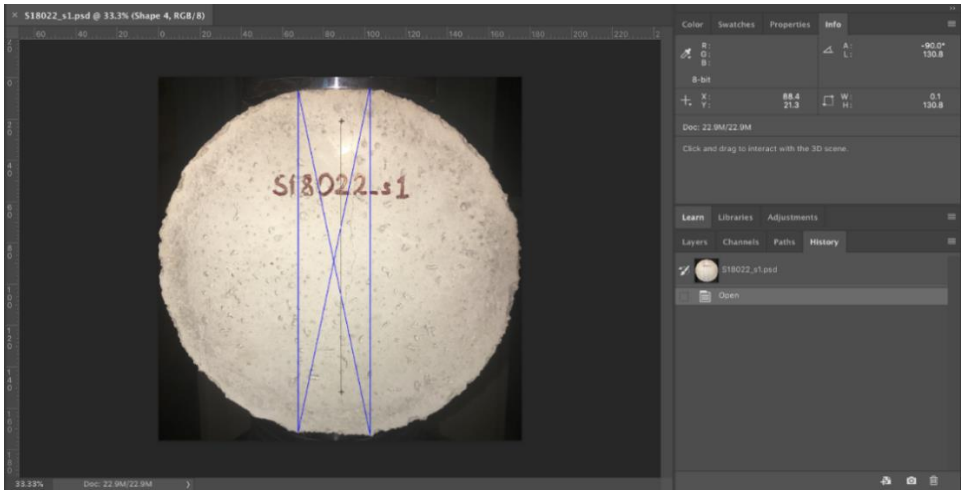

Figure 0.82. FBD test crack measurement of the sample S180_s1

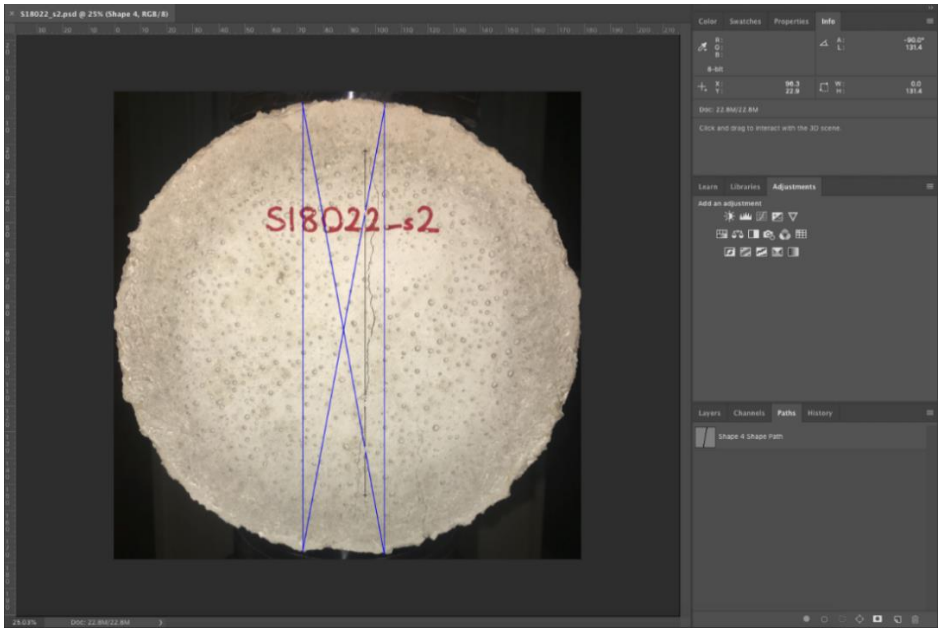

Figure 0.83. FBD test crack measurement of the sample S180_s2

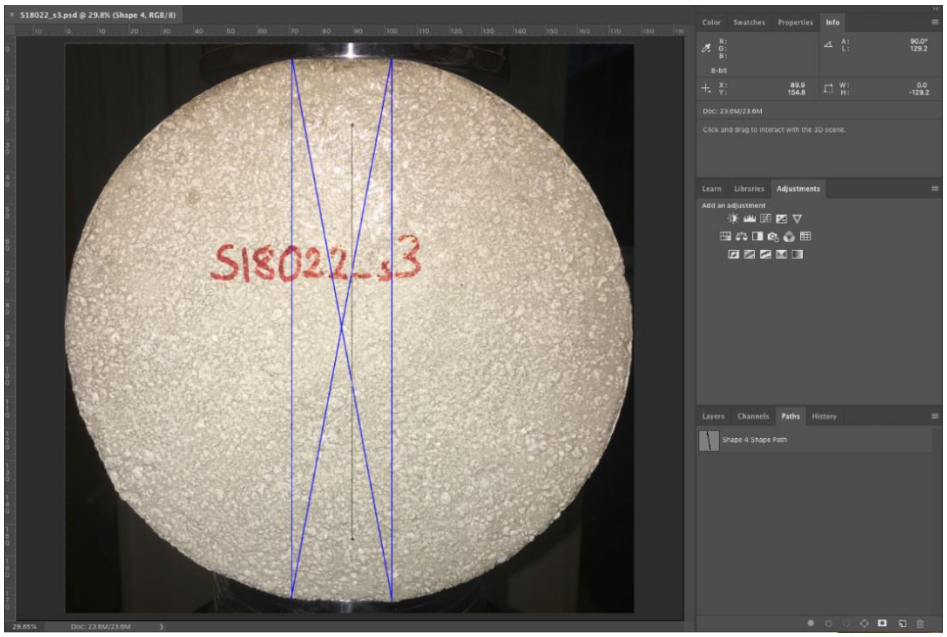

Figure 0.84. FBD test crack measurement of the sample S180_s3

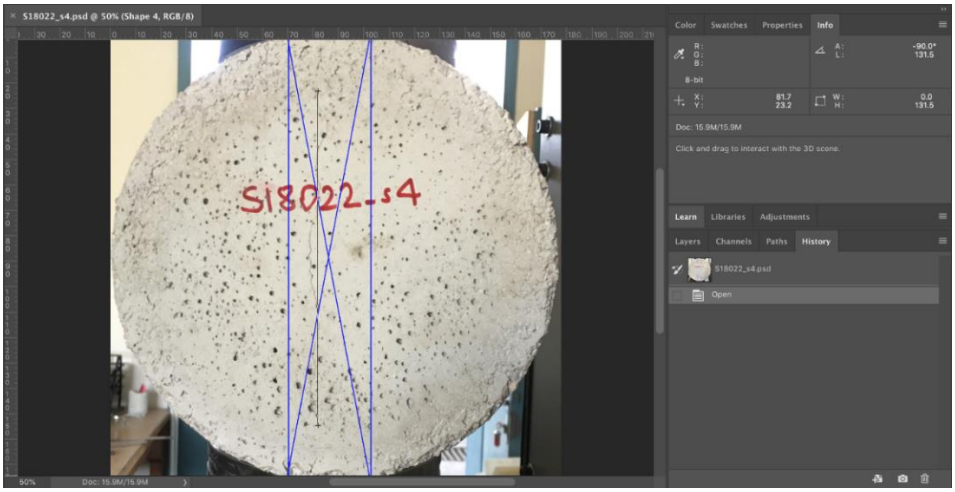

Figure 0.85. FBD test crack measurement of the sample S180_s4

Figure 0.86. FBD test crack measurement of the sample S180_s5

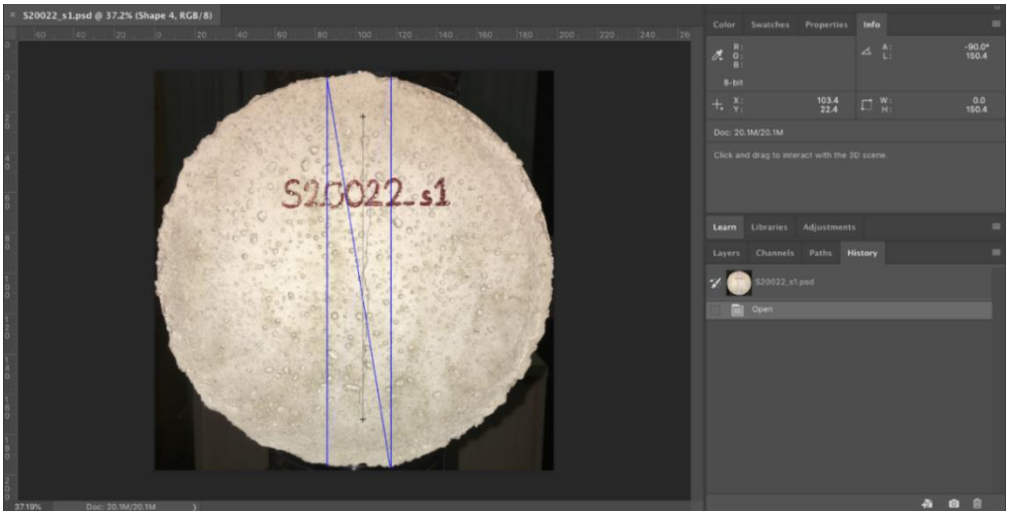

Figure 0.87. FBD test crack measurement of the sample S200_s1

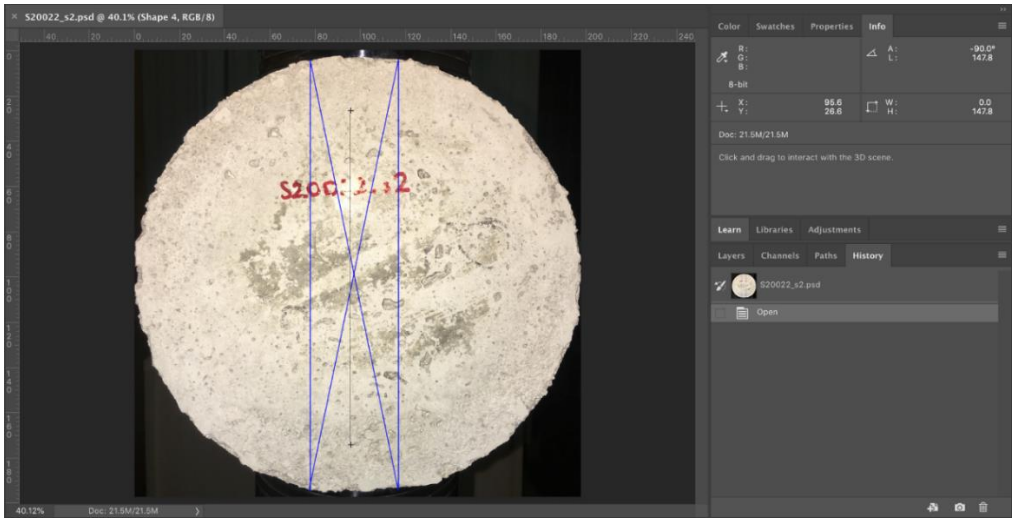

Figure 0.88. FBD test crack measurement of the sample S200_s2

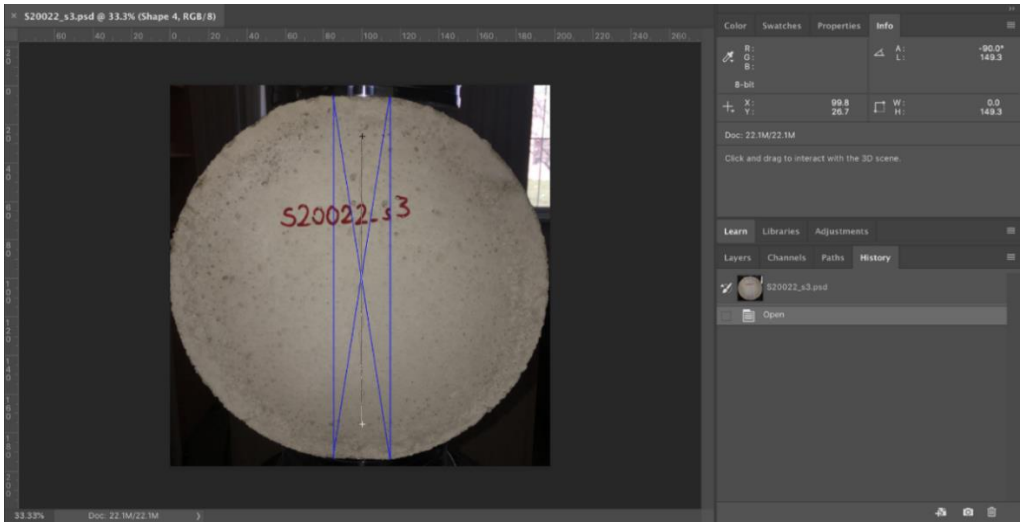

Figure 0.89. FBD test crack measurement of the sample S200_s3

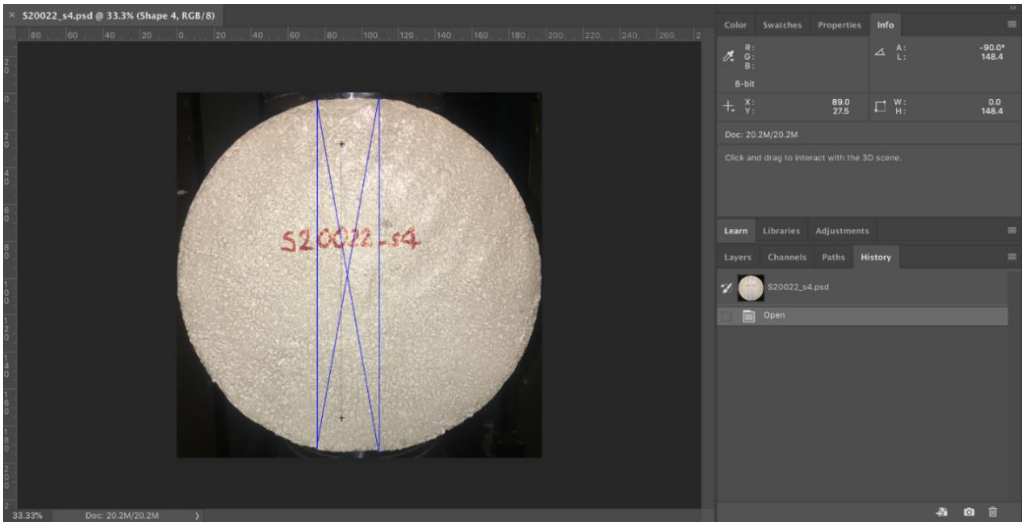

Figure 0.90. FBD test crack measurement of the sample S200_s4